Summer 2010

Functionalization and patterning of monolayers on silicon(111) and polydicyclopentadiene

Mathew Ian Perring
University of Iowa

FUNCTIONALIZATION AND PATTERNING OF MONOLAYERS ON SILICON(111) AND POLYDICYCLOPENTADIENE

by

Mathew Ian Perring

An Abstract

Of a thesis submitted in partial fulfillment
of the requirements for the Doctor of
Philosophy degree in Chemistry
in the Graduate College of
The University of Iowa

July 2010

Thesis Supervisor: Associate Professor Ned Bowden

ABSTRACT

The formation of a functional surface combines the properties of a substrate and monolayer to produce a new hybrid that can combine aspects of each. Monolayers can be made on many surfaces, and well defined functionalized monolayers were assembled on silicon(111) and polydicyclopentadiene (PDCPD).

Acid terminated monolayers were assembled on silicon(111) and their functionalization chemistry explored. It was shown that using trifluoroacetic anhydride to generate an intermediate reactive anhydride, the surface could be functionalized with amines. It was further shown that using soft lithography these functionalized surfaces could be patterned.

Mixed monolayers of methyl and olefin terminated surfaces on silicon(111) were used to develop a new soft lithographic technique with polydimethylsiloxane (PDMS). PDMS can be controllably etched using fluoride species. The surface is first activated by the attachment of the Grubbs' 1st generation catalyst. A PDMS microfluidic device is then placed on the surface. By using a cross metathesis reaction, the exposed channel can be pacified. The next step, a fluoride etchant is used to remove PDMS, exposing an unreacted surface. Polymer brushes were then grown by ring opening metathesis polymerization (ROMP) in this region.

Functionalization of the emerging polymer PDCPD was conducted through two different routes. ROMP formed PDCPD has double bonds that can be functionalized. In the first process, the double bonds were reacted with bromine. This is a rapid reaction and proceeds to a significant depth in the material. Bromines can then be displaced with amines in a substitution reaction. This was demonstrated with a fluorinated amine that when examined by XPS were shown to be present only at the surface, further more we were able to pattern this surface too. Secondly, a process using epoxides was developed. The epoxidation reaction could not be quantified, but formation in the second step of an

amine functionalized surfaces was observed by XPS. Further reaction of surface hydroxyls was also observed. This was also used to grow polyethylimine from the surface to sufficient thickness that it became observable by infrared spectroscopy.

Abstract Approved: _____
Thesis Supervisor

_____
Title and Department

_____
Date

FUNCTIONALIZATION AND PATTERNING OF MONOLAYERS ON SILICON(111) AND POLYDICYCLOPENTADIENE

by

Mathew Ian Perring

A thesis submitted in partial fulfillment
of the requirements for the Doctor of
Philosophy degree in Chemistry
in the Graduate College of
The University of Iowa

July 2010

Thesis Supervisor: Associate Professor Ned Bowden

Graduate College
The University of Iowa
Iowa City, Iowa

CERTIFICATE OF APPROVAL

_____

PH.D. THESIS

_____

This is to certify that the Ph.D. thesis of

Mathew Ian Perring

has been approved by the Examining Committee
for the thesis requirement for the Doctor of Philosophy
degree in Chemistry at the July 2010 graduation.

Thesis Committee: _____
Ned Bowden, Thesis Supervisor

_____
Edward Gillan

_____
Sarah Larsen

_____
Greg Friestad

_____
David Rethwisch

To my wife Patricia and children Carlos and Eleanor.

TABLE OF CONTENTS

LIST OF TABLES

LIST OF FIGURES

INTRODUCTION

Monolayers

Definition of a monolayer

A monolayers is an ordered arrangement of molecules on a surface that is one molecule thick. Monolayers are distinct from bilayers or multilayers that are composed of many layers, or a submonolayer which is a layer that fills less than the maximum space allowed. Monolayers are known to exist on many surfaces, with much work done on gold, glass, silicon oxide, and silicon. On polymers, monolayers are often referred to as 'functionalized' surfaces. Polymer surfaces do not exhibit the crystalline structure of metals, semiconductors, or oxides and do not exhibit the well-ordered coverings often achieved on these surfaces. However, complete coverage is not important for all applications and both types of surfaces have their uses. Monolayers may be formed through chemisorption, in which a chemical bond is formed between substrate and overlayer or by physiorption. Chemisorption tends to produce more robust monolayers than a physiabsorption, but labile bonds or unwanted surface reactions can make them less permanent than otherwise expected. Physisorbed monolayers are often removed by a change in the environment, a useful property for certain applications such as delayed drug release.[1,2]

The types of surfaces that can support monolayers range from nanoparticles[3,4] to large flat wafers.[5] This makes the formation of self-assembled monolayers (SAMs) a versatile tool. The same methods can often be applied to materials of various sizes for different applications.

The surface properties of a monolayer are determined by the terminal groups that occupy the surface. Therefore, it is possible to tailor a surface to have a specific property through the careful selection of terminal functional groups. Applications of monolayers often combine some property of the bulk material with that of a surface covering, such as

a sensor incorporating a conducting substrate with a monolayer that has molecular recognition so responses are measured electronically.[6-9] Other monolayers have been synthesized for protection of the substrate from unwanted reactions.[10-12] In some cases, the substrate is simply the support for the monolayer that contains functionality for an application and is not dependent on the substrate; such applications include surface bound catalysts[13-16] and fluorescent molecular recognition.[17,18]

Another use of the term monolayer is for the coating of a surface, sometimes through chemical bonds, of a single layer of nanoparticles, (e.g. nano-crystalline zeolites on gold[19] and silicon[20] or silica particles on silicon.[21]) However, this discussion will be limited to the first type of monolayer.

Examples of Monolayers

Monolayers are known for many types of surfaces. Gold has been used extensively for the formation of monolayers. Other metals that have been studied include silver,[22-25] platinum,[26-28] and copper.[29,30] Semiconductors such as silicon, gallium arsenide[31-34] indium phosphate,[35] and, most recently, diamond[36-39] have been used to assemble monolayers as well as other crystalline materials such as silica, zeolites,[40] and zirconia.[41] Less ordered substrates such as glass and polymers can be used as substrates for monolayers, but would be expected to have less ordered layers. The range of applications for a surface coated with a monolayer is a combination of the monolayer's and the substrate's properties.

Monolayers on Gold

Much of the work on monolayers has been informed by studies of monolayer formation on gold, making gold an important substrate for the understanding of other systems (Figure 1). The most widely used method for the formation of monolayers on gold of thiols[42-52] (recently analogous selonates[53] and tellurides[54] have also been used). Some monolayer on gold can be formed by immersion in a thiol solution. Monolayers

can be assembled in as little as a few minutes. The precautions required to produce high quality monolayers are dependent on the thiol being used.

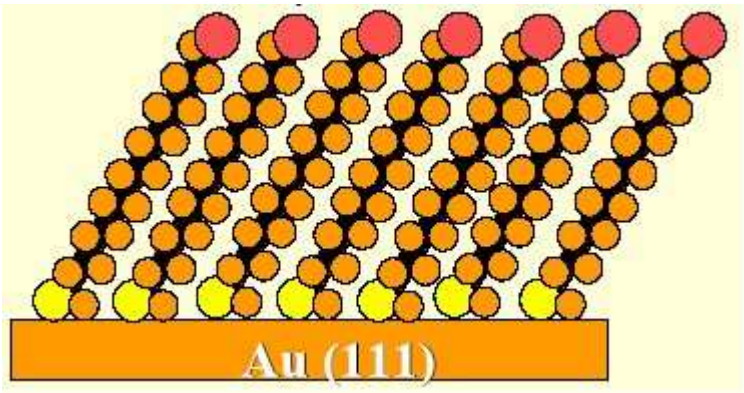

Figure 1. Schematic representation of alkyl thiols self assembled monolayers (SAM) on gold. From reference 48.

Because the spacing of gold atoms is very similar to the diameter of an alkane chain, monolayers can assemble into well-packed and ordered layers. The formation of gold-thiol bonds is governed by thermodynamics at room temperature and the monolayer is in equilibrium with the thiol solution; thus, nearly all the available sites on the gold are occupied. However, this advantage in the formation of highly packed layers reduces the stability of the resulting surface as the labile gold-thiol bonds[55,56] are susceptible to breaking and reducing the monolayer coverage in applications.

The labile nature of gold-thiol bonds can be used to modify the surface after the formation of the monolayer by partial displacement of ligands by other functionalized molecules.[57-62] Partial displacement is particularly useful if the thiols do not form a well ordered, high coverage monolayer when assembled directly from solution due to sterics or charge repulsion. Partial displacement is one method of forming mixed monolayers containing two or more ligands. Mixed monolayers may also be assembled by having

more than one ligand present during assembly, with the ratio in solution determining the ratio on the surface. However, it has been shown that the ratio of surface moieties will not necessarily reflect that found in solution. This method has been used to assemble monolayers incorporating biotin. If the concentration of biotin in the monolayer is too high they are unable to bind streptavidin in solution because of steric crowding.[63,64]

Chemical modifications of the terminal groups have been shown with gold. Modification can be through the conversion of the terminal group to a different functional group or attachment of another molecule. Examples of reactions on monolayers on gold include bromine substitution by amines[65] and reactions of carboxylic acids to amides via surface anhydrides.[66,67]

A variety of molecules have been attached to gold monolayers including DNA[68-73] and proteins.[74-77] Much of the work on other substrates has been stimulated by the original work on gold, with the transfer of techniques initially undertaken on gold to other surfaces. The patterning of monolayers has been demonstrated on gold, including micro contact printing of thiols.[78-84]

Monolayers on Glass and Silica

Monolayers on glass and silica are made by reacting surface hydroxyl groups with reactive species, normally to yield Si-O-Si-C bond.[85-89] Typical attachments involve reacting molecules with trichlorosilanes, Si-O-CH_2R or Si-CH_2R. These can polymerize in solution and the resulting attachment may be a single site linking a long polymer chain rather than individual molecules attaching to a surface. The disadvantage of these monolayers is the susceptibility of the Si-O bond to undergo further reaction, thereby destroying the monolayer. Alternatively, a chlorinated surface can be formed on a silicon oxide and then reacted with alcohols, Grignard reagents, or alkyl lithium reagents.[90]

Monolayers on Silicon

The interest in monolayers on silicon is largely due to the semi conducting properties of silicon and the potential to combine electronic components with molecular applications. While silicon-carbon bonds are less labile than thiol-Au bonds, the substrate is vulnerable to oxidation. Oxidation is slowed with the formation of dense monolayers that decrease the diffusion of small molecules, such as water and oxygen, to the surface. The spacing between silicon atoms in silicon(111) is 3.84 Å and the diameter of an alkyl chain is 4.2 Å. Because of this difference not every silicon atom can be capped by an alkyl chain. The formation of a monolayer on Si(111) leaves behind unreacted silicon hydrides that can become oxidized and introduce defects.

Types of silicon

Silicon surfaces are described in terms of their Miller indices to orientate the crystal structure relative to the surface. The two most widely used surfaces for the assembly of monolayers are silicon(100) and silicon(111).

Silicon(100) surfaces are not atomically flat but are comprised of a series of planes that produce steps with widths of approximately 6 silicon atoms. The prepared hydride surface has two silicon hydride bonds per silicon atom. Silicon(100) is the type of silicon most widely used in semiconductor applications.

Silicon(111) presents an atomically flat face in the prepared hydride surface each silicon atom possesses a single terminal hydrogen. This arrangement yields fewer defects, as well as better coverage and reduced surface oxidation. Si(111) is the slowest face of silicon to etch.

Reactions of the Silicon Surface

To assemble monolayers on silicon, the native oxide layer must be removed first. Methods exist to produce monolayers on the native oxide layer through Si-O-Si linkages[90] and share much in common with monolayer formation on glass and silica.

However, as this silicon oxide layer is insulating, it limits potential applications. Methods of attachment that do away with the oxidized layer are desirable. The three methods most widely used to form organic monolayers on silicon are reconstruction of the silicon surface, reactions with a halogenated surface, and formation of a reactive hydride surface.

Surface reconstruction occurs in silicon(111) and silicon(100) under ultrahigh vacuum at elevated temperatures around 700^{o}C.[91,92] The new surface configuration contains dangling bonds. Dangling bonds react with molecules introduced to the chamber to yield monolayers. The disadvantage of this method is that the structure of the silicon at the surface is changed. Introduction of a new layer of material alters some properties of the silicon such as its conductivity. This method also requires the use of specialized equipment which limits who can utilize it.

The second method of reconstruction to form organic monolayers is scribing.[93,94] Here, a silicon wafer is exposed to a molecule and mechanical force or other ablation technique (i.e. a laser) is applied to the surface to remove the top layers of silicon. The underlying layer is left with reactive dangling bonds that will form the monolayer with proximate molecules. However, this method leaves behind an uneven surface and only occurs in the region that has been scribed making it suitable for patterning but not for functionalization of a large area.

Silicon surfaces with silicon hydrides (see below) can be converted to a surface with silicon halides through a number of methods.[95] Chlorinated surfaces may be generated by the use of PCl_5 or Cl_2 with benzyl peroxides[96,97] or UV light.[98,99] Brominated surfaces can be formed from CCl_3Br with benzyl peroxide[100] or light[99] and iodinated surfaces from I_2[101,102] or CH_3I.[103] These halide surfaces react with Grignard and alkyl lithium reagents, but due to the reactivity of these molecules the functional groups that can be included in a monolayer is limited. Restrictions on the terminal groups that can be displayed limit the utility of this approach. These surfaces also react

with alcohols, but these reactions yield undesirable Si-O-C bonds that are susceptible to cleavage.

The other major route to monolayers on silicon is through the reaction of silicon hydride surfaces. Silicon(111) can be functionalized with hydrogen to yield an atomically flat surface with each silicon capped with a single hydrogen. Chabal[104] showed that it was possible to take HF buffered at high pH in ammonium fluoride with silicon to produce a highly ordered surface. When this surface was examined by p-polarized infrared light, a peak at 2087 cm^{-1} was observed while no peak was observed using s-polarized light as shown in Figure 2. The IR spectrum corresponds to an Si-H bond orientated perpendicular to the surface.

Others[105,106] took this work further to reduce the presence of defects caused by oxygen etch pits by the degassing of etchants and the use of single side polished wafers. This method provided cathodic protection from superoxide etching by the rough side acting as a sacrificial anode. It was seen[104,107,108] that etching with HF at low pH led to rougher surfaces than etching at high pH (*i.e.* ammonium fluoride). This work led to the acceptance of the step-flow mechanism which explains the smoothing of the Si(111)–H surface. The mechanism was further refined[106,109-113] and shown to be initiated by a rate limiting oxidative addition of hydroxide on a silicon atom at a step edge followed by displacement of the hydroxide by fluoride ion. This leads eventually to the removal of silicon from the surface in the form of SiF_3OH and the capping of the surface silicon atoms by hydrogen.

Formation of Monolayers on Silicon Hydride Surfaces

A number of different methods for the formation of monolayers from the Si(111) surface are known. Some methods rely on the formation of radicals, such as those generated by heat, UV light, or a radical initiator. Other methods involve the use of reagents such as Grignards or chlorosilanes. All of these methods limit which functional

groups can be used and therefore limit the possible function groups expressed on a surface.

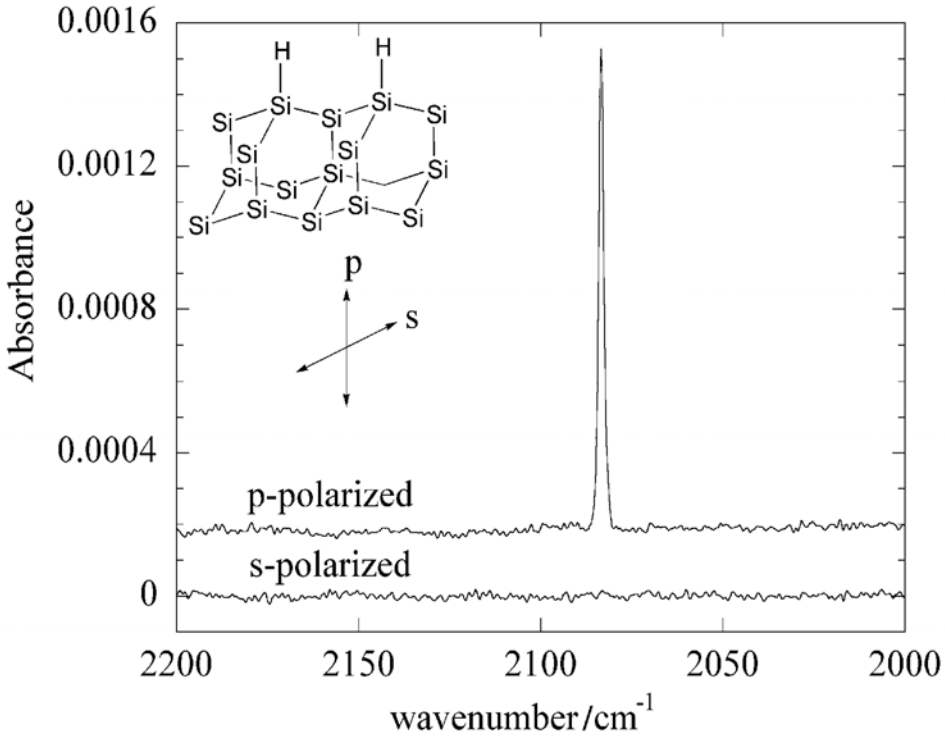

Figure 2 Infrared spectra of a silicon (111) surface terminated with hydrogen showing that the Si-H bonds are perpendicular to the surface, from reference 104

It was shown by Chidesy and Linford that organic molecules possessing a double bond can be attached to hydrogen-terminated silicon.[114] The alkyl monolayers were prepared by adding 1-alkenes into the Si-H group in the presence of a diacyl peroxide radical initiator at 100 ^{o}C. The proposed mechanism of monolayer formation is based on a series of free radical reactions and is shown in Figure 3. The currently accepted mechanism for formation of a monolayer involves the formation of a radical on the surface. In the first step, the initiator, diacyl peroxide, dissociates by homolytic cleavage

to form two acyloxy radicals which eventually break apart to form an alkyl radical and carbon dioxide. In the second step, the alkyl radical abstracts the hydrogen atom from the hydrogen-terminated Si surface to produce a silicon radical. In the final step, the silicon radical reacts with alkenes to form a Si-C bond. The reaction is a chain reaction which leads to formation of a monolayer by a random walk on the surface. Because this is a kinetic process, not all available Si-H are reacted which will result in pinhole defects. In a similar fashion, alkenyl monolayers can be grafted using alkyne molecules.

It has been found that at temperatures >150 ^{o}C, the Si-H bond undergoes a homolytic cleavage, Si-H→Si$\cdot$ +H$\cdot$, and yields a silicon radical at the surface, which then reacts with alkenes as described above. This process is called "thermally induced hydrosilylation."[115] The hydrosilylation by homolytic cleavage can also been promoted by UV irradiation known as "photochemical hydrosilylation." [116,117] In this case the radical is generated by homolytic cleavage of Si-H and the formation of electron holes by light in the bulk silicon. Organic monolayers have also been attached to the Si-H surface using electrochemical methods.[118]

The use of visible[119] wavelengths of light, in the presence of olefins, has been shown to produce monolayers. The use of visible light requires significantly longer times to form monolayers than UV light, but has the advantage that a wider range of molecules, that would not tolerate harsh UV light conditions, can be used to assemble a monolayer. The energy of visible light is insufficient to cause homolytic cleavage of Si-H so an alternative mechanism must be responsible for the assembly of the monolayer through the generation of electron hole pairs in silicon.

Functionalization of Monolayers

Most early work to assemble monolayers on surfaces utilized alkyl chains. These pack well and allow dense, well-ordered monolayers to be assembled, which make them ideal to study how monolayers are formed. Alkyl chains do not have many desirable

properties other than surface passivation, which limits their use. To increase the potential applications of monolayers it is necessary to assemble monolayers with functionalized surfaces. One method of functionalizing an alkyl chain on silicon has been shown by Chidsey where a surface was first chlorosulfonated by a photo initiated free radical reaction followed by sulfonamide formation by reaction of the sulfonyl chloride with an amine.[120]

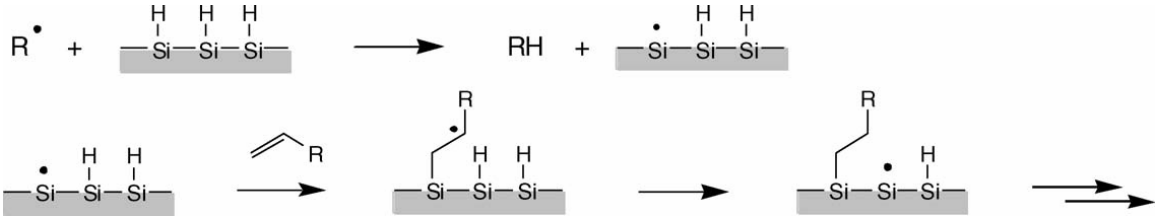

Figure 3 Radical initiation and step wise reaction of monolayer formation

To assemble a functionalized surface, a suitable molecule must be used that incorporates two compatible end groups. Because not all functional groups can be assembled into monolayers through a one step reaction, various methods have been developed to further functionalize a surface. When multiple steps are needed a suitable functionalized surface must be first assembled. Examples of monolayers on silicon containing functional groups assembled in a single step include esters[121-125], carboxylic acids,[121,124-126] aldehydes,[127] alkyl bromides,[128] alcohols,[121,124,129] olefins,[5,130] amides,[131] and amines.[124,132,133] Because of steric crowding, a functionalized surface will often be assembled in the presence of an alkyl chain molecule to dilute the functional group concentration in a mixed monolayer. The incorporation of alkyl chains serves two purposes. First, alkyl chains can make the functional groups more accessible. Second, they can add greater stability because they pack more densely than chains with non-CH_3 terminal groups.

Reactions on surfaces normally have precedents in homogeneous reactions in solution chemistry. But due to the confined nature of a surface, steric crowding is a significant limitation. Reactions take longer and their progress is difficult to monitor. In typical organic reactions aliquots can be removed and TLC or NMR spectroscopy can be used to check the progress. No similar technique is available for surface reactions. Separating a monolayer surface from a reaction mixture is easy, with washing and sonication being the preferred methods. These ensure that only chemisorbed species are present on the surface. Unwanted side products on surfaces are difficult to control. It is not possible to purify the surface after reaction so anything covalently bonded to the surface will remain. In addition, certain reaction conditions promote the growth of defects such as through oxidation of the underlying substrate.

Esters are versatile and have many potential reactions. Esters have low reactivity towards silicon surfaces and have been chosen to assemble well-ordered monalayers with the ester groups presented on the surface. Ester surfaces can also be generated by the conversion of carboxylic acids[124,134] and olefins by oxidation with an aqueous solution of $KMnO_4/NaIO_4/K_2CO_3$.[134]

On silicon surfaces, esters have been converted to carboxylic acids.[121,124] Esters have been reduced to alcohols with sodium borohydride[124] and lithium aluminum hydride,[121] the subsequent alcohols were converted to esters by reaction with acetyl chloride.[124] Esters have been reacted with Gringard agents. This reaction added two alkyl chains to each ester.[124] Carboxylic acids have been activated by N-hydroxysuccinimide to attach amines including amine terminated single stranded DNA.[135]

Amine surfaces can be accessed by assembling the amine monolayers while the amine is protected. Monolayers assembled using phthalimide and acetamide as protecting groups have been deprotected and reacted with trifluroacetic anhydride.[132] Alternatively, the protecting group tertbutoxycarbonyl has been used and when deprotected the amine reacted with thiol modified DNA using a heterobifunctional

linker.[136] Amines have been converted to amides,[137] and amines have also been used to attach C_{60} to silicon.[131]

Monolayers assembled from protected alcohols have been used to grow nucleotides from a surface. Dimethoxytriphenylmethyl protected alcohols were assembled then deprotected with methylamine. The alcohol was used as the base to grow DNA using a DNA synthesizer.[138]

Bromine terminated monolayers have undergone S_N2 displacements with azides, thiocyanate, and cysteine. These reactions were shown to be slow due to the hindered nature of the alkyl chains, but the bromines were present at the surface.[139]

Formation of Monolayers on Silicon (111) using TEMPO

It was shown by the Bowden group[140] that it was possible to assemble monolayers on silicon (111) using the stable radical 2,2,6,6-tetramethyl-1-piperidinyloxy (TEMPO) and 1-octadecene. TEMPO is stable at room temperature and unreactive towards many functional groups, making it an ideal initiator to assemble monolayers under mild conditions.

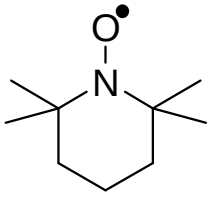

Figure 4. 2,2,6,6-Tetramethyl-1-piperidinyloxy (TEMPO)

Silicon hydride surfaces were prepared in HF buffered at high pH as outlined before.[104,105] Studies were undertaken to determine the best conditions for the assembly of monolayers and arrangement of the reactants on the surface. The surfaces were studied by XPS, elipsometry, and contact angle goniometry. In prior work, well-ordered

monolayers with exposed methyl groups were found to have contact angles in the 110-113^{o} [117,141-143] range, while those that were disordered and showing CH_2 groups at the surface had contact angles of 102^{o}.[144] Monolayers assembled from octadecene with 1.0 or 0.1 mol% TEMPO produced surfaces with contact angles of 110^{o}.

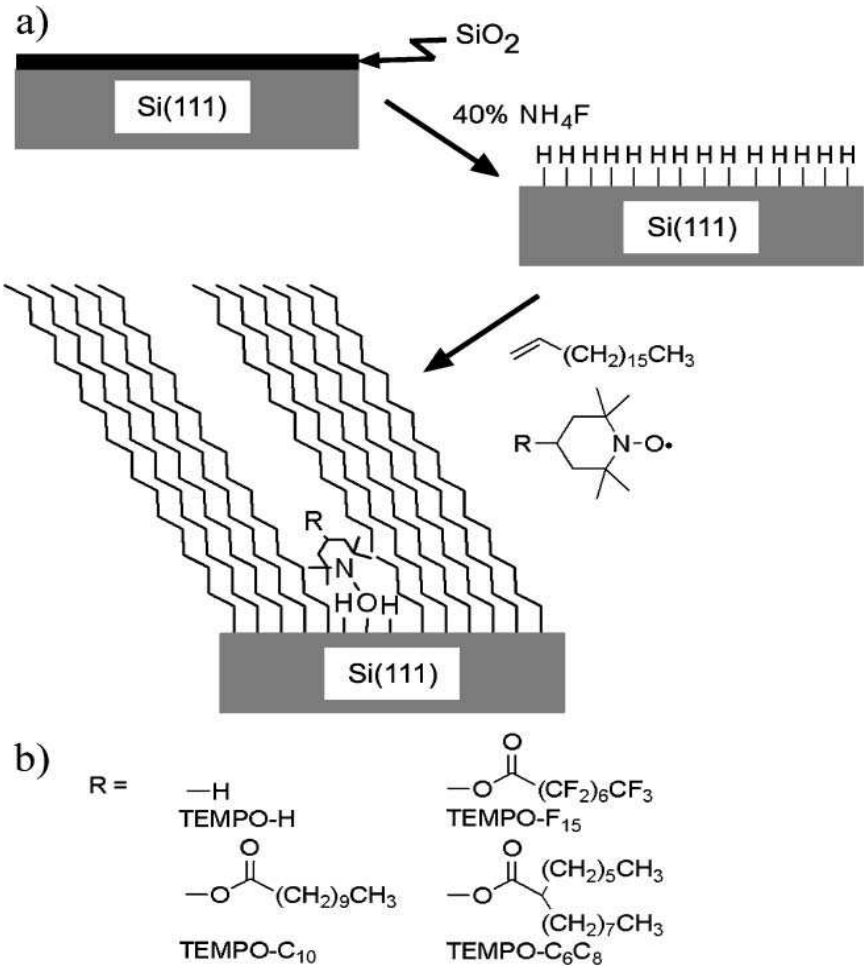

Figure 5. Assembly of monolayers on silicon a) A Si(111)-H surface is generated by reacting a clean silicon wafer with 40% NH_4F under N_2. This surface is reacted with different concentrations of TEMPO or derivatives of TEMPO in 1-octadecene to form well-ordered monolayers. b) The different derivatives of TEMPO used to assemble the monolayers. From ref 139

It was found that TEMPO molecules were attached to the surface presumably through their oxygen. Therefore, to reduce the disorder that TEMPO would introduce, derivates were used that incorporated extended chains to space fill the region above the point of attachment of TEMPO. Surfaces functionalized with octadecene, and these derivatives of TEMPO had contact angles of 111^{o}-112^{o}.

The assembly of monolayers of 1-octodecene monolayers without TEMPO had contact angles of 102^{o}. The disordered monolayer was most likely formed by ambient light.[119] When TEMPO was used in a solvent without 1-octadecene, a contact angle of 85^{o} was recorded suggesting that TEMPO does bind to the surface, but that incomplete coverage was observed. The monolayers were studied for their stabilities on exposure to different solvents. The most stable surfaces were stable to refluxing toluene and chloroform over extended periods and oxidized slightly in water. Significant oxidation occurred on exposure to refluxing chloroform and water after a few hours.

XPS was used to show that the monolayers protected the underlying silicon under ambient conditions; however the wafers that were exposed to water showed formation of silicon oxides in the XPS spectra. XPS was also used to demonstrate that TEMPO attached to the surface by using a fluorinated derivative of TEMPO which showed an F(1s) signal in the XPS after assembly. It was seen that the amount of fluorine was related to the initial concentration of TEMPO-F_{15}. The relationship between initiator concentration and TEMPO on the surface was not determined though.

It was further shown (see Figure 6) that it was possible to pattern these monolayers by soft lithography using polydimethylsiloxane (PDMS). Silicon hydride surfaces were partially covered by a patterned PDMS stamp, leaving open channels that were filled by capillary action with a solution of 11-undecylenic acid and TEMPO. After 24 hours the PDMS was removed and the silicon cleaned. Then the whole wafer was immersed in a solution of 1-octadecene which reacted only on the previously covered portion. The pattern was visualized by water condensation which preferentially formed

on the region terminated with carboxylic acids. The UV curable Nordland optical adhesive 61 preferentially assembled on the region terminated with carboxylic acids, was cured and imaged by light microscopy. Scanning electron microscopy also showed a difference between the two patterned regions.

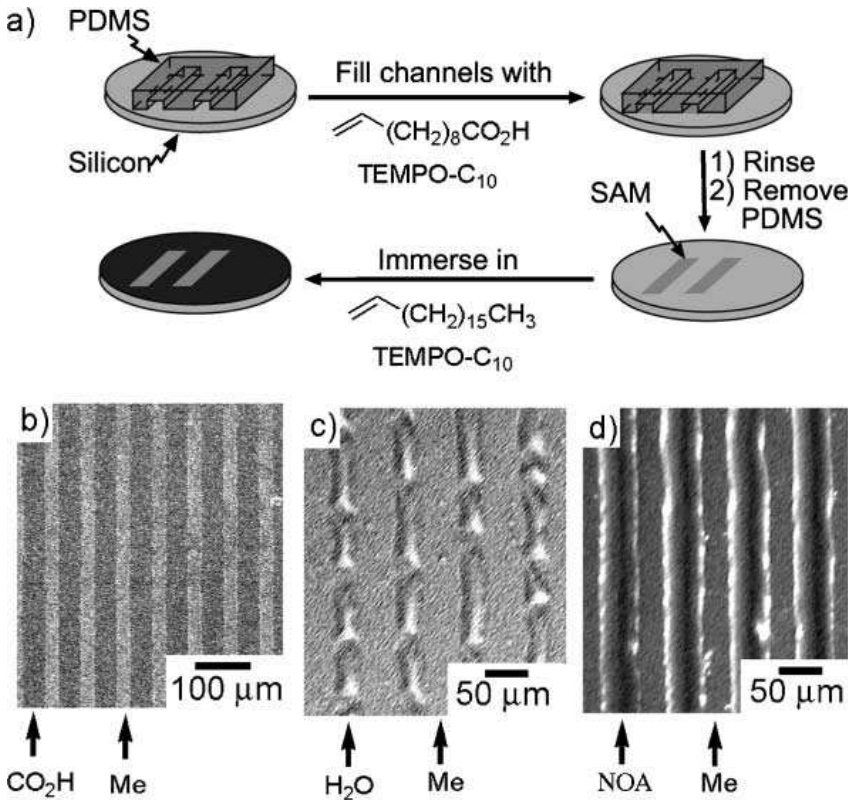

Figure 6 SAMs on Silicon patterned using PDMS containing acid and methyl terminated monolayers. a) shows the reaction scheme for the patterning of silicon by the assembly of undecalynic acid and octadecene b) show an electron micrograph of a patterned monolayer c) shows a water condensation image where the water drops appear on the acid terminated region and d) shows the condensation of Norland optical adhesive 61 on the acid terminated regions. From ref 139

This research was the basis for the assembly and patterning of monolayers in Chapters 1, 2 and appendix A. Monolayers with sufficient resilience were assembled that could be further functionalized and patterned.

Monolayers on Polymers

Principles of Polymer Surface Functionalization

A monolayer on a polymer surface is normally referred to as a 'functionalized surfaces.' Polymers lack the well-defined structures that are typical of crystals used to assemble monolayers. However, this difference does not necessarily limit their utility as they have different properties from crystals that can be exploited, such as permeability, optical transparency, and ability to be cast into a desired shape.

Functionalization of polymers has been shown on polystyrene (PS), polytetrafluoroethylene (PTFE), polyethylene terephthalate (PETP), polyethylene (PE), poly α-hydroxyacids (PAH), polypyrrole (PP), polydimethyl siloxane (PDMS), and polymethyl methacrylate (PMMA). There are several methods to functionalize polymer surfaces. These different methods include generating new reactive species on a surface, and the use of functional groups contained in the polymer material. These functional groups can be from residual functionalities unconsumed in the polymerization procedure, or from functional groups formed in polymerization.

Many wet chemical processes can be used to generate oxygen containing functional groups. PE and PP can be oxidized by chromic acid and potassium permanganate.[145-147] Sodium hydroxide can be used to generate carboxylic acids on PMMA.[148,149] PMMA can also be reduced to hydroxyls with lithium aluminum hydride.[150] These reactions may introduce a range of oxygen groups that are then functionalized. But due to the different functional groups that can be formed under these

conditions, it can be difficult to control their surface chemistry. These reagents can also cause the surface to be etched.[151]

Plasmas are high energy gases of charged particles that can be used to modify a surface. Many parameters can be altered to tailor the resulting surface such as the gas used, temperature, pressure, flow rates, etc. Plasmas typically only affect the first few nanometers of a surface, unlike wet chemical techniques that can affect the bulk. Oxygen plasmas can be used to incorporate a range of oxygenated species, but tend to yield several different functional groups on the surface.[152] Carbon dioxide plasmas have been used to incorporate carbonyl groups on PP[153] and PS.[154] Nitrogen and ammonia have been used to add amines on PTFE[155,156] and PS.[154] Inert gases such as argon can be used to produce radicals on the surface that will react in the presence of monomers for graft polymerization.[157-159] However, plasma generated surfaces are difficult to replicate because many parameters are difficult to control and optimization with one apparatus can not be easily repeated at another location.

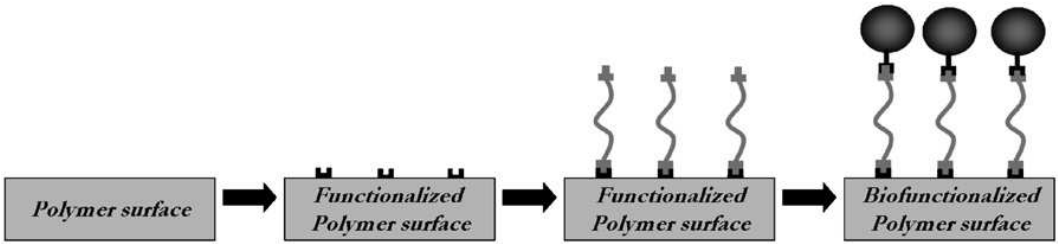

Figure 7 Generalized outline of how biomolecules are attached to polymer surfaces. From reference 166

When exposed to UV light, polymer surfaces generate reactive sites which can be functionalized upon exposure to gas or can be used to initiate UV-induced graft polymerization. This technique differs from plasma treatments by the ability to tailor the

depth of the surface that reacts by varying the wavelength. UV irradiation has been used to introduce carboxylic acids to PMMA[160] as well as to activate PS[161] surfaces for enzyme attachment. UV irradiation has also been used to initiate radical graft polymerization of bioactive compounds. For instance, *N*-vinylpyrrolidone has been photo grafted to the surface of PP films to generate antimicrobial materials.[162] UV treatment can, however, affect the optical properties of the polymer.

Silanes can be attached to either chemically modified or plasma modified surfaces. They can be added by wet chemical methods or by vapor deposition. Silanes have been attached to surfaces to display groups such as polyethylene glycol, vinyl and bromine. Silanes have been added to PMMA,[150,163] PTFE,[164] and PETP.[165]

Applications for the attachment of biomolecules to polymers are found in biomedicine, textiles, microelectronics, bioprocessing, and food packaging.[166] The general process is outlined in Figure 7. After a surface is functionalized, a spacer is added to the surface and the relevant biomolecule is attached to the spacer to reduce the steric crowding of biomolecules. One challenge of fabricating functionalized surfaces on polymers is that they can undergo reconstruction. The surface of the polymer can rearrange to a lower energy configuration, which can bury the attached layer.

Polydicyclopentadiene

Dicyclopentadiene is polymerized to form polydicylopentadiene by ring opening metathesis polymerization (ROMP). The recent development of highly active ROMP catalysts, such as the Grubbs catalyst, allows for the polymerization, at low catalyst loading, of many monomers including dicyclopentadiene. Polydyclopentadiene (PDCPD) has many desirable properties such as hardness, transparency to visible light, and low reactivity towards many organic reagents. PDCPD from ROMP contains double bonds that can be exploited for further functionalization. Prior to our work there was

only one report of the surface functionalization of PDCPD[167] using an ATRP initiator grafted to the double bonds.

Mercaptoethanol was attached to the double bonds in the presence of benzyl peroxide. 2-Bromoisobutyryl bromide was then reacted with the mercaptoethanol on the surface. XPS results showed the amount of mercaptoethanol on the surface was low compared to surface 2-bromoisobutyryl bromide in the next step. The author suggests that the bromide compound must also attach through surface hydroxyls from advantageous oxidation. The bromide was used as the ATRP initiator for the growth of poly(methylmethacrylate) from the surface.

Characterization

The analysis of a surface is not a straightforward task compared to the analysis of a compound of small molecular size. For example, impurities cannot be removed from a surface and can hinder characterization, whereas small molecules can be purified to remove unwanted side products. A compound in solution can often be unambiguously identified by a simple ^{1}H NMR spectrum and functional groups can be seen with infrared spectra. Mass spectrometry can be used to identify many compounds from the fragmentation patterns or parent ions. When mass spectrometry is applied to a surface, there is a significant chance of secondary products from the destruction of the surface when generating the ions. No single technique can provide a definite answer to the structure of a surface, instead a combination is needed. Each technique provides a different piece of information that is used to construct a picture of the surface. However, due to the nature of each technique, information from the surface may come from different depths. A careful analysis of data from each technique is needed to determine the structure of the surface.

One of the problems with surface analysis is the inherent sensitivity of a thin layer attached to the bulk. Therefore, the analysis must be undertaken by methods that

measure phenomena that are surface localized or use a setup that can be used to enhance the signal from the surface relative to the bulk. The choice of which techniques to apply to surfaces is a combination of the information to be obtained, cost, time, and availability. The analysis of surfaces often require expensive instruments with high vacuums or those that use electron beams. Therefore, it is not feasible to use all possible techniques due to limited resources. Thus it was necessary to confine our analysis to the most informative techniques and those that can be undertaken most cost effectively. Rapid feedback could be obtained from simple techniques such as contact angle measurements whereas extensive chemical information could be obtained from XPS.

XPS

Principles of XPS

X-ray Photoelectron Spectroscopy (XPS) is a technique that is used to examine surfaces. The technique is inherently surface localized because electrons are unable to escape from depth to be captured by the detector.

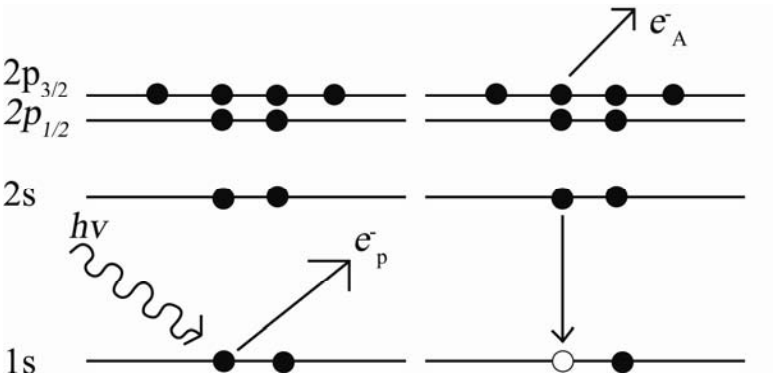

Figure 8 Electronic diagram of the XPS (e^-_p) and Auger (e^-_A) process Adapted from Surface Analysis D. Briggs, J. T. Grant, IM Publications and Surface Spectra Limited, 2003

X-rays are used to illuminate a target, and this radiation causes inner core electrons to be ejected. The energy of the electron is equal to the incoming radiation minus the energy needed to remove the electron from the atom, called the binding energy, and a factor related to the individual instrument. It is the energy of these electrons that is measured when XPS spectra are taken. Holes can be refilled by electrons falling from the outer shells and the excess energy can then be lost as a photon by fluorescence. This effect is measured by X-ray fluorescence spectroscopy (XRF). Alternatively, excess energy can be lost by the ejection of a second photoelectron, referred to as Auger electron, from an outer orbital. These electrons are measured in an Auger spectrum. In normal Auger applications, electron holes are generated by an electron gun instead of an X-ray source, but Auger series are observed in XPS spectra. The incorporation of an electron gun in an XPS instrument allows SEM images to be obtained, although with lower quality images than a dedicated SEM instrument because the optimum location for the electron gun is occupied by the XPS detector.

The surface region from which electrons can escape and be detected is generally regarded to be three times the attenuation length. The attenuation length is the distance component of a decay function for electrons in a medium. The attenuation length is related to and is similar in value to the inelastic mean free path (IMFP) that is the average distance between inelastic collisions. The IMFP is an easier value to determine and is often used to approximate the AL, IMFPs can also be used to calculate an AL. There are two widely used formulas for the calculation of the IMFP, one is by Greis[168] and the other by Tanuma, Powell, and Penn.[169] They use different properties of the material being analyzed to calculate a IMFP. It is possible to choose the most appropriate method to calculate an IMFP based on the known values. For our work, the Greis' method was favored since the band gap energy was unknown for PDCPD and this value is required for the method by Tanuma, Powell, and Penn.

XPS provides information on the elemental surface composition and also can provide information on the chemical environment of an element. Bonding to different elements, bonding with different bond orders, or possessing a different charge state creates small shifts that are discernable in XPS. Examples include carbonyl vs. single bonded oxygen; carbon bonded to electronegative atoms vs. a carbon with only carbon-carbon and carbon-hydrogen bonds; and protonated vs. unprotonated amines. The location of a peak is characteristic of these groups and can be used to assign the functional groups in a sample. The area of a peak in an XPS spectrum is proportional to the concentration at the surface which allows the percent atomic compositions to be calculated.

In XPS, electrons are ejected from the sample and the binding energy is related to the environment that an electron comes from. It is possible that the sample will itself become charged during analysis. For conductors and semiconductors, electrons are free to move and prevent charging from occurring. But for insulating samples, such as PDCPD, this charging can be significant, with peaks moving hundreds of eV. Modern XPS instruments include a charge neutralizer, which is an electron gun that supplies electrons to the surface at a rate that counteracts the loss due to X-rays. The current is carefully controlled to eliminate surface charging.

Auger has a higher spatial resolution than XPS and is therefore useful in mapping elements. Mapping is possible with XPS but has a lower resolution. Auger spectra do not contain as much structural information as can be found within an XPS spectra.

Distribution in a Surface by Inelastic Background Analysis

$$D = A_p / B$$

Equation 1. Inelastic background distribution where D is the distribution value, A_p is the peak area with a linear background and B the Increase in background 30 eV below the peak.

A method to find the depth of an atom on a surface from peaks in XPS spectrum was found by Tougaard. In a series of papers[170-172] he examined the effect of distribution of elements in the surface region to the background in XPS spectra. It was found that the background after the peak appeared was affected by the depth profile of atoms in the surface layer. This difference was due to the to the signal at the peak being composed of electrons passing out of the sample without collision or only from elastic collisions. Electrons that experienced inelastic collisions lose energy, therefore it was predicted that the background of the lower energy region adjacent to the peak would be of higher intensity than the background of the higher energy side of the peak. The number of electrons that lost energy was expected to be related to the depth of emission as there were more opportunities for inelastic collisions to occur. The concentration would also be a factor in the number of electrons in this region, which is why the peak area is also taken into account.

It was calculated for an uniform ideal sample the area of the element peak, A_p, divided by the rise in background, B, 30 eV above the peak would be 23.7 eV.[170,171] Experiments[172] with deposited transition metal films showed that it this value worked in practice and was in good agreement over a wide range of materials. This result led to the general outline that values of 20-30 eV denoted a uniform distribution, values above 30 eV denoted a surface layer, and values below 20 eV denoted a buried layer. This method has been used to measure SiO_x/Si film thickness,[173] organic molecule distribution in cellulosic fibres,[174] and titanium oxide adhesion to pyroles overlayers on titanium substrates.[175] However, a note of caution should be emphasized because a film sandwiched at the right depth will also produce a value that indicates a uniform distribution. The depth of a layer that would have this result would be dependent on the attenuation length of the element. Other methods[176] are available to differentiate these two possibilities, but are beyond the scope of this review as there were no samples where this layering would be observed. This method can be used non-destructively to obtain a

profile of the depth of atoms from information contained within an XPS spectra. Other XPS data analysis methods have been developed for the non-destructive profiling, including methods to generate 3D images.[177]

Infrared Spectroscopy

Infrared (IR) spectroscopy is a widely applied technique that can provide information on functional groups and geometry. Normally IR spectroscopy is used to study bulk properties of a sample; however certain instrumental attachments have been developed to confine the area of interrogation to a surface region. These various attachments are based on a change of refractive index between the sample and another medium. IR spectroscopy can be used to identify functional groups present in the assembled monolayers. Due to the absorption of bulk silicon below 1400 cm^{-1}, direct evidence of the formation of Si-C bonds, which would be expected to show absorptions around 780 cm^{-1}, cannot be observed.

One important piece of information obtainable through IR spectroscopy is the density of packing of the assembled monolayer. The asymmetric methylene stretch of disordered aliphatic liquids typically are near 2925 cm^{-1}, while for crystalline materials it is as low as 2915 cm^{-1}. The shift to higher frequency is associated with an increase in the number of gauche defects in the alkyl chains. Highly ordered films tend to adopt an all trans geometry of the methylenes.[178] Well-ordered monolayers on gold have a value of 2918 cm^{-1} for this peak. IR peaks can be used to determine a measure of order in a monolayer.

Attenuated Total Reflectance

Attenuated total reflectance (ATR) uses the difference of refractive (RF) index between a crystalline material and the overlayer to obtain a spectrum. Silicon has an RF of 2.5 while the RF of air is defined as 1.0; therefore when light is passed through silicon at angles greater than the critical angle, an evanescent wave is formed that continues

outside of the silicon before being refracted in the air to pass back into the silicon. Multiple refractions can be achieved in a crystal and the refraction occurs in the thickness of a surface monolayer. Also, multiple refractions increase the sensitivity of this measurement of the surface. Special crystals designed for ATR must be used, on which a monolayer is directly assembled.

GATR

GATR is a special type of ATR marketed by Harrick. The GATR contains a germanium crystal (refractive index 4.0) that can be brought in to intimate contact with a substrate. Mirrors set up an incident angle of 65^{o} to produce an evanescent wave at the surface of the germanium crystal. The GATR works differently depending on the nature of the substrate. Silicon is a reflective substance and an enhancement of signal is achieved by sandwiching a layer between the germanium and silicon.[179]

For a polymer sample, the depth of penetration is governed by the refractive index of the polymer. The depth of penetration of most polymers is 150-200 nm depending on the wavelength of radiation.[180] When examining a surface it is possible that the spectrum will be dominated by the bulk if the concentration of surface features is low.

Grazing Angle IR Spectroscopy

In a grazing angle IR attachment light is diverted through a series of mirrors to focus at an angle on a surface. This technique can only be used on reflective surfaces such as metals or silicon and would not be suitable for a polymer sample. By using a high incident angle a long footprint on the sample can be achieved.

Contact Angle Measurements

Contact angles can be used to examine certain characteristics of a surface. This technique relies on the affinity of a surface for a liquid such as water. A water drop placed on a hydrophilic surface will spread while a drop of water on a hydrophobic

surface will bead up. Contact angle goniometry is best used to compare two surfaces to see any differences. The largest difference in angles can be seen between a polar or charged surface and a nonpolar surface. Well-ordered monolayers of alkanes have contact angles of water of 114^{o} on gold[181] and 110-113^{o} on silicon.[117,141,142] Here well-ordered alkyl chains are aligned and terminate with CH_3 groups rather than CH_2, which is known to possess lower contact angles. For instance, non-crystalline polyethylene gives a contact angle of 102^{o} [182] and has its CH_2 groups on the surface.

Contact angle measurements are one method to determine if a chemical transition of the terminal area of the monolayer has been affected. The change of a hydrophobic surface to a hydrophilic surface by the addition of a surface alkyl chain is easily observed with an increasing contact angle. Reaction conditions that cause oxidative damage to a monolayer can also be observed by a reduction in contact angle.

Contact angle goniometry is an easy, fast and nondestructive technique allowing samples to be analyzed by other techniques after initial evaluation by this method. This is a useful technique for characterizing surfaces before being analyzed by another costly or destructive technique to ensure that the monolayer has assembled as expected.

Scanning Electron Microscopy

Scanning electron microscopy (SEM) has been used to image many types of surfaces. SEM imaging requires conducting samples, so in most applications the surface is covered with a metallic layer which is most commonly a mixture of gold and palladium. For a surface patterned with a monolayer this coating would obscure the surface chemistry but would allow imaging of variation in surface relief. Silicon is sufficiently conductive to eliminate any charging of the surface so no coating is needed for imaging.

Electron microscopy utilizes a beam of electrons focused on the surface. Electrons that leave the surface are captured by the detectors. There are two types' of

electrons that are detected. Backscattered electrons are electrons that are generated by the electron gun, collide with the surface, and are deflected back towards the detector. Secondary elections are generated when incoming electrons collide with an atom and cause electrons from the orbitals to be removed, the ejected electrons are the secondary electrons. Secondary electrons are lower in energy than backscattered electrons. Substrates for monolayers are typically composed of heavier elements, such as gold or silicon that yield high secondary electron count. Most secondary electrons are generated in the substrate. It has been shown[183-186] that thicker overlayers cause increased scattering, resulting in a reduction in electron count. Therefore, thick monolayers will appear as darker regions relative to a thin monolayer covering.

Heavier elements generate many secondary electrons that can be used to help differentiate patterned areas. This concept was used to visualize patterns on PPCPD in which a carbon substrate was decorated with a nitrogen containing polymer. By reacting with a heavy element, copper, it was possible to differentiate the patterned areas because copper bound to the amines.

Polymers are susceptible to melting when exposed to the energy of an electron beam. To image monolayers on PDCPD it was necessary to use an SEM with variable pressure settings. At higher pressure the melting point is suppressed; however a reduction in the image quality is observed because electrons can collide with gas molecules in the chamber.

SEM is the primary technique to image surface patterns. Although other techniques can be employed, the resolution and ease of use of SEM made it a good choice for imaging.

Patterning with Soft Lithography

Soft lithography refers to a family of techniques that use an elastomer. Polyurethanes, epoxides, and polyimides have been used as liquid prepolymers and are

commercially available, but the most common material used in soft lithography is polydimethylsiloxane (PDMS). To produce a pattern it is first necessary to produce a master out of a hard material. Available methods to fabricate the master include photolithography, electron beam lithography, focused ion beam, and polymer masks.[187-190]

Once a master has been produced, a negative in bas-relief is made by casting a mixture of PDMS with crosslinking agent against it and allowing it to harden. Sylgard 184 is a commercial two part PDMS kit that is widely used for many types of soft lithography. The master can be used repeatedly to make many replicas, depending on the durability of the master used. There are size limitations of the features that can be produced, but patterns from nm to mm are routinely obtained. Harder formulations of PDMS are available that can make features of 100 nm when backed with a softer PDMS.[191,192] PDMS is a useful material because it is optically transparent to ~300 nm, thermally stable to 150 ^{o}C, inert to many of the chemicals used to form monolayers, and has desirable physical properties.[193] Its low surface energy allows easy release from templates and surfaces.[194] It contains no solvent to evaporate, and it has a low thermal expansion coeffecient.[195] A number of soft lithographic techniques have been developed for the patterning of materials inside channels of PDMS that do not relate to functionalization of a surface.[196]

Micro Contact Printing (μCP)

μCP is a technique that uses a patterned stamp made of PDMS. A solution of a molecule is allowed to permeate the PDMS. The solvent is allowed to evaporate and the molecule can then be transferred to a surface like an ink. The molecule was only found on the surface in the area that was in contact with the stamp. μCP has been used to pattern molecules (such as thiols on gold) with dimensions down to 50 nm.[197] The limits of μCP include the lateral diffusion of molecules through PDMS,[198] incomplete

coverage,[199] and the poorly defined edges. Microcontact printing has been used to pattern on a wide variety of surfaces and molecules and for various applications.[78,79,81-84,200-216]

Patterning with Microfluidic Devices

Microfluidic devices can be fabricated from PDMS patterned in bas relief. PDMS pieces have been joined together to fabricate microfluidic devices[217-220] for purposes such as biological assays[221-223] and surface bound catalyzed reactions.[224] Alternatively a pattered PDMS slab can be brought into contact with a surface to form microfluidic channels. The surface with open channel can then be selectively reacted by passing reagents through the an open channel. For simple one step reactions, an open ended PDMS microfluidic device can be filled by capillary action with a solution placed in contact with the end of the channel. Removal of the reactant is achieved by solvent washing.

By attaching tubing and utilizing a syringe pump, it is possible to controllably pass several reagents across a surface to complete many steps. When completing reactions it is important that all solvents or reagents are compatible with PDMS. Whitesides et al,[225] studied how solvents and common reagents swell and react with PDMS. They measured how solvents swell PDMS by finding the change in length of a slab of PDMS before and after immersion in a solvent for 24 hours. This data can be used to find suitable solvents for various applications. Only very polar solvents, such as water, DMF, and nitromethane were found to be compatible with PDMS devices attached to a silicon surface or silicon monolayer. Other solvents cause PDMS to swell and lead to detachment from the surface. Also, various solvent and reagents were found to cause the decomposition of PDMS.

Summary of Research

For monolayers to be used in many applications it will be necessary to functionalize them after the initial monolayer is attached. In Chapter 1 it was shown that a carboxylic acid terminated monolayer could be functionalized with an amine to form an amide. The carboxylic acid was first activated with an anhydride in an intermediate step. This process that has a precedent with SAMs on gold.[66,67] It is possible to pattern this type of surface with the use of a PDMS microfluidic device.

Along with the ability to produce a well ordered monolayer it is necessary to pattern them on the nm to micrometer size range. In Chapter 2 a new technique is reported that we developed to exploit the ability to etch PDMS with fluoride. The etching was found to be dependent on the identity of the fluoride species and time. When combined with previously synthesized and functionalized monolayers (see Appendix A), nanoscale patterns were obtained by the growth of a polymer brush of norbornene derivatives by ROMP

Briefly, a monolayer terminated with olefins was assembled on silicon. The Grubbs catalyst was attached to this surface and then a PDMS slab was placed on it to generate microfluidic channels. An olefin was passed through the channel to remove the catalyst within the channel. PDMS was then etched to expose nm to µm sized areas containing the Grubbs catalyst. A polymer was grown from these newly exposed areas.

In Chapter 3 PDCPD was functionalized by exploiting the functional group in the polymer. Bromine reacted with the double bonds, and in a subsequent step, a displacement reaction of the bromine was used to functionalize the surface with an amine. These surfaces were characterized to calculate surface coverage and to demonstrate the functionalization. Another method was developed using epoxides formed from the reaction of 3-chloroperoxybenzoic acid (*m*CPBA) with PDCPD. These were also reacted with amines, and in a subsequent step, further reacted with an anhydride to form a new functionalized surface. In an alternative procedure, the

epoxidized surface was reacted with polyethyleneimine (PEI). The PEI layer was then allowed to grow thicker by using a diepoxide and PEI. The surface was identical when compared to cross linked PEI by IR spectroscopy using the GATR attachment which has a depth of analysis of approximately 200 nm.

CHAPTER 1 SIMPLE METHODS FOR THE DIRECT ASSEMBLY, FUNCTIONALIZATION, AND PATTERNING OF ACID-TERMINATED MONOLAYERS ON SI (111)

Abstract

This paper describes mild methods to directly assemble, functionalize, and pattern monolayers of undecylenic acid on hydrogen-terminated Si (111). These monolayers were assembled under very mild conditions from a neat solution of undecylenic acid containing 0.1 mole percent of 4-(decanoate)-2,2,6,6-tetramethylpiperidinoxy at room temperature without the need for UV light. Because of these mild conditions, monolayers exposing carboxylic acids could be assembled in one step without the need to protect the acid prior to its assembly. The monolayers were extensively characterized by horizontal attenuated total reflection infrared spectroscopy, X-ray photoelectron spectroscopy (XPS), and contact angle goniometry. The monolayers bonded to the silicon surface preferentially through the olefin with no detectable bonds between the carboxylic acids and silicon. The cystallinity of the monolayer was studied by infrared spectroscopy through the antisymmetric – $\nu_a(CH_2)$ – and symmetric – $\nu_s(CH_2)$ – stretches for methylene. Because it is important for future applications to assemble functional surfaces, methods to react the acid-terminated monolayers with trifluoroacetic anhydride and triethylamine to yield a symmetric anhydride on the monolayer were studied. These anhydrides were reacted with a variety of milligram quantities of amines to yield amide-terminated surfaces. This method was general and a variety of amines could be bonded to the monolayer. The stabilities of these monolayers upon exposure to ambient conditions and under a variety of solvents were described. As patterned monolayers have found wide applications, we developed methods to pattern 1-octadecylamine and poly(ethylenimine) on the micrometer-size scale using soft lithography. In addition, polymer brushes of polynorbornene with thicknesses from 32 to 150 nm were grown

from monolayers patterned with the Grubbs' catalyst. The patterned surfaces were imaged by scanning electron microscopy, scanning probe microscopy, and ellipsometry to determine the thicknesses of the patterns and the fidelity of the method.

Introduction

Self-assembled monolayers (SAMs) on silicon is an area of intense study due to their applications in the development of new biomolecular and molecular electronic devices.[226-256] SAMs are directly assembled onto silicon without an intervening layer of silicon dioxide such that the electrical properties of silicon can be addressed through the SAMs. These surfaces are exciting as the display of important functional groups – such as single stranded DNA, carbohydrates, or proteins – can be detected using electrochemistry.[234,242,251,253,256-260] Recently, new biosensors based on SAMs on silicon and fundamental studies of electron tunneling through SAMs on silicon have been reported.[233,240-242,245,246,250,251,253,256-262]

Interest in this area is driven by opportunities to combine the selectivity of organic chemistry to display well-defined functional groups on SAMs with the terrific electronic properties of silicon. Silicon is the most important electronic material in the electronics industry; yet, its applications in biotechnology and nanotechnology are lacking due to limited methods to assemble, functionalize, and pattern SAMs directly on silicon. Mild methods to assemble and pattern functional SAMs on silicon are needed to advance these fields such that a wide variety of small molecules and nanomaterials can be both readily displayed and patterned on a silicon wafer.

New methods to assemble SAMs on hydrogen-terminated Si(111) from olefins, aldehydes, alcohols, or Grignard reagents were recently reported.[226-230,235,236,243,248,249,257-259,261,263-277] Methods to assemble monolayers on Si(111) use heat, acyl peroxides, UV light, chlorination of the surface followed by reaction with Grignard reagents or alcohols, iodination of the surface followed by exposure to olefins and light, or scribing. Many of

these methods are harsh and limit the range of functional groups that can be assembled on the surface. Mild methods to assemble well-ordered SAMs on silicon are still needed.[230,235,236]

The results reported in this paper build on our previous work to assemble well-ordered monolayers on hydrogen-terminated Si(111) from olefins and 2,2,6,6-tetramethyl-1-piperidinyloxy (TEMPO, Scheme 5).[230] Previously, we discovered that 1-octadecene in the presence of trace amounts of TEMPO formed crystalline monolayers when assembled at room temperature without the need for UV light. This very mild method for assembly prompted us to question whether SAMs terminated interesting functional groups such as carboxylic acids could be assembled directly onto silicon.

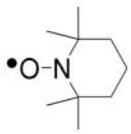

Figure 9 The structure of TEMPO is shown.

Previous work to assemble SAMs on Si(111) that display reactive functional groups on the surface yielded promising results. SAMs terminated with alcohols, esters, olefins, and ethers have been assembled, but more reactive groups such as carboxylic acids are challenging as they can oxidize hydrogen-terminated Si(111) prior to the assembly of the monolayer.[226-228,230,235,236,243,248,249,263-274,278] Only one paper reports the direct assembly of an acid-terminated SAM onto Si(111) using UV light, but the SAM was not fully characterized.[249,260,279] Acid-terminated monolayers are important as they are readily activated and reacted with amines or alcohols to yield amides or esters. Interest in assembling acid-terminated surfaces is shown by the numerous examples of

these SAMs on other surfaces being activated to yield more functional surfaces.[243,246,248,249,257-261,270,279,280]

In this paper we report extremely mild methods to assemble, functionalize, and pattern SAMs terminated with carboxylic acids onto Si(111). Our methods do not require heat or exposure to UV light, thus enabling the assembly of a wide variety of monolayers. SAMs are assembled in the presence of undecylenic acid and a derivative of TEMPO. These SAMs are further functionalized by activation with trifluoroacetic anhydride and reaction with a variety of amines to expose amide-terminated SAMs. We will demonstrate that these SAMs are stable in apolar solvents and can be patterned on the micrometer-size scale using microfluidic channels formed through soft lithography.

Experimental Section

Materials and Methods.

Distilled water, 1-octadecene (90%), hexane, 10-undecenoic acid, trifluoroacetic anhydride, polyethylenimine (water-free), 1-dodecylamine (98%), 1-butylamine (99.5%), 1-octylamine (99+%), 1-hexadecylamine (90%), 1-octadecylamine (90%), and 48% hydrofluoric acid were purchased from Acros or Aldrich and used as received. 40% NH_4F was purchased from J.T. Baker and used as received. All solvents were purchased from Acros and used as received. Single-side polished Si(111) wafers (n-type) were purchased from Silicon Inc, Boise, Idaho.

The synthesis of TEMPO-C_{10} was described in a previous paper and stored in a glove box freezer under N_2 at 30 ºC.[230] 10-undecenoic acid (Bp 275°, Bp_{15} 165°) was distilled with a Vigreux column under reduced pressure. Typically 500 mL were distilled at one time. The first 100 mL of distilled 10-undecenoic acid was discarded. We collected the next 300 mL and transferred it to a Kontes flask. The Kontes flask was evacuated under reduced pressure for 48 hours and back filled with N_2, this process was

repeated three times. The Kontes flask was stored in the glove box. The same process was followed for the purification of 1-octadecene.

Assembly of Monolayers of Undecylenic Acid.

Shards of Si(111) wafers were washed with hexanes, acetone, and methanol and then sonicated in acetone for 5 min. The shards were rinsed with water and treated with 5:1 (v/v) 40% $NH_4F_{(aq)}$/48% $HF_{(aq)}$ for 30 sec to remove the native silicon dioxide layer. The samples were then placed in 3:1 (v/v) of concentrated H_2SO_4/30% $H_2O_{2(aq)}$ (Piranha solution) for 1 h at 90 °C to clean the surfaces and oxidize the surface of the silicon shards. *Warning: Piranha solution is exceedingly dangerous and should be kept from organic materials and treated with care.* The wafers were removed from the Piranha solution and washed with copious amounts of water. The wafers were hydrophilic after this treatment.

To form hydrogen-terminated Si(111), 40% NH_4F was placed in a cup within a larger cup covered with a cap. Argon was purged through the NH_4F for 30 min to remove O_2 before the Si(111) shards were immersed. The larger cup was continuously purged with Ar while the Si(111) shards were immersed in NH_4F for 20 min. The shards were removed and the NH_4F spontaneously dewetted from the surface. The shards were dried under a stream of N_2.

The shards were immediately taken into the glove box as is and immersed into a neat solution of undecylenic acid with 0.1 mole % TEMPO-C_{10}. Transferring the silicon shards into a glove box immediately after forming the hydrogen-terminated surface is important as the surface rapidly oxidizes to silicon dioxide under ambient conditions. The monolayers were assembled at room temperature in a sealed Schlenk flask under N_2 for 24 h. After 24 h the shards were removed and washed with copious amounts of hexane, acetone, and methanol. Finally, the shards were sonicated twice for 3 min in CH_2Cl_2. New CH_2Cl_2 was used for each sonication.

Activation of Carboxylic Acids with Trifluoroacetic Anhydride and Reaction with Amines.

SAMs terminated with carboxylic acids were immersed in 0.1 M acetic anhydride and 0.2 M triethylamine in DMF. After 15 min the wafers were removed and immediately immersed in a 0.01 M solution of an amine in methylene chloride or THF for 30 min. The wafers were removed and rinsed with acetone, methanol, and water.

X-ray Photoelectron Spectroscopy (XPS).

The samples were studied by XPS at the University of Illinois at the Center for Microanalysis of Materials (CMM) with the help of Rick Haasch. The instrument was a Kratos axis ultra X-Ray photoelectron spectrometer. The dimension of the image area was 300 by 700 μm and the take-off angle was 45°. The pass energy on the survey scan (0 to 1100 eV) was 160 eV. High resolution scans of Si(2p) (92 to 108 eV binding energy), C(1s) (274 to 300 eV binding energy), O(1s) (523 to 539 eV binding energy), and F(1s) (680 to 696 eV binding energy) were performed. The atomic compositions were corrected for the atomic sensitivities and measured from the high-resolution scans. The atomic sensitivities were 1.000 for F(1s), 0.780 for O(1s), 0.278 for C(1s), and 0.328 for Si(2p).

Contact Angle Goniometry.

Contact angles were measured on a Ramé-Hart model 100 goniometer at room temperature and ambient humidity. An Eppendorf EDOS 5222 was used to dispense distilled water. Small drops of water (5 μL) were dispensed and the contact angles were measured immediately. A minimum of 15 measurements at two different spots on the surface were collected for each sample. The error in the measurements of advancing contact angles was typically small; for contact angles of greater than 100° most of the measurements came within ±1° of the reported value. Contact angles less than 100° had errors of ±2°.

Infrared Spectroscopy.

All measurements were made with a Bruker Tensor 27 spectrometer with a liquid nitrogen cooled mercury cadmium telluride (MCT) detector. Monolayers were assembled on silicon ATR crystals with dimensions of 80X10X5 mm. The crystals were fabricated such that the Si(111) face was exposed along the long face. The spectrometer and sample chamber were continuously purged with water and carbon dioxide depleted air.

The backgrounds for the samples were freshly prepared silicon dioxide surfaces on the ATR crystals. The ATR crystals were first cleaned with organic solvents and then immersed in Piranha solution for 60 min to remove residual organics on the surface. These ATR crystals were immediately used to measure the background scans. Spectra of SAMs were collected at a resolution of 4 cm^{-1} and spectra for hydrogen-terminated Si(111) were collected at a resolution of 2 cm^{-1}.

Scanning Probe Microscopy.

We used the MFP-3D scanning probe microscope from Asylum Research. The instrument was operated in AC-mode with a frequency of 55.58 kHz and the spring constant of the tips were 1 N m^{-1}.

Results and Discussion

Assembly of SAMs from Undecylenic Acid.

The monolayers were assembled using 0.1 mole percent of a derivative of TEMPO in neat undecylenic acid as described in detail in the experimental section (Figure 10). This method is based on our previous results for the assembly of well-ordered monolayers of 1-octadecene in the presence of TEMPO or derivatives of TEMPO.[230] SAMs of 1-octadecene were characterized by contact angle goniometry, ellipsometry, and XPS. These measurements showed that our method of assembly

resulted in crystalline monolayers of 1-octadecene with a small concentration of TEMPO on the surface. Although the role of TEMPO in the assembly of monolayers was not determined, its presence was necessary for the assembly of well-ordered SAMs. This paper extends our prior work to describe the assembly, functionalization, and patterning of monolayers terminated with carboxylic acids.

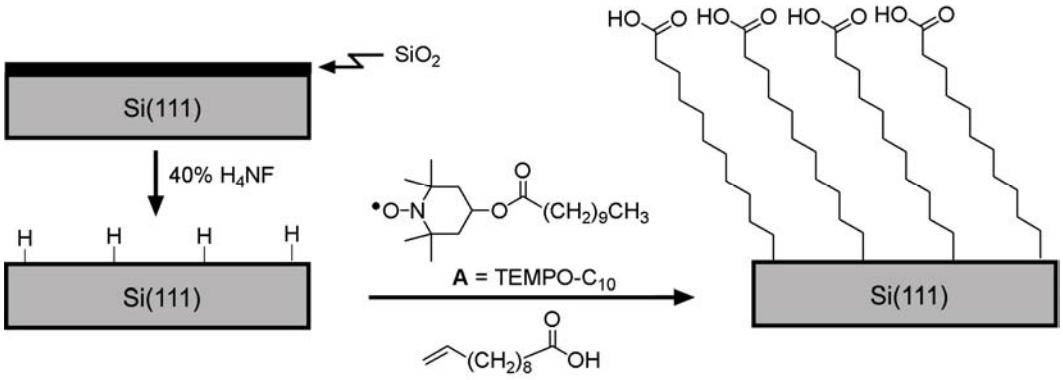

Figure 10 Our method to assemble monolayers of undecylenic acid. Silicon wafers with a native silicon dioxide layer were immersed in 40% NH_4F for 20 min under an argon purge. The silicon dioxide was etched to yield hydrogen-terminated Si(111). The wafer was immersed in a solution of undecylenic acid with 0.1 mole percent TEMPO-C_{10} (**A**) for 24 h.

To unambiguously characterize a SAM, multiple methods must be used. Here, we characterized SAMs of undecylenic acid by X-ray photoelectron spectroscopy (XPS) and horizontal attenuated total reflection infrared (HATR-IR) spectroscopy. XPS was chosen as it describes the chemical composition of the surface and can detect the presence of oxidized silicon. HATR-IR spectroscopy was chosen as C-H and C=O regions describe the degree of crystallinity of SAMs and the presence of acids and amides.

The XPS spectrum of a monolayer of undecylenic acid is shown in Figure 11. In Figure 11a we show a survey scan of the surface that clearly describes the presence of only O, Si, and C. High resolution scans of the surface were done to further quantify the surface composition as 21% O, 36% Si, 0% F, and 42% C. The high resolution scan of fluorine confirmed that Si-F and C-F bonds were not present. The high resolution scan for carbon shows a peak for the methylene carbons at 283 eV and the carbonyl carbon at 288 eV. This result is expected as the carbonyl peak is seen at higher binding energies on acid-terminated SAMs.[259]

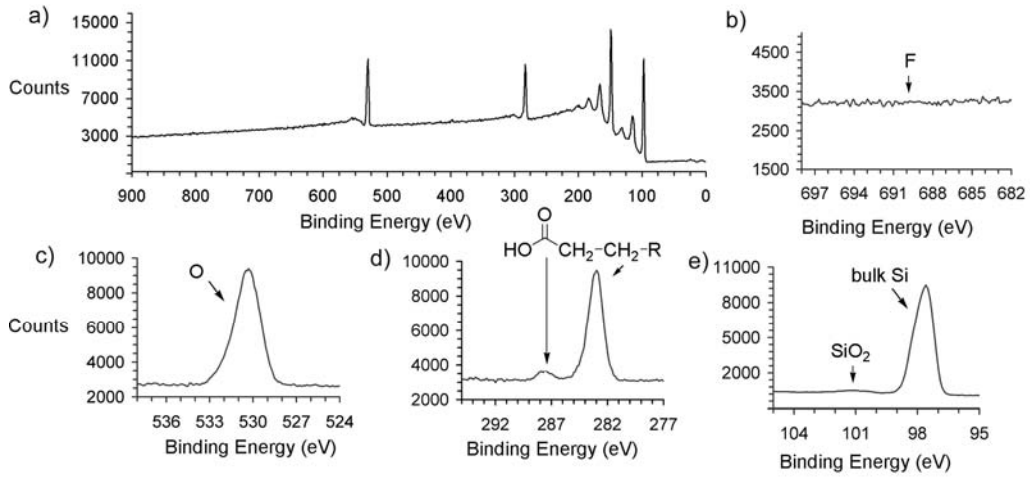

Figure 11 XPS spectra of our monolayers. In a) a XPS survey scan of a SAM of undecylenic acid is shown. The high resolution scans for b) fluorine, c) oxygen, d) carbon, and e) silicon are shown. We assign peaks for carbon and silicon based on literature references.

The high resolution scans of Si and O reveal important information about the surface. The XPS spectrum of Si shows one peak for bulk Si and only trace amounts of SiO_x at 102 eV. This result proves that the silicon surface underwent minimal oxidation during the assembly of the monolayer. The amount of SiO_x was much less than 1% of the surface composition for many different samples.

The peak for oxygen in the XPS spectrum is broadly centered at approximately 531 eV. Possible sources of oxygen include carboxylic acids from undecylenic acid, TEMPO-C_{10} (**A** in Figure 10), and SiO_x on the surface. In our previous work on the assembly of SAMs from 1-octadecene and derivatives of TEMPO, we know that trace amounts of TEMPO-C_{10} assemble onto silicon and account for some of the oxygen observed by XPS.[230] The lack of a peak in the silicon region for SiO_x indicates that little of the observed oxygen is due to oxidized silicon. Thus, we attribute the observed oxygen peak to the presence of TEMPO-C_{10} on the surface and the terminal carboxylic acids on the end of the SAMs. Due to the multiple sources for oxygen, we can not make further assignments to this peak.

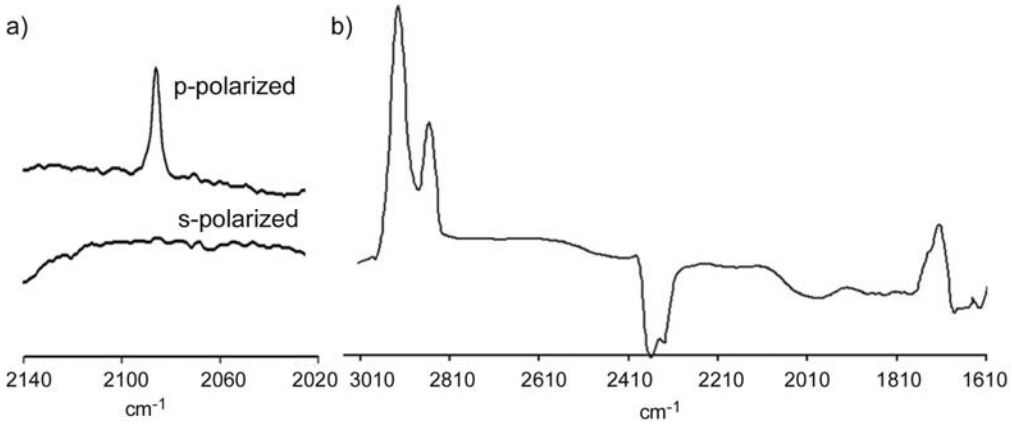

Figure 12 Infrared spectra (a) The HATR spectra of the Si(111)-H peak with *p*- and *s*-polarized light. (b) The HATR spectrum of a SAM of undecylenic acid.

The HATR-IR spectra of hydrogen-terminated Si(111) and a SAM of undecylenic acid are shown in Figure 12. The assembly of our monolayer begins with the formation of a surface of hydrogen-terminated Si(111). Higashi et al. reported that etching the native oxide layer from a Si(111) wafer in argon-purged 40% NH_4F results in a

hydrogen-terminated Si(111) surface with a defect density of 0.5%.[281] The Si(111)-H bonds are perpendicular to the exposed plane of the silicon wafer; thus, these bonds are IR-active only with *p*-polarized light. The literature reference for the shift of the Si(111)-H peak is 2083.7 cm^{-1} with a FWHM of 0.95 cm^{-1}.[281] Dihydrogen and trihydrogen defects appear as peaks at 2111, 2120, and 2139 cm^{-1} under both *s*- and *p*-polarized light.[282,283]

In the HATR-IR spectra of Si(111)-H surfaces with *s*- and *p*-polarized light (Figure 12a) we see only one peak at 2084 cm^{-1} with a FWHM of 3.8 cm^{-1} with *p*-polarized light. The HATR-IR spectrum of Si(111)-H with *s*-polarized light showed an absence of peaks. These results demonstrate that we formed well-ordered Si(111)-H surfaces.

The HATR-IR spectrum of undecylenic acid SAMs shows three important peaks. The peaks corresponding to the antisymmetric – $\nu_a(CH_2)$ – and symmetric – $\nu_s(CH_2)$ – stretches for methylene appear at 2923 and 2853 cm^{-1} (Table 1). These results are significant as the $\nu_a(CH_2)$ peak for crystalline SAMs ranges from 2918 to 2920 cm^{-1} but for disordered SAMs it ranges from 2925 to 2928 cm^{-1}.[226,284,285] Similarly, the $\nu_s(CH_2)$ peak for crystalline SAMs appears at 2850 cm^{-1} but for disordered SAMs it appears at 2858 cm^{-1}.[226,284,285] The location of $\nu_a(CH_2)$ and $\nu_s(CH_2)$ peaks within these ranges describes the crystallinity of SAMs. Our results show that we assembled monolayers with some degree of order but the monolayers were not quite crystalline. This result was not unexpected as Chidsey *et al.* reported that SAMs of 11-mercaptoundecanioc acid on Au had values of 2925 cm^{-1} for $\nu_a(CH_2)$ and 2853 cm^{-1} for $\nu_s(CH_2)$, but that SAMs of 1-decanethiol had values of 2920.5 cm^{-1} for $\nu_a(CH_2)$ and 2850.5 cm^{-1} for $\nu_s(CH_2)$.[286] Based on these data, the presence of carboxylic acids on the thiols prevented 11-mercaptoundecanoic acid from assembling into crystalline monolayers.

Silicon hydrides on Si(111) are 3.84 Å from each other and the diameter of an alkyl chain is approximately 4.2 Å.[227] Thus, simple geometric arguments about the

spacing of hydrides on silicon and the cross-sectional area of an alkane chain in a monolayer yield the result that approximately half of the silicon hydrides react when a monolayer is assembled.[227,228,267,287] Despite the expected presence of Si(111)-H peaks in the HATR-IR spectra of alkyl SAMs, this peak has not been observed by us or others.

Mode of Bonding of Undecylenic Acid.

Undecylenic acid can bond to hydrogen-terminated Si(111) through the acid or olefin. In our previous work, we demonstrated that 1-octadecene assembled into SAMs on Si(111)-H through its olefin. Thus, 1-alkenes terminated with methyl groups assemble into ordered monolayers through their olefins, but the carboxylic acid of undecylenic acid provides another mode of bonding to Si(111)-H. We wished to study which functional group – the olefin or acid – bonded to the surface.

Table 1 Select peaks from the HATR-IR spectra of monolayers of thiols on gold (entries one and two) and olefins on silicon (entries three through five).

Entry	Monolayer	$\nu_a(CH_2)$ (cm^{-1})	$\nu_s(CH_2)$ (cm^{-1})	C=O (cm^{-1})
1	Au-$(CH_2)_9$-CH_3	2920.5[a]	2850.5[a]	
2	Au-$(CH_2)_{10}$-CO_2H	2925[a]	2853[a]	1744[b], 1720[b]
3	Si-$(CH_2)_{10}$-CO_2H	2923	2853	1710
4	Si-$(CH_2)_{10}$-C(O)OC(O)-$(CH_2)_{10}$-Si	2927	2856	1742, 1633
5	Si-$(CH_2)_{10}$-CONH-$(CH_2)_x$-CH_3 Si-$(CH_2)_{10}$-CO_2H	2925	2856	1722, 1593

[a]From reference 31b.
[b]From reference 34. These peaks were measured on SAMs of 16-mercaptohexdecanoic acid.

The advancing contact angle of water was 65° for SAMs of undecylenic acid. This value is consistent with a monolayer terminated with acids rather than olefins as they would be expected to exhibit a contact angle close to 100°. Our value for an advancing contact angle of water does not eliminate the possibility that a significant fraction of the undecylenic acid is bonded to the silicon surface through the acid group but it provides evidence that acids are displayed on the surface.

A second piece of evidence for the assembly of monolayers through olefins rather than acids is outlined in Figure 13. We studied the assembly of monolayers from 1 mole percent of TEMPO-C_{10}, 2.37 g (3.0 mL, 9.4 mmole) of 1-octadecene, and 1.00 g (3.3 mmole) of **B** in 3 mL of diglyme. The diglyme was needed to dissolve the reagents as **B** had poor solubility in 1-octadecene. **B** was added to the assembly to provide a unique handle in the XPS to determine whether acids bond to the surface. We synthesized **B** as it has a pKa and nucleophilicity similar to that of undecylenic acid, but it can only bond to the surface through its acid. Thus, if acids bond to Si(111)-H, we will see fluorine in the XPS spectrum. If carboxylic acids do not bond to Si(111)-H we will not see a peak due to fluorine in the XPS spectrum.

The advancing and receding contact angles of water on these SAMs were 111º and 107º, respectively. These values were the same as we observed for SAMs assembled from 1-octadecene and TEMPO-C_{10} in the absence of **B**. The compositions of these surfaces measured by XPS were 66% C, 10% O, 24% Si, and 0% F. In Figure 13b we show the high resolution scans of the fluorine and silicon regions to show the lack of fluorine and SiO_x on these surfaces.

The absence of F and SiO_x in the XPS combined with the contact angles of water demonstrate that olefins selectively bonded to Si(111)-H in the presence of acids. The bonding of acids to a Si(111)-H surface was not detectable when an olefin was present in solution. Thus, SAMs assembled from undecylenic acid bond to the surface through olefins and exposed acids on the surface of the SAMs.

Functionalization of Acids on the Surface with Amines.

We wished to develop a mild method to functionalize carboxylic acid-terminated monolayers on silicon. Our method to assemble SAMs uses approximately 5 g of olefin to functionalize a shard of silicon. This method would be prohibitively expensive for some olefins terminated with other functional groups. Here, we report a method to functionalize SAMs that uses commercially available undecylenic acid and milligram quantities of amines.

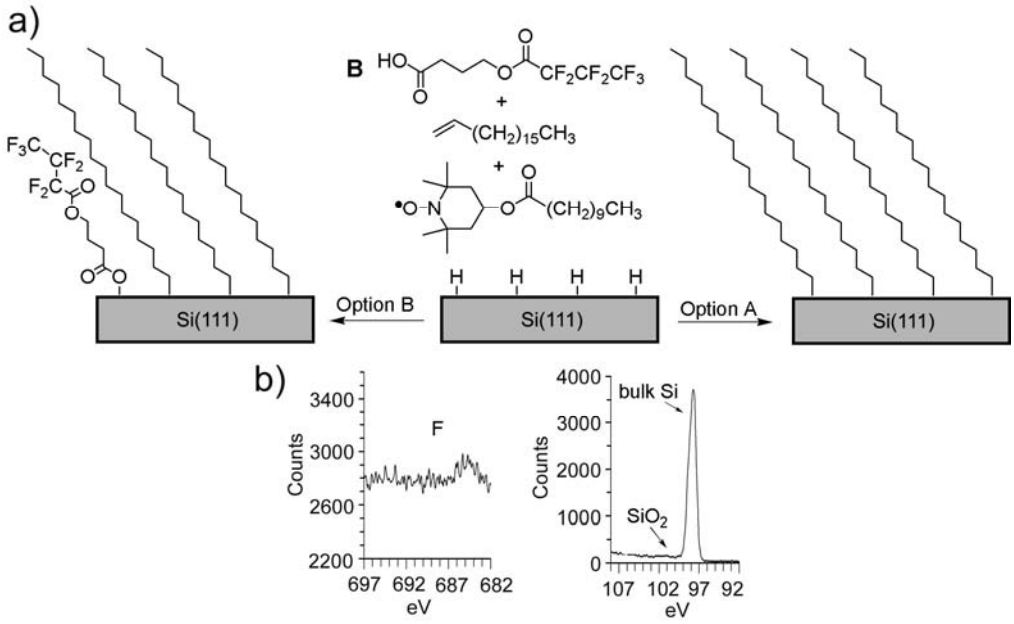

Figure 13 Assembly of monolayers a) We assembled monolayers from **B**, 1-octadecene, and TEMPO-C_{10} in diglyme to study whether acids bonded to the surface at rates competitive with olefins. In option A only olefins bonded to the surfaces and the monolayer is composed of 1-octadecene. In option B both the acids and olefins bond to Si(111)-H at competitive rates. b) High resolution XPS spectra of the fluorine and silicon regions for these monolayers showed no fluorine or SiO_x. These results were consistent with option A.

Our method is outlined in Figure 14 and is based on work by others to activate acids to bond amines to the surface.[260,288] We activated acid-terminated surfaces with

trifluoroacetic anhydride to yield an anhydride-terminated SAM. This SAM was then reacted with amines to assemble amide-terminated SAMs. We tried a variety of different solvents for each step, and DMF and $CHCl_3$ gave the best results.

We characterized these results by XPS and HATR-IR spectroscopy. The XPS of anhydride surfaces did not show the presence of fluorine. Activation of surface carboxylic acids could yield symmetric anhydrides as shown in Figure 14 or mixed anhydrides with the following structure: $CF_3C(O)OC(O)(CH_2)_{10}$-Si. The absence of fluorine in the XPS of anhydride monolayers suggests that the surface is composed of symmetric anhydrides. The HATR-IR spectra show the progression of acid to anhydride to amide (Table 1 and Figure 14). These spectra are consistent with previous results for these surfaces on Au and demonstrate that the SAMs were functionalized.[288]

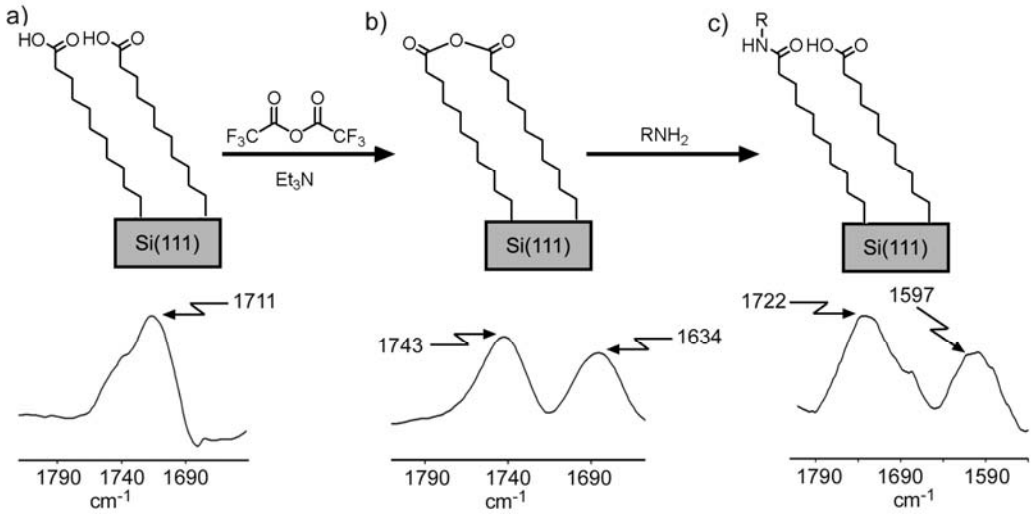

Figure 14 This Figure shows how acid-terminated SAMs were functionalized. On top of the Figure we show a schematic of SAMs at several steps in the process and beneath each is the HATR-IR spectrum of the carbonyl region. (a) The acids were activated with trifluoroacetic anhydride to yield a (b) anhydride surface. (c) This surface was reacted with amines to yield a mixed monolayer of amides and acids.

To test this method we assembled amide-terminated surfaces with alkyl amines of increasing lengths. We reacted the amide surfaces with amines of the general formula $H_2NC_nH_{2n+1}$ where n equals 4, 8, 12, 16, and 18. A plot of advancing contact angles of water on these surfaces versus the number of carbons in the amine is shown in Figure 15. Longer amines result in more hydrophobic surfaces as expected. The most hydrophobic surface was synthesized from 1-octadecylamine and yielded an advancing contact angle of water of 94°.

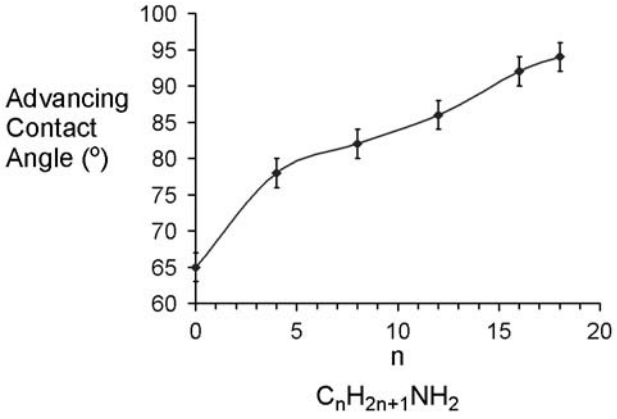

Figure 15 Advancing contact angles of water on amide-terminated SAMs as a function of the number of carbons in the amines. Anhydride surfaces were reacted with amines as in Figure 14. The line is drawn as a guide to view the data.

Stabilities of SAMs Assembled from Undecylenic Acid.

We wished to measure the stabilities of undecylenic acid monolayers functionalized with 1-octadecylamine as in Figure 14. These monolayers are representative of surfaces that we and others may wish to use in further studies; thus, knowledge of their stabilities over time is important. Their stabilities in water are particularly important for potential biological applications in DNA sensing, biosensors, or as surfaces to grow cells.

One method that we found particularly useful to study the stability of SAMs is contact angle goniometry. Contact angles can be measured quickly and provide information about which functional groups are exposed on a surface.[228,262,280,289-293] We began with a hydrophobic SAM with a large contact angle of 94° and expect that as the silicon is slowly oxidized to yield a glassy, hydrophilic layer on the surface the contact angle will decrease. Silicon wafers readily oxidize to yield a thin layer of silicon dioxide on the surface, but well-ordered alkyl monolayers greatly inhibit the rate of this oxidation.[227,228,275] Thus, by measuring the decrease of advancing contact angles as a function of time we will learn how well our SAMs protect silicon from oxidation.

Table 2. Changes in advancing contact angles of water on amide-terminated SAMs assembled with 1-octadecylamine after immersion in solvents for 12 or 72 h.

Solvent	Dielectric Constant	Duration (h)	Decrease of Contact Angle (º)
None	1.0	12	0
		72	0
Hexanes	1.9	12	3
		72	4
$CHCl_3$	4.8	12	1
		72	7
THF	7.5	12	9
		72	16
H_2O	79	12	12
		72	21

We exposed amide-terminated SAMs to air and immersed them in various solvents taken directly from the manufacturer's bottle for 12 and 72 hours. Silicon shards

exposed to air for two months exhibited no change in their contact angles; these wafers are stable in air for long periods of time. Silicon shards immersed in hexanes or chloroform had small changes in their contact angles, but those immersed in tetrahydrofuran or water were quickly degraded after 12 h.

Measurement of advancing contact angles provides a simple method to address the stability of these monolayers. As we know that water can readily oxidize a silicon surface to SiO_x, we tried to correlate our results to the dielectric constant of the solvents. Our results indicate that the monolayers are stable in solvents with low dielectric constants, but they are unstable in solvents with high dielectric constants. These results are meant as a guide for future work with these monolayers and effects such as the presence of O_2, trace water in the solvents, trace peroxides in THF, or HCl in chloroform must be examined. In future work we will analyze the stabilities of our monolayers over time using XPS and HATR.

Patterning on the Micron-Size Scale Using Soft Lithography.

We developed mild methods to assemble and functionalize monolayers of undecylenic acid, and in this section we describe a mild method to pattern these monolayers. We choose to use "soft lithography" for our patterning. Soft lithography is a series of techniques based on polydimethylsiloxane (PDMS) and developed by Whitesides *et al.* that can be used to pattern features from nanometer to micrometer sizes.[294-301]

In our method we take advantage of the microfluidic channels formed by PDMS patterned in bas-relief in contact with a silicon wafer (Figure 16). Since PDMS is soft and compliant, it makes conformal contact with a flat surface. We begin by functionalizing acid-terminated SAMs to anhydrides using trifluoroacetic anhydride. Next, we place a PDMS mold in contact with the surface to form microchannels. Then,

we use capillarity to flow a solution of an amine through the microfluidic channels. The amine only contacts anhydrides in the microfluidic channels, while anhydrides covered by PDMS were protected from reaction. After 15 min the amines were washed from the microchannels and the PDMS mold was removed.

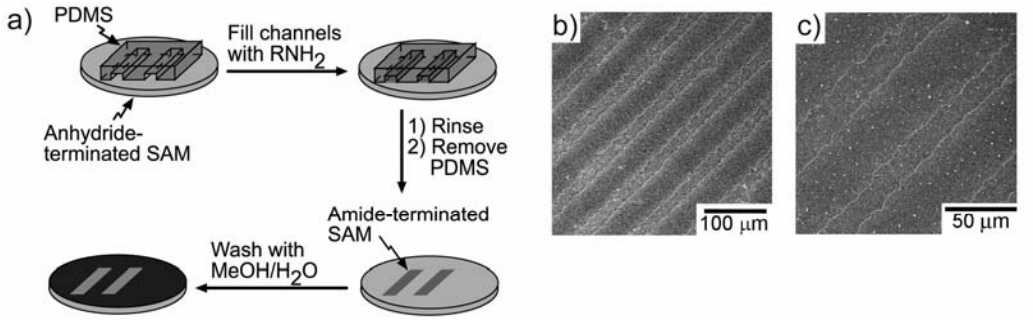

Figure 16 Patterning of an acid surface a) A PDMS slab patterned in bas-relief is placed on an anhydride-terminated SAM. The channels were filled with amines dissolved in DMF. After 15 min the channels were rinsed and the PDMS was removed to expose an amide-terminated surface. The surface was washed with methanol and then water to quench the remaining anhydrides. b) SEM micrographs of 30 μm-wide lines of amide-terminated SAMs synthesized using 1-octadecylamine. The thin, bright lines are amide-terminated SAMs and the wide, dark lines are acid/ester-terminated SAMs.

Pattern with 1-octadecylamine.

A solution of 1-octadecylamine in DMF was used to pattern a silicon wafer with micron-sized lines (Figure 16b). Roughness of the patterned SAM is due to the roughness of the sides of the PDMS microchannels. These microchannels were fabricated using rapid prototyping, which involves the use of transparency masks with an edge resolution of about 5 micrometers. This roughness transferred into the PDMS molds and the resulting patterns on Si(111).

Pattern with Polyethylenimine.

A solution of polyethylenimine (M_n = 10,000 g mol^{-1}) in DMF was used to pattern SAMs (Figure 17). We choose this polymer as it has many amines along the backbone to bond to the surface and it demonstrates that polymers can also be patterned with this technique. SEM images of patterned SAMs showed bright lines for the polyethylenimine-patterned regions separated by dark lines of unpatterned SAMs.

To further characterize the patterns we used scanning probe microscopy (Figure 17c, d). The SPM micrograph of the surface showed that the polymer was approximately 1.0 nm thick and uniformly coated along the patterned region.

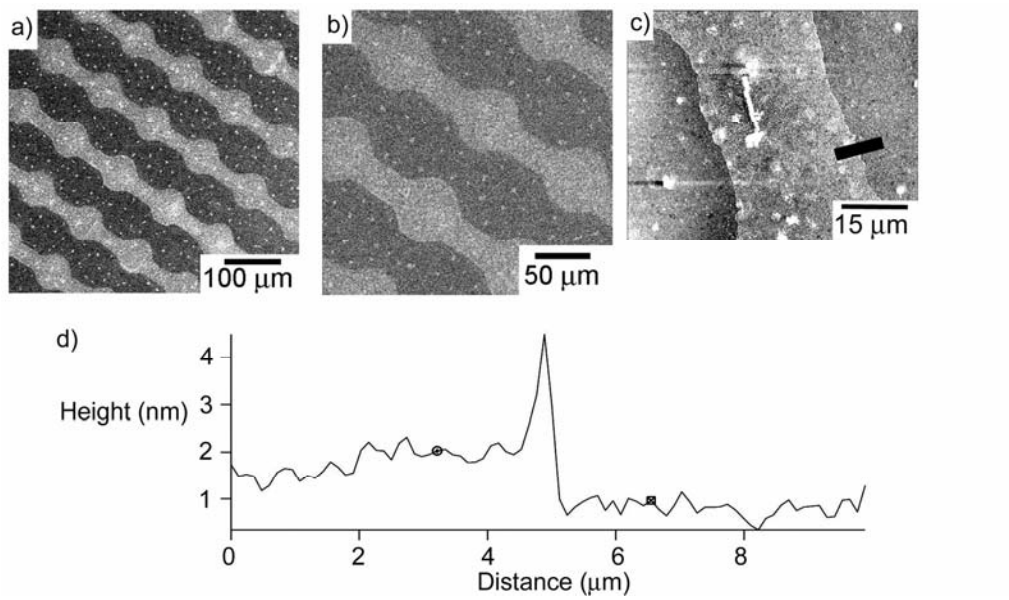

Figure 17 Patterned monolayers (a) and (b) SEM micrographs of patterned polyethylenimine on a silicon wafer. The light areas are polyethylenimine bonded to anhydrides on the surface. The small bright spots in the dark, unpatterned regions are due to polyethylenimine that was not washed from the channels prior to removal of PDMS. (c) A SPM micrograph of a patterned surface. The center region is the polyethylenimine-coated SAM, and the left and right regions are uncoated SAMs. The bright spots were dust particles on the surface. The dark line indicates the area that was integrated to give the thickness plot in (d). The average thickness of the polymer layer was 1.0 nm.

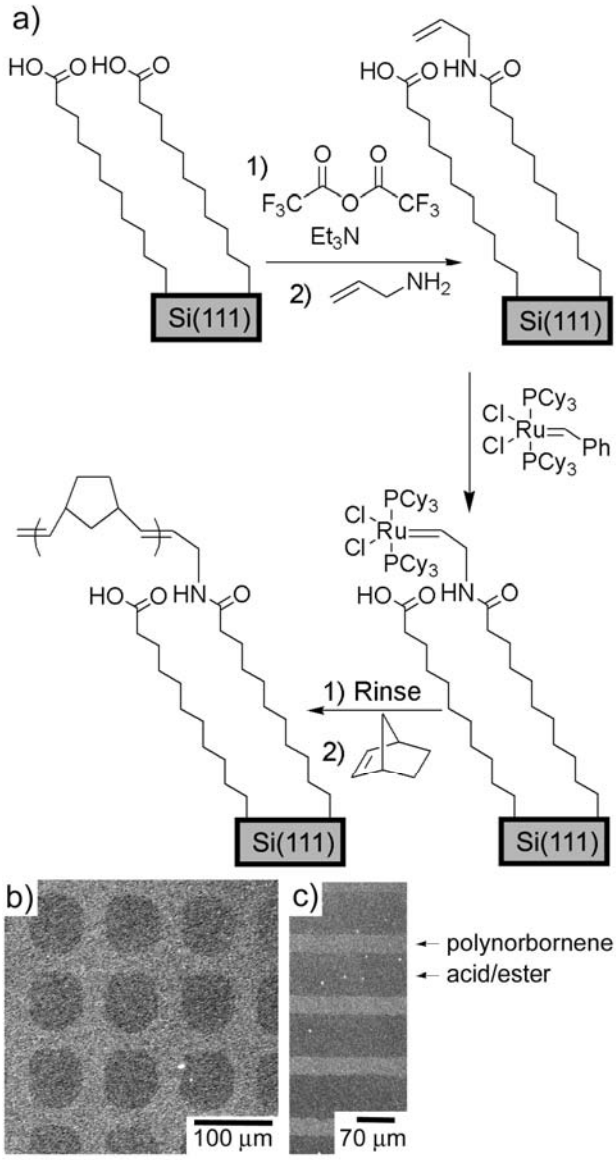

Figure 18 Functionalized monolayers (a) We functionalized anhydride-terminated SAMs with allyl amine to yield an olefin-terminated SAM. This SAM was immersed in a solution of the Grubbs' first generation catalyst for 30 min in a glove box. The wafer was removed, rinsed, and immersed in norbornene to yield a polynorbornene surface. SEM micrographs of (b) a two-dimensional grid and (c) parallel lines of SAMs exposing polynorbornene are shown.

Pattern with Poly(norbornene).

We grew polynorbornene from SAMs using the Grubbs' first generation catalyst by patterning a two-dimensional grid of allyl amine on the SAMs using the method described in Figure 18a. The olefin-terminated SAM was immersed in a solution of the

Grubbs' catalyst in xylenes for 30 minutes in a glove box (Figure 18a). The wafer was removed, rinsed thoroughly with xylenes, and placed in a 0.1 g mL^{-1} solution of norbornene in xylenes.

After one or fifteen hours the wafer was removed from the glove box, washed thoroughly to remove excess norbornene, and imaged under an SEM (Figure 18b, c). Control experiments where the monolayer was not reacted with the Grubbs' catalyst did not show any polymer on the surface by ellipsometry or SEM. The thickness of polynorbornene was measured with an ellipsometer on large, unpatterned sections of silicon wafers. The thicknesses were 32 nm after 1 h and 150 nm after 15 h.

Conclusions

This paper describes three general methods to assemble SAMs with reactive end groups on silicon. We described mild methods to assemble undecylenic acid on a Si(111)-H surface, to functionalize an acid-terminated monolayer on silicon, and to pattern these monolayers on the micrometer-size scale. SAMs of undecylenic acid were characterized by contact angle goniometry, HATR-IR spectroscopy, and XPS. No detectable reaction between the carboxylic acid and Si(111)-H surface was measured.

The direct assembly of acid-terminated monolayers on silicon is important as acids are readily functionalized to expose other chemical groups. In our method commercially available undecylenic acid is assembled directly on silicon without an intervening layer of silicon dioxide. The further functionalization and patterning of these SAMs are important as these methods extend the potential range of applications of SAMs on silicon. We demonstrated how these monolayers could be patterned by assembling an amide-terminated surface with a small molecule, a polymer, and a catalyst that was used to grow a polymer from the surface. These methods are generally applicable and will allow other, more functional surfaces to be assembled and patterned on silicon for

applications in the areas of electronics, (bio)chemical sensors, microchemical systems, nanoscience, and beyond.

CHAPTER 2 PATTERNING BY ETCHING AT THE NANOSCALE (PENS) ON SI(111) THROUGH THE CONTROLLED ETCHING OF PDMS

Abstract

Patterned polymer brushes were grown from organic monolayers on Si(111) using ring opening metathesis polymerization catalyzed by the Grubbs' first generation catalyst. The Grubbs' catalyst reacted through cross metathesis with an olefin-terminated monolayer on Si(111) such that it was attached to the monolayer. Next, a polydimethylsiloxane slab patterned in bas-relief was placed on this surface to form microchannels. Undecenoic acid was added to the microchannels to react with and remove the Grubbs' catalyst from the surface exposed in the microchannels. Next, the microchannels were etched by tens of nanometers to several micrometers with F^-. This etching exposed fresh monolayers on the silicon terminated with the Grubbs' catalyst. A solution of bicyclo[2.2.1]hept-5-ene-2-carboxylic acid was added to the microchannels and polymer brushes grew by ring opening metathesis polymerization only on the newly exposed surface. A range of polymer brushes with widths from 70 nm to several micrometers was fabricated. This method is exciting because an entire surface can be patterned simultaneously, and it is not limited by the wavelength of light. Rather, the width of the polymer brushes is determined by the amount of polydimethylsiloxane that is etched from the microchannels. In addition, this method can be used to pattern surfaces inside of existing microchannels. These polymer brushes were characterized by a combination of methods including X-ray photoelectron spectroscopy, scanning Auger spectroscopy, scanning electron microscopy, and optical microscopy.

Introduction

Nanometer to micrometer wide patterns of well-defined organic compounds on surfaces have accelerated advances in nanoscience in fields ranging from medicine to

molecular electronics.[302-310] These patterns allow for the spatial engineering of smart surfaces to display well-defined arrays of molecules that can recognize metals, DNA, RNA, or proteins in solution; act as molecular wires; or provide the basis for devices fabricated for molecular electronics. Numerous methods to pattern surface chemistries on the micrometer-size scale exist, but patterning surfaces with nanometer-sized dimensions is considerably more challenging. Current methods to pattern surfaces with nm-sized features of organic molecules include dip pen lithography,[311,312] electron-beam lithography,[313-315] focused ion beam lithography,[316,317] nano-imprint lithography,[318-320] and microcontact printing.[321] These methods are exciting alternatives to photolithography as they combine patterning on the nm-size scale with the placement of well-defined and tailored organic functional groups on a surface and exploit the opportunity to generate many patterns quickly without the need for new chrome masks to be manufactured. This combination of patterning on the nm-size scale with well-defined chemistries is critical for new applications in nanoscience.

In this chapter, we report a mild method to pattern polymer brushes from 70 nanometers to several micrometers in width from monolayers on Si(111) using ring opening metathesis polymerization (ROMP) catalyzed by the Grubbs' first generation catalyst. This method uses F^- to etch polydimethylsiloxane (PDMS) microchannels to pattern an entire silicon wafer with polymer brushes that are readily integrated with microfluidic systems. Although these polymers were decorated with carboxylic acids or anhydrides, a wide range of functional groups is possible as ROMP is insensitive to many functional groups. Recently, polymers have been synthesized with ROMP that exposed alcohols, carboxylic acids, Pd catalysts, anhydrides, esters, amides, sugars, ethylene glycols, and ethers to name a few examples.[322-326] Clearly, ROMP is an important polymerization method that can be used to grow polymers displaying many functional groups. In this article we choose to grow polymer brushes exposing anhydrides and carboxylic acids as these functional groups demonstrate our method and they can be

further reacted in subsequent steps. We call this method “patterning by etching at the nanoscale” or PENs for short.

We choose to use PDMS microchannels and silicon for two reasons. First, silicon is the most important electronic material; yet methods to pattern and control its surface chemistry lag behind that of coinage metals and glass.[226,235,236,248,265,269,270,272,273,327-336] Combining the successes of nanotechnology with silicon technology will open up opportunities to fabricate materials with new properties that take advantage of the semiconducting properties of silicon.[239,245,246,250,251,259,337-339] Patterning with polymer brushes is exciting as they combine the selectivity of organic chemistry with the multiplying effect of polymers. Polymer brushes can be used to add more functional groups per unit area of surface than monolayers and still maintain atomic level control over surface chemistry. Second, PDMS microfluidic channels have gained widespread acceptance as a useful tool. Our work is exciting as we are growing well-defined polymer brushes inside of microfluidic channels that will allow their surface chemistries to be patterned from the nm to μm size scales in new ways that will extend the applications of these microchannels.

Experimental Section.

Materials.

We purchased 10-undecanoic acid (98%), 48% HF, cyclooctene, bicyclo[2.2.1]hept-5-ene-2-carboxylic acid (98% pure as an endo/exo mixture), norbornene, the Grubbs’ first generation catalyst, and all solvents from Aldrich or Acros chemicals and used as received. Exo-7-oxa-bicyclo(2.2.1)-heptane-2,3-dicarboxylic anhydride was synthesized according to literature precedent.[340] Single-side polished Si(111) wafers (n-type) were purchased from Silicon Inc, Boise, ID.

Instrumentation.

A Hitachi S-4000 scanning electron microscope was used to gather the SEM images. An accelerating voltage of 5 kV was used to image the patterns on the surface. A micromaster optical microscope with image capturing software (Micron) was used to obtain the optical micrographs of the surface.

The samples were studied by XPS and scanning Auger spectroscopy using a Kratos Axis Ultra at the University of Iowa. For XPS, the dimension of the image area was 300 by 700 μm and the take-off angle was 45°. The pass energy on the survey scan (0 to 1100 eV) was 160 eV. High resolution scans of Si(2p) (92 to 108 eV binding energy), C(1s) (274 to 300 eV binding energy), O(1s) (523 to 539 eV binding energy), and F(1s) (680 to 696 eV binding energy) were performed. The atomic compositions were corrected for the atomic sensitivities and measured from the high-resolution scans. The atomic sensitivities were 1.000 for F(1s), 0.780 for O(1s), 0.278 for C(1s), and 0.328 for Si(2p). For scanning Auger spectroscopy, the voltage was 5 kv and the lateral resolution was 200 nm.

Patterning of polymer brushes

We will describe how we patterned polymer brushes with Bu_4NF and bicyclo[2.2.1]hept-5-ene-2-carboxylic acid, this method was followed for all patterns. The Grubbs' catalyst was removed from a glove box where it was stored under N_2 and exposed to ambient atmosphere. All further steps in this procedure were carried out under ambient conditions. We mixed a 1.22 mM solution of the Grubbs' first generation catalyst in CH_2Cl_2 and immersed a silicon wafer with an olefin-terminated monolayer in it for 30 min. The wafer was removed from the solution of catalyst and rinsed. A PDMS stamp was placed on the monolayer and a 0.48 M solution of undecenoic acid in nitromethane was added to the microchannels for 60 min. The undecenoic acid reacted with the Grubbs' catalyst on the surface to yield an acid terminated monolayer that was

free of the Grubbs' catalyst. 0.5 M Bu_4NF in THF/nitromethane was added to the microchannels for different periods of time. This solution was removed from the channels with fresh nitromethane. A 58 mM solution of the monomer in DMF was added to the microchannels for 3 to 33 h. This addition of monomer resulted in polymer brushes only along the newly exposed Grubbs' catalyst-terminated monolayer. The polymerization time varied to obtain clear images by optical microscopy or scanning electron microscopy. The microchannels were rinsed with fresh nitromethane and the PDMS stamp was removed. The surface was rinsed and imaged by optical and scanning electron microscopy.

Results and Discussion

Our method to pattern micrometer to nanometer-sized polymer brushes begins with the assembly of an olefin-terminated monolayer on Si(111) as shown in Figure 19. The assembly and characterization of these monolayers was reported in a previous publication, and we will only repeat the important details here.

We assembled mixed monolayers of a diolefin and 1-octadecene to form monolayers terminated with olefins and methyl groups. We demonstrated that these monolayers readily react by cross metathesis or ring opening metathesis polymerization (ROMP) with the Grubbs' first generation catalyst.[341-343] Metathesis is an important class of organic reactions that can be used to synthesize small molecules and large polymers.[344-353] In our previous work we used cross metathesis and ROMP to pattern surfaces with carboxylic acid-terminated monolayers and polymer brushes.[341] These monolayers on Si(111) are stable to atmospheric conditions for months and to immersion in aqueous or organic solvents for days to weeks. They are stable enough to have a wide range of application in fields that currently use monolayers on electrically conducting substrates such as gold or electrically insulating substrates such as glass.

Method to Fabricate Polymer Brushes Inside Microfluidic Channels.

In this chapter, we report a method to pattern polymer brushes on monolayers on Si(111). This method relies on the controlled etching of PDMS by HF or Bu_4NF within microfluidic channels (Figure 20). PDMS is a commercially available polymer that is extensively used in "soft lithography" for numerous applications including patterning of monolayers or as scaffolds to generate microfluidic channels.[295,299,354] A PDMS mold maintains its shape when placed on a surface and it is flexible enough to seal in conformal contact with a surface. Thus, fluids flowing through PDMS microchannels do not come into contact with surfaces covered with PDMS.

The structure of cross-linked PDMS is comprised of strong silicon-oxygen bonds [formula: $(–O–SiMe_2–)$] with a bond dissociation energy of approximately 522 kJ/mol.[355] These bonds are unreactive towards most reagents with an important exception of the fluoride ion, F^-, which readily cleaves the polydimethylsiloxane network into small molecules. We took advantage of this property of PDMS and passed solutions of HF or Bu_4NF through PDMS microfluidic channels to etch PDMS. By controlling the time of exposure of the channels to a solution of certain $[F^-]$, we were able to control how much PDMS was etched to reveal a fresh surface of Grubbs' catalyst-terminated monolayer that subsequently could be functionalized by ROMP. Two key features of this method is its potential to pattern sub-100 nm wide lines on a surface because it is not limited by the wavelength of light, and its potential to pattern an entire wafer concurrently.

Our method demonstrates the tolerance of the Grubbs' catalysts to these conditions. Only the Grubbs' catalysts are stored in a glove box, the remaining steps are carried out under ambient conditions. The Grubbs' catalysts bonded to the monolayer are exposed to aqueous solutions of HF or Bu_4NF and O_2, yet they still catalyze the growth of polymer brushes from the surface. This result is unexpected but welcome as it makes the formation of patterned polymer brushes rather simple and easy to carry out.

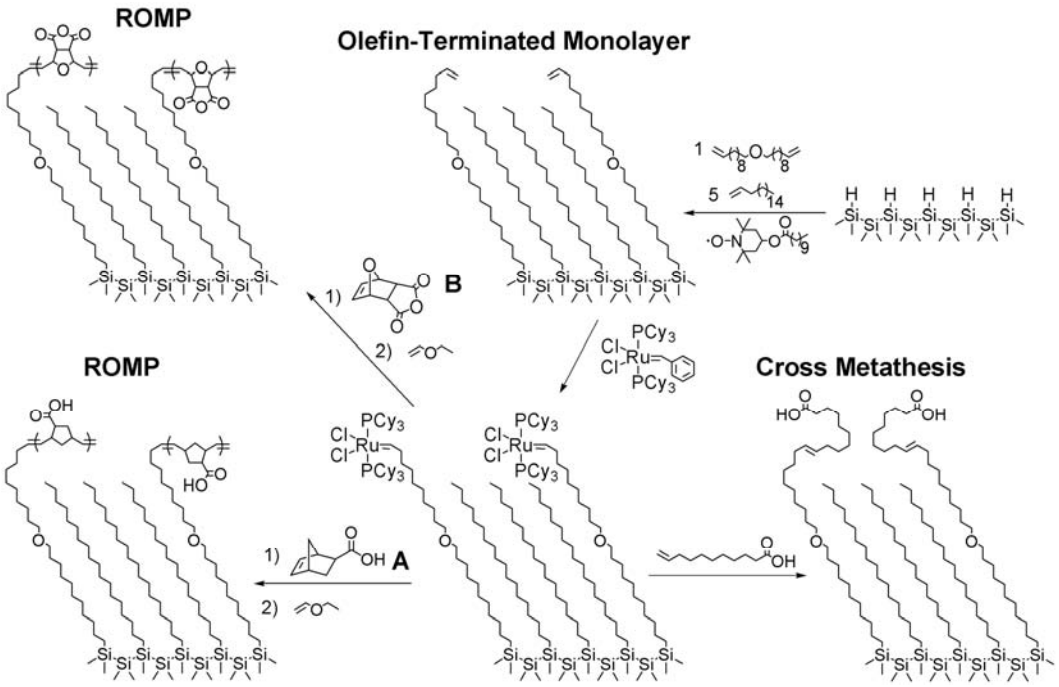

Figure 19 This Figure illustrates the reactions and monolayers used in this study; the full characterization and reactions conditions are reported in the literature. Monolayers terminated with olefins and methyl groups were assembled directly on Si(111) without an intervening layer of silicon dioxide. We first synthesized hydrogen-terminated Si(111) and reacted this surface with 1-octadecene and a diolefin with 0.1 mole % of TEMPO-C_{10}. Next, these surfaces were exposed to a solution of the Grubbs' catalyst to yield a surface with this catalyst covalently bonded to it. This monolayer was reacted with 10-undecenoic acid to yield a carboxylic acid-terminated monolayer by cross metathesis. Alternatively, it was reacted with bicyclo[2.2.1]hept-5-ene-2-carboxylic acid, **A**, or exo-7-oxa-bicyclo(2.2.1)-heptane-2,3-dicarboxylic anhydride, **B**, to yield polymer brushes by ROMP.

Rates of Etching of PDMS

We first measured the rate at which PDMS is etched when immersed in either 0.5 M Bu_4NF dissolved in 1/1 v/v $MeNO_2$/THF or 5% HF in H_2O (Figure 21). To measure the amount of PDMS that was etched, we cut a slab of PDMS that was patterned in bas-

relief with microchannels to expose a series of features raised by 50 microns on PDMS. We measured the widths of at least ten microchannels before and after etching the PDMS to learn how much had been removed. From our results it is clear that 0.5M Bu_4NF etches PDMS faster than 5% HF ($[F^-] = 4$ M). These results indicate that PDMS can be readily etched with Bu_4NF, but to etch sub-micrometer wide stripes of PDMS from the walls of microchannels it is better to use 5% HF.

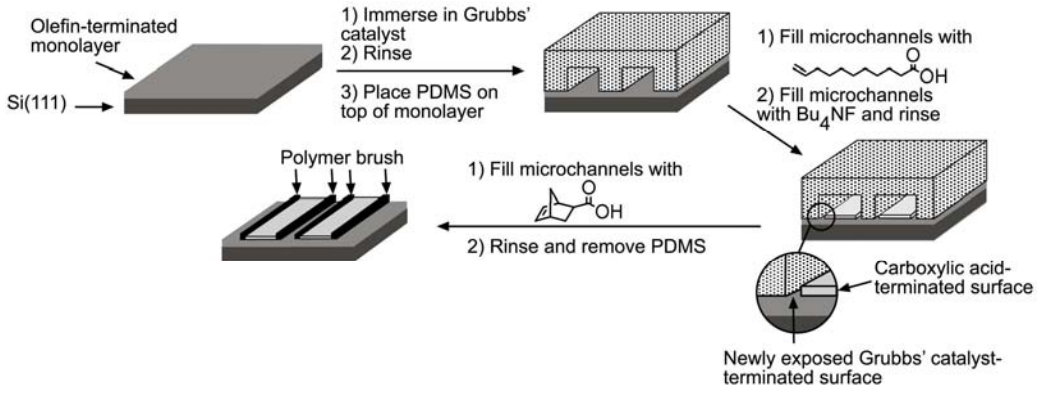

Figure 20 The growth of patterned polymer brush lines began with the assembly of an olefin-terminated monolayer as shown in Figure 19. The silicon wafer is immersed in a solution of the Grubbs' first generation catalyst and removed. The Grubbs' catalyst reacts with the olefins on the surface and is bonded to the monolayer. After rinsing with fresh solvent, a PDMS slab with microchannels is placed on the surface. The microchannels are filled with undecenoic acid to cross metathesize with exposed Grubbs' catalyst and remove it from the surface. Bu_4NF or HF is added to the PDMS microchannels to etch the walls and expose fresh Grubbs' catalyst-terminated surface. A solution of monomer for ROMP is added to the microchannels to grow polymer brushes only on the newly exposed surface. The entire method outlined here is performed outside of a glove box under ambient conditions.

Interestingly, if we immerse PDMS into a solution of undecenoic acid in nitromethane prior to etching, the amount of PDMS that was etched was lowered relative to slabs of PDMS that had not been immersed in undecenoic acid. It is possible that

undecenoic acid can diffuse into PDMS and affect the etching rate by buffering the F^- and offering a barrier to its diffusion into PDMS. It is well known that the rate at which SiO_2 is etched is highly dependent on the pH of the solution with acidic solutions more reactive than basic solutions, but though HF has a lower pH than Bu_4NF, they are present in different solvents which accounts for their different etch rates. Also, undecenoic acid can affect the rate at which F^- reacts with PDMS by offering a barrier through which it must diffuse to react. The actual reasons for the retarded rate is unknown and is beyond the scope of this paper. It is important to note that undecenoic acid had an important effect and that it must be taken into consideration when etching PDMS.

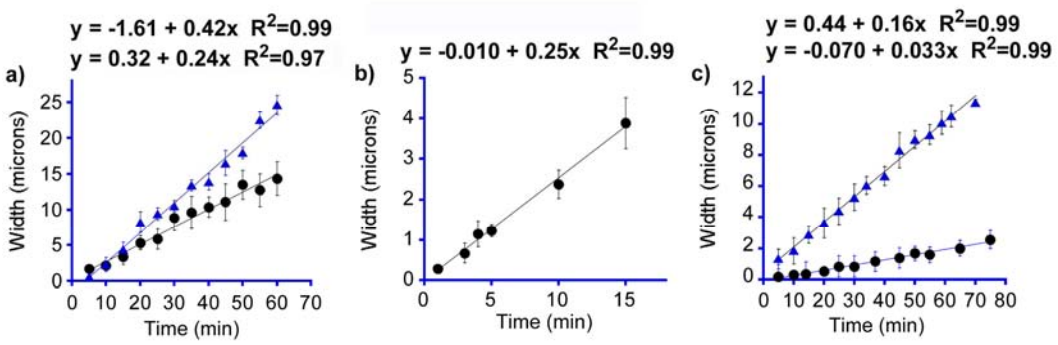

Figure 21 This Figure shows the amount of PDMS that was etched under a variety of conditions. The equations above each graph describe the linear fits to the data as shown by the lines through the data. a) Calibration curves for etching PDMS microchannels in 0.5 M Bu_4NF after the PDMS was immersed in 10% by volume solution of undecenoic acid in $MeNO_2$ for 60 min (●) and without exposure to undecenoic acid (▲). b) The width of polymer brushes fabricated using the 0.5 M Bu_4NF as the etchant and as measured from SEM micrographs. c) Calibration curves for etching PDMS microchannels in 5% HF after the PDMS was immersed in a 10% by volume solution of undecenoic acid in nitromethane for 60 min (●) and without exposure to undecenoic acid (▲). The error bars are the standard deviations for at least ten measurements at each point.

In the next section, we will further describe how the width of the polymer brush patterns closely match the calibration curve set using PDMS immersed in undecenoic

acid prior to etching. This result is not unexpected as undecenoic is flown through the microfluidic channels prior to etching.

Growth of Polymer Brushes and Characterization by Optical Microscopy and SEM.

After treatment with etchant solution, polymer lines were grown on the newly exposed surface according to the procedure of Figure 20 and characterized by optical and scanning electron microscopy (Figure 22). For these experiments we used monomer **A** in Figure 19 to synthesize a polymer brush exposing carboxylic acids. There is a limitation in viewing these patterns by SEM as the lines are narrow (widths of tens of nanometers to several micrometers) and do not show up well at low magnifications. Therefore, we grew thick polymers that were easily viewed as bright lines under optical microscopy and show SEM micrographs at high and low magnifications where the lines were still clearly visible.

We wished to show that this technique works over a large area for both straight and curvy microchannels. The images in Figure 22 are representative of what we observed over numerous samples, the polymer lines were continuous over the entire length of the microchannels – greater than a centimeter in length. Although there were very few defects on these surfaces, occasionally a microchannel did not fill with the liquid so a polymer line was not patterned in it. In addition, it is clear from Figure 22e that curvy channels can be patterned. Figure 22d shows polymer lines that followed the contours of the end of the microchannels. This method is both robust over large areas and can be used to pattern polymer brushes in straight and curvy microchannels. To better characterize the polymer lines, we imaged them under high magnification by SEM (Figures 22f, g, h, and i). These images clearly demonstrate that the lines were continuous. The walls of the microchannels were not smooth (as expected from the use of transparency masks to create the microchannels), the polymer brushes followed their

uneven contours. Thus, this method successfully replicated the contours of the walls of the microchannels. It is forgiving of imperfections in the roughness of the walls and allows curves on the submicron to tens of microns size scale to be patterned.

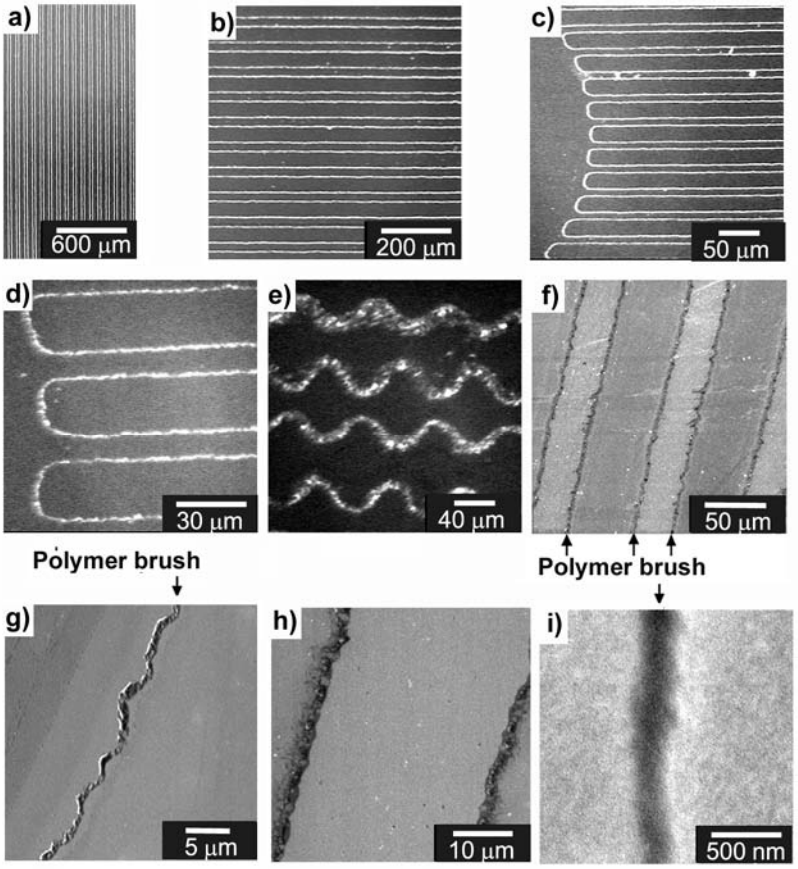

Figure 22 Optical micrographs of polymer brushes (bright lines) that were grown in a), b), c) and d) straight and e) curvy microchannels. In c) and d) we show the ends of the microchannels to emphasize that the polymer lines followed the curves of their shapes. f), g), h), and i) SEM micrographs of polymer brushes (dark lines). The polymer lines appear curvy under high magnification due to imperfections in the walls of the PDMS microchannels used to fabricate them. i) A SEM micrograph of a polymer brush with a width of 270 nm. In each of these experiments we used monomer **A** from Figure 19 to synthesize the polymers.

The widths of the patterns were measured as a function of time that the microchannels were exposed to Bu_4NF and the data was plotted in Figure 21b. The agreement between the measured widths of the lines and the amount of PDMS etched after exposure to undecenoic acid was excellent (slopes of 0.25 and 0.24 μm per min) and demonstrated that this method could be used to grow patterned polymer brushes with widths from 270 nm to at least 3.7 μm. Control experiments where we did not add monomer to the microchannels after etching did not show any polymer lines.

To grow polymer brushes with widths of less than 250 nm we had to use an etchant solution different from 0.5 M Bu_4NF. Based on the calibration curves, to etch 100 nm from microchannel walls they must be exposed to 0.5 M Bu_4NF for only 26 second – a time that we found challenging to control. Decreasing the concentration of Bu_4NF did not provide reproducible results for the widths of polymer brushes so we switched to 5% HF as the etchant due to its slower rate of etching as shown in Figure 21c. With this etchant 100 nm of PDMS would be etched from the microchannel walls upon exposure to HF for approximately 5 min. In Figure 23 we show polymer brushes with widths of 70, 90, and 140 nm that were fabricated by following the method outlined in Figure 20 and replacing the etchant with 5% HF in H_2O. From the results in Figures 22 and 5, it is clear that the edge resolution of the polymer brushes increases with their widths. For the smallest lines the edge resolutions were much less than 50 nm, but for the widest lines exceeding one micron the edge resolution increased to over 50 nm.

To further demonstrate the potential of this method, we patterned crossed lines of different polymer brushes by first growing polymer brushes of monomer **A** in Figure 19 along microchannels of PDMS. Next, the surface was immersed in a solution of the Grubbs' catalyst again to bond Grubbs' catalyst throughout the entire surface. The PDMS stamp was rotated and placed back on the surface. The procedure outlined in Figure 19 was repeated to grow polymer brushes of monomer **B** at an angle relative to the first lines. Because we replenished the Grubbs' catalyst on the surface prior to growing the

second set of polymer brushes, we grew crossed polymer lines as shown in Figures 23d and e.

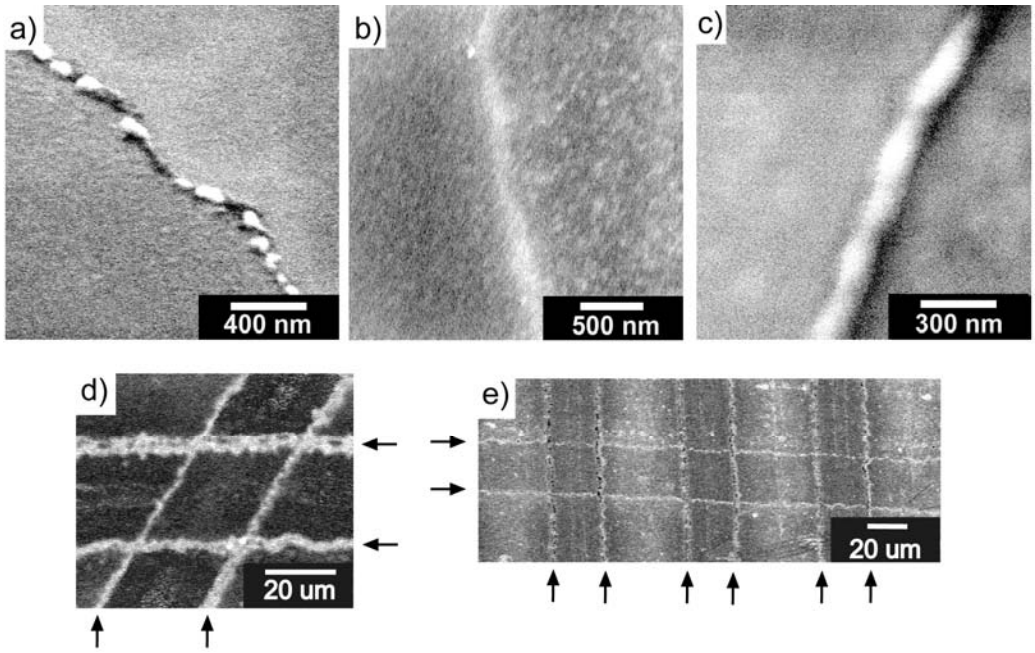

Figure 23 SEM micrographs of patterned polymer brushes that were grown from PDMS microchannels after etching with 5% HF and using monomer **B** in Figure 19. The polymer brush lines had widths of a) 70, b) 90, and c) 140 nm. d) and e) Crossed polymer brush lines that were fabricated by growing one set of polymer lines, removing the PDMS, immersing the wafer in a solution of the Grubbs' catalyst, and following the method in Figure 20 to grow a second set of polymer lines on the surface. The arrows point to the lines of polymer brushes.

Characterization of Polymer Brushes by XPS and Auger Spectroscopy.

We further characterized these polymer brushes by XPS and Auger spectroscopy. We first looked at these surfaces by XPS to characterize the change in the C(1s) peak that would show evidence of growth of polymer. Polymer brushes of monomer **A** were grown on the entire surface of a Si(111) wafer for measurements by XPS. A nonpatterned

surface was imaged because our polymer brushes were narrower than the smallest pixel size that could be measured by scanning XPS. In Figure 24 we show the evolution of the C(1s) peak in the original monolayer, the Grubbs' catalyst-terminated surface, and the polymer brush. These results demonstrate that we are growing polymers that were bonded to the surface (they were not removed with extensive washing in organic solvents). In addition, the Ru(3p) and Ru (3d) peaks clearly show that the Grubbs' catalyst was bonded to the monolayer as described in Figure 19.

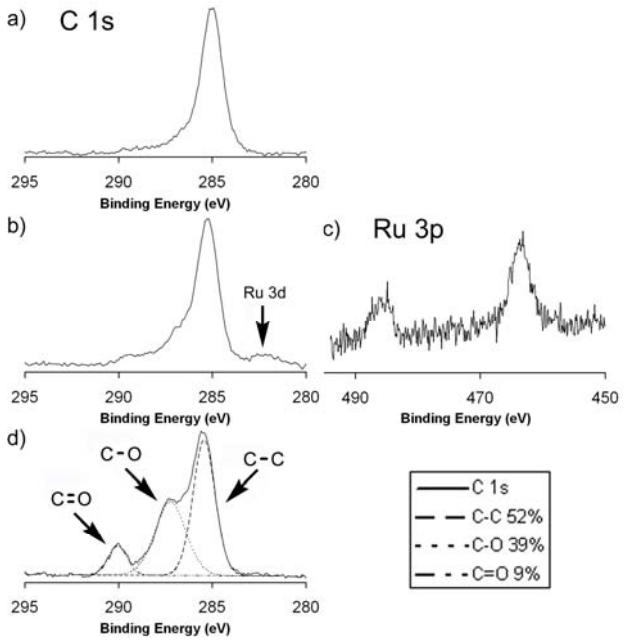

Figure 24 The change of the C(1s) peak in the XPS spectra for a) a mixed monolayer terminated with methyls and olefins, b) after reaction with the Grubbs' catalyst, and d) after reaction of the surface with monomer. c) The Ru(3p) peak clearly shows that it is bonded to the surface.

Because XPS is a bulk measurement over a large (approximately 0.24 mm^2) section of a surface, we grew patterned polymer brushes using monomer **A** and imaged

them by scanning Auger spectroscopy. Auger spectroscopy has the advantage that it can be image small area with a lateral resolution approaching 200 nm. In Figure 25 we show a SEM of a patterned surface with a dark, horizontal line that indicates where the surface was imaged by scanning Auger spectroscopy. When the Auger imaged the polymer brush, it detected a spike in the amount of C and a decrease in the amount of O and Si. These results are consistent with the growth of a polymer brush with high amounts of C that shields the Si peak. The O(KLL) peak decreases when the polymer brush is imaged because the area between the polymer brushes the surface is terminated with acids as described in Figure 19.

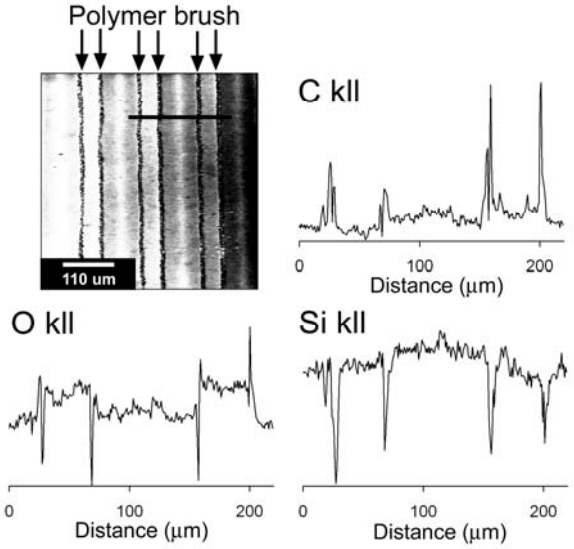

Figure 25 This Figure shows a SEM of a patterned surface taken in the Auger spectrometer. The gradient in darkness is due to the unoptimized location of the detector due to the location of the XPS detector. The dark vertical lines are the polymer brushes and the one dark horizontal line is where the surface was imaged by Auger spectroscopy. The C(KLL), O(KLL), and Si(KLL) scans show spikes where the polymer brushes were found.

Conclusions and Summary

We report a new method to pattern polymer brushes inside of PDMS microchannels with widths from several micrometers down to 70 nanometers. All of the steps of this method are carried out under ambient conditions using simple PDMS slabs. This method uses the controlled etching of PDMS with different sources of F^- to expose fresh surfaces of Grubbs' catalyst-terminated monolayer within microchannels. Although we patterned lines with widths down to 70 nm, this method probably can be extended to patterns with smaller widths by using lower exposures to F^- or low molecular weight polymer brushes. We expect that the true widths of the polymer lines where they attach to the surface is smaller than the widths measured here because polymer brushes will spread onto adjacent surfaces that did not grow polymer brushes. The spreading of polymer brushes and increasing difficulty of imaging nm-wide polymer lines by SEM kept us from learning the lower limit of this method.

Growing polymer brushes patterned along the edges of microfluidic channels is exciting for several reasons. One potential application will be the study of fluid flow directly along the edges of complex microchannels. Because our method relies on etching the PDMS walls with continually refreshed sources of F^-, it should be possible to study how fluid flows along the walls of microchannels through the width of polymer brushes along the surface. Another exciting option with this method is control of spatial chemistry inside of microfluidic devices for use in micro total analysis systems (μTAS). In "these lab on a chip" systems, the increasingly small dimensions of the microfluidic channels increases the importance of controlling their surface chemistry. To pattern the surface chemistry inside of a microfluidic device the surface is either patterned and then another slab is bonded onto the surface to form channels, or the channels are modified using lamellar flow in the channels. These patterned surfaces can direct the flow of liquids or the growth of substrates in the channels. Our method allows the edges of the channels to be patterned selectively from the rest of the surface and will allow for further

control over the surface chemistry. Finally, we can imagine coating the newly formed polymer brushes with other nanomaterials or inorganics. A hard shell could be grown over the polymer brush lines, and after the polymers are etched a new, nanofluidic device would remain that would be readily integrated with a microfluidic channel. This method is also promising because it can be integrated with monolayers on coinage metals. In future work we will explore some of these applications, study the lower limits of line widths of polymer brushes that can be obtained with this method, and investigate the growth of block copolymer brushes.

CHAPTER 3 ASSEMBLY OF ORGANIC MONOLAYERS ON POLYDICYCLOPENTADIENE THROUGH BROMINATION

Abstract

The first well-defined organic monolayers assembled on polydicyclopentadiene is reported. Commercial grade dicyclopentadiene 90%+, mixture of endo exo, without any purification, was polymerized with the Grubbs' second-generation catalyst in a fume hood under ambient conditions at very low catalyst to monomer loadings of 1 to 20,000. This simple method resulted in a polymer that was a hard solid and appeared slightly yellow. Brief exposures of a few seconds of this polymer to Br_2 lead to a surface with approximately half of the olefins brominated as shown by X-ray photoelectron spectroscopy (XPS) and attenuated total reflection-infrared (ATR-IR) spectroscopy. The ATR-IR spectroscopy was carried out with the polymer in contact with a Ge hemisphere housed in a GATR accessory from Harrick. This brominated polydicyclopentadiene was immersed in DMF with 4-(trifluoromethyl)benzylamine to assemble a monolayer. The amines displaced Br on the surface to form a monolayer that exposed a CF_3 group on the surface. The surface was extensively studied by XPS using the method described by Tougaard to find the distribution of F within the surface layer. The ratio for the peak area, Ap, to the background height, B, measured 30 eV below the peak maximum was 109.8 eV. This value clearly indicated that the F was found only at the surface and was not found within the polymer. A surface coverage of 1.37 amines per nm^2 was estimated and indicated that the monolayer was 28% as dense as a similar monolayer assembled from thiols on gold. Finally, a simple method to pattern these monolayers using soft lithography is described. This work is critically important because it reports the first monolayers on a relatively new and emerging polymer that has many desirable physical characteristics such as high hardness, chemical stability, and ease of forming different shapes.

Introduction

Control over surface chemistry on organic and inorganic substrates is critically important in many industrial devices and in academic research.[298,309,332,339,356-363] Surface chemistry is typically controlled either by assembling organic monolayers – such as thiols on gold or siloxanes on glass – or through the assembly or growth of polymers on surfaces.[244,285,290,291,301,364-370] One set of examples to illustrate the importance of surface chemistry is the use of DNA and protein arrays in medicine and biology.[371,372] These arrays require complex patterns of single-stranded DNA or proteins bonded to a surface with high loadings. In these arrays and other materials, the surface chemistry must be well defined and controlled such that the functional groups exposed on a surface are known and react with selected molecules. Because of the importance of well-defined surface chemistry in areas as diverse as chromatography, DNA arrays, biosensors, tribology, and others, developing methods to control surface chemistry is a very active area of research. The assembly of organic monolayers on polymeric surfaces is well studied with a variety of polymers studied including polydimethylsiloxane,[373-375] poly(methyl methacrylate),[376] polycaprolactone,[377,378] polylactide,[379-381] cellulose,[382,383] and polyethylene[384-386]. Unfortunately, all of these polymers have limitations ranging from surface reconstruction that buries some functional groups into the bulk of the polymer, surface etching that limits the lifetimes of displayed functional groups, poorly defined surfaces with many functional groups present, harsh conditions needed functionalize their surfaces, or undesired physical properties of the polymers.

Recently, polydicyclopentadiene (PDCPD) emerged as a new material with applications in surface science and chromatography.[167,387-395] Dicyclopentadiene is commonly polymerized by two mechanisms: radical polymerization or ring opening metathesis polymerization (Figure 26). The radical polymerization yields a highly cross-linked polymer with only a low concentration of unreacted olefins present. Alternatively, the synthesis of PDCPD by ROMP yields a highly cross-linked material with olefins

present at high concentrations due to the presence of four sp^2 hybridized carbons for every ten carbons in the polymer. We hypothesized that the presence of these olefins at high concentrations would make it possible to yield a highly functionalized PDCPD surface. This material has become more accessible because of the relatively recent development of highly active, homogeneous Grubbs' metathesis catalysts that polymerize DCPD at low loadings of catalyst under simple conditions.

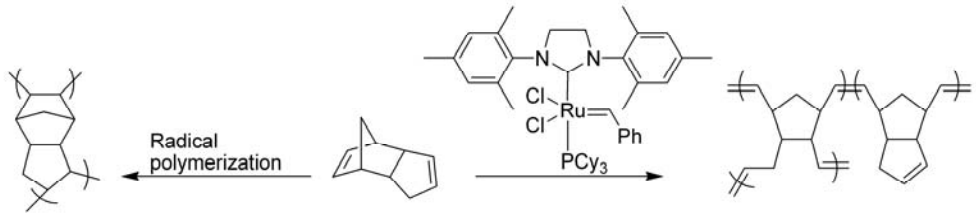

Figure 26 Dicyclopentadiene has traditionally been polymerized by radical methods to yield a highly cross-linked, stable polymer. Development of the very active Grubbs' second generation metathesis catalyst made it simple to synthesize PDCPD that is highly cross-linked and exposes a high concentration of reactive olefins.

PDCPD has found many applications because of its toughness and, more recently, the presence of a high density of olefins. Because of its toughness and resistance to fracture, this material is used to make the covers on snowmobile sleds and as a protective material for hoods on semitrucks.[388,391-394] PDCPD is also being explored for uses as the solid phase in chromatography because of its ease of synthesis in a variety of containers, its highly cross-linked structure, and the presence of olefins that can be functionalized to introduce additional selectively to separations.[167,387,388]

We wished to study the surface chemistry of this polymer because its properties and low price may lend it to a variety of applications where other polymers are currently used. Others studied the functionalization of PDCPD by growing new polymers from the

surface, but no one has reported the assembly of monolayers on its surface. In prior work, Buchmeiser et al. polymerized DCPD into porous beads using the Grubbs' catalyst and used the residual catalyst to graft a second polymer onto the beads.[396] Hilborn et al. reported the surface functionalization of PDCPD by grafting atom transfer radical initiators onto the surface using olefins present on PDCPD and growing polyacrylates through radical polymerizations.[167,387] They did not report the density of the initiator on the surface or whether it was only bonded to the surface or also present in the bulk but still near the surface. We decided to study this emerging polymer by functionalizing the olefins in PDCPD with Br_2 and then reacting resulting surface with amines. These reactions are well precedented in organic chemistry and proceed with high yields using a variety of different amines under different reaction conditions. The compatibility of this approach with different amines will make this approach potentially useful in fields that require the presentation of well-defined surfaces on inexpensive, transparent polymers.

Results and Discussion

Synthesis and Characterization of PDCPD.

The overall reaction sequence to yield functionalized PDCPD is shown in Figure 27 along with the abbreviations for each surface. The first step was the synthesis and characterization of PDCPD to use as a suitable substrate.

The conditions to synthesize highly cross-linked PDCPD with minimal catalyst loadings were investigated with the Grubbs' first and second generation catalysts. An important consideration in this work is that the low vapor pressure and reactive olefins of dicyclopentadiene made its use in a glove box unfeasible due to its probable contamination of other reactions in the glove box. It could not be used on a benchtop due to its strong, unpleasant odor. These conditions necessitated the use of DCPD in a fume hood. Although the Grubbs' catalysts are mildly air sensitive, they are stable in the solid state and can be readily handled under ambient conditions if solutions are used

immediately after mixing the catalyst with solvent.[345,347,397,398] Because of these issues, all polymerizations were carried out in a fume hood with catalyst solutions that were mixed and then immediately used. No care was taken to degas the monomer or other solvents.

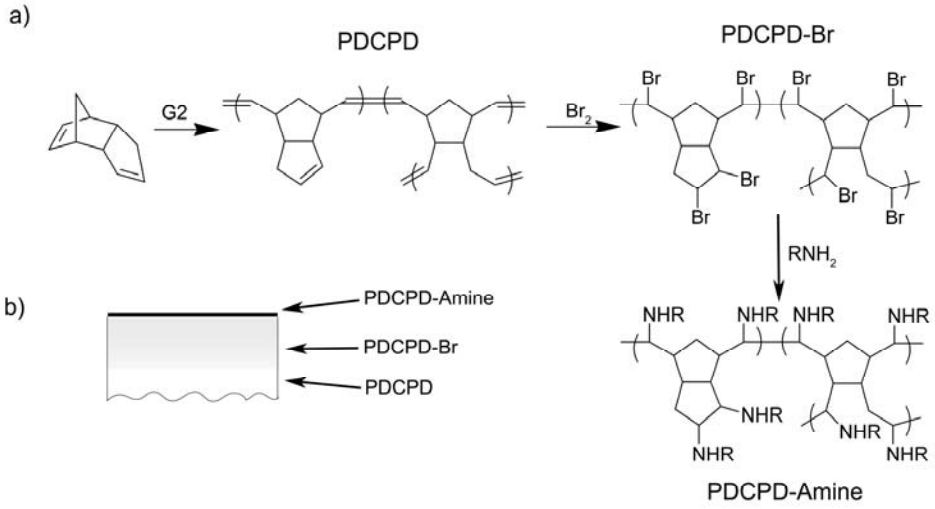

Figure 27 Formation and functionalization of PDCPD a) Our method to functionalize PDCPD to assemble amines into monolayers. b) A schematic of PDCPD-amine to illustrate that the amine bonds to the surface and PDCPD-Br extends into the bulk that eventually is solely PDCPD.

The first generation Grubbs' catalyst was initially studied because of its lower cost relative to the second generation Grubbs' catalyst (Table 3). DCPD was quickly polymerized with this catalyst at monomer to catalyst loadings of 1,000 to 1, but the polymer was darkly colored. Lower catalyst loadings were attempted at evaluated temperatures by immersing DCPD in a glass flask into an oil bath and adding the catalyst after the DCPD thermally equilibrated. These polymerizations yielded viscous liquids or gels due to incomplete polymerizations.

Table 3 Polymerization of dicyclopentadiene with the Grubbs' catalysts.

Entry	Monomer/Catalyst	Catalyst	Temp (^{o}C)	[a]Time	[b]State
1	1,000	G1	RT	3 min	Solid
2	10,000	G1	60	72 h	Liquid
3	100,000	G1	60	72 h	Liquid
4	1,000,000	G1	60	72 h	Liquid
5	10,000	G1	90	48 h	Soft Solid
6	100,000	G1	90	48 h	Gel
7	1,000,000	G1	90	48 h	Liquid
8	10,000	G2	25	18 h	Soft Solid
9	10,000	G2	[c]25 -> 50	16 h	Soft Solid
10	100,000	G2	[c]25 -> 50	16 h	Liquid
11	1,000,000	G2	[c]25 -> 50	16 h	Liquid
12	10,000	G2	50	1 min	Solid
13	100,000	G2	50	4 h	Liquid
14	1,000,000	G2	50	4 h	Liquid
15	10,000	G2	55	3 min	Solid
16	20,000	G2	55	3 min	Solid
17	30,000	G2	55	3 min	Solid
18	80,000	G2	55	24 h	Liquid
19	100,000	G2	55	24 h	Liquid
20	1,000,000	G2	55	24 h	Liquid
21	10,000	G2	80	[d]1 s	Solid
22	100,000	G2	80	16 h	Soft Solid

[a]The time each polymerization was allowed to proceed before the observation of its final state. [b]The physical state of the final polymer. [c]The catalyst and DCPD were added at room temperature and the vial was immediately immersed into an oil bath set at 50°C. [d]An approximate time was used because this polymerization was very rapid.

Because the best polymerization with the Grubbs' first generation catalyst yielded a darkly colored polymer due to residual Ru in the sample, the second generation Grubbs' catalyst was investigated. This catalyst is much more active than the first generation catalyst while still maintaining acceptable stabilities towards oxygen and elevated temperatures.[347]

Initial attempts to yield a hard polymer by carrying out the polymerization at room temperature or by mixing catalyst and monomer at room temperature followed by gradual heating to 50°C failed. When the monomer was heated prior to the addition of catalyst, it polymerized to yield a hard polymer in less than a minute at monomer to catalyst loadings of 10,000 to 1, but did not yield a hard polymer at much higher loadings of 100,000 or 1,000,000 to 1. A temperature of 55°C was chosen based on literature reports that indicated the catalyst was highly active at this temperature but did not decompose rapidly. A range of monomer to catalyst loadings were attempted, and the highest loading of monomer that yielded a hard polymer was 30,000 to 1. Higher temperatures did not yield hard polymers at monomer to catalyst loadings above 30,000 to 1. Monomer to catalyst loadings of 20,000 to 1 were used throughout the remainder of the experiments due to a very slight, but still noticeable, odor of DCPD in the polymer produced from monomer to catalyst loadings of 30,000 to 1.

This method was followed for most samples, but a slightly modified method was used to yield large, flat samples. In this method, PDCPD was heated to 55°C and the Grubbs' catalyst (at monomer to catalyst loadings of 20,000 to 1) was added. The solution was immediately transferred to a glass petri dish within a glass vacuum desiccator. The atmosphere was evacuated and the sample was placed under N_2. The sample was added to an 80°C oven for 30 min to complete the polymerization. Polymers produced by both methods appeared slightly yellow, but were mostly transparent even for samples over an inch thick. The latter method was used for all of the characterization experiments due to the ease of working with a flat, rather than a curved, surface.

PDCPD was studied by XPS and attenuated total reflection-infrared (ATR-IR) spectroscopy with a Ge hemisphere in contact with the polymer sample to confirm its composition and presence of functional groups (Table 4 and Figure 29). The XPS spectrum showed that the sample was composed of carbon (98.6%) with a small amount of oxygen (0.9%) and, surprisingly, silicon (0.4%). Ruthenium was not observed due to its low concentration in the polymer.

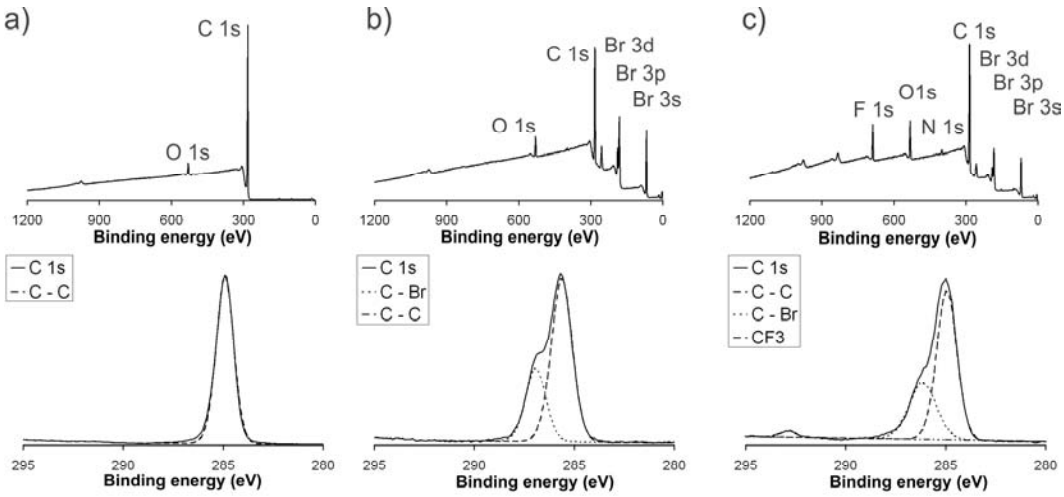

Figure 28 The survey and high resolution scans of C for a) PDCPD, b) PDCPD-Br, and c) PDCPD-amine. Fits to the high resolution scans are shown.

Although the presence of oxygen is not surprising because olefins are readily oxidized via radicals or by ozone and these reactions would be accelerated at elevated temperatures such as those used for the polymerization; the presence of silicon was unexpected. In work by Hilborn et al., they polymerized DCPD with Grubbs' catalyst and observed at surface with 14.21% of oxygen and 6.11% of silicon by XPS.[167] They attributed the presence of silicon and oxygen to either glass particles embedded in the polymer or siloxane contamination with only minimal oxidation of the olefins in PDCPD.

Interestingly, our results also showed some Si and O but at significantly lower amounts, yet still in a nearly 2:1 ratio.

An experiment was carried out to determine if Si originated from advantageous, small glass shards embedded in the surface or from siloxane found in vacuum oils or other materials in contact with the polymer. Dicyclopentadiene polymerized rapidly at the elevated temperatures used in these experiments – the polymer is a hard solid within three minutes – and underwent a slight contraction as it polymerizes. These conditions might allow small, residual glass to become imbedded in the surface. If this was the source of Si and O in the polymer, the glass would only be located on the surface of PDCPD and not in its interior, so a slab of PDCPD was cut in half and the interior was characterized by XPS. Similar levels of Si and O were seen in the interior of PDCPD, which indicated that it was not due to glass particles embedded during the polymerization process. The presence of Si and some of the O were mostly likely due to contamination by silicones such as from exhaust from vacuum oils. Slabs of PDCPD were placed under vacuum for extended periods prior to being loaded into the XPS chamber; it is possible that the polymer became contaminated from the oil vapor at this stage or from silicon greased joints. Although we were unable to eliminate the source of the O and Si, they were only small impurities in the XPS spectra of PDCPD.

ATR-IR spectroscopy was used rather than a bulk measurement, such as by passing IR light through a PDCPD sample, so the surface chemistry could be studied (Figure 29a). In ATR-IR spectroscopy with a GATR accessory from Harrick, a polymer sample is placed into contact with the flat section of a Ge hemisphere.[399-401] IR light is passed through the hemisphere and reflected from the flat surface. Only the top 100 to 200 nm of the surface of the solid in contact with the Ge hemisphere is imaged by the IR light. The distance into the material that is imaged depends on several factors including the index of refraction of the material and the wavelength of light, but a good estimate for PDCPD is 100 to 200 nm for the range of the IR spectrum that is shown in Figure 29a.

These values for the penetration of the IR light are explained in more detail in the Apendix B. The IR spectrum shows a strong peak for the Csp^2-H peak at 3044 cm^{-1} and a weaker peak at 3004 cm cm^{-1}. These peaks are smaller than the Csp^3-H peaks that fall below 3000 cm^{-1} as expected from the composition of this polymer. The presence of olefins was further confirmed by the appearance of a weak peak for C=C at 1620 cm^{-1}. The presence of oxygen in the XPS spectrum suggested the presence of alcohols or carbonyl groups, but no peaks could be conclusively assigned to either of these functional groups. The absence of these peaks was not surprising and attributed to the low amounts of oxygen in the XPS spectrum and its possible presence due to siloxane contamination. In summary, the data from the XPS and ATR-IR strongly suggest that PDCPD was formed with very low levels of oxidation of the olefins.

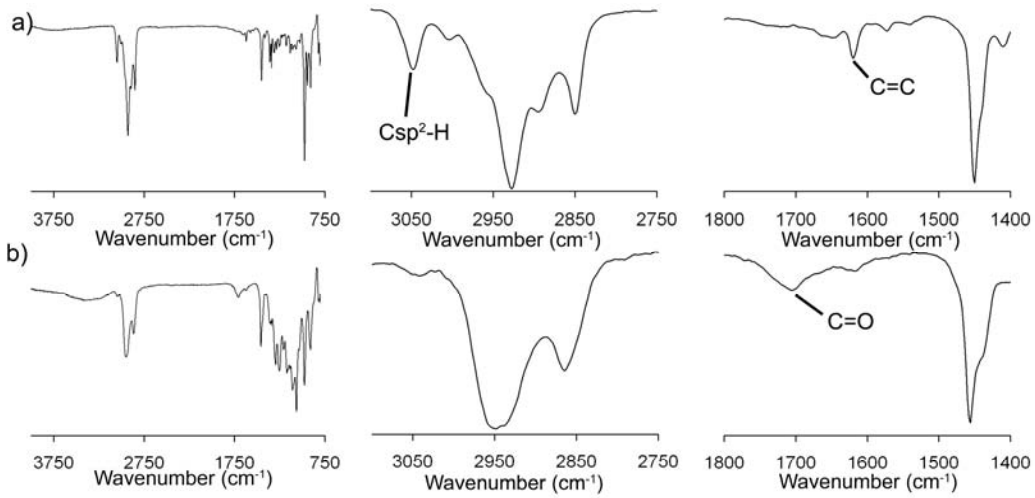

Figure 29 ATR-IR spectrum of a) PCDPD and b) PDCPD-Br.

Synthesis and Characterization of PDCPD-Br.

Br_2 is a dense, dark liquid with a low boiling point (58.8°C) and high vapor pressure at room temperature (175 mm Hg). It rapidly reacts with olefins; in fact, Br_2 is used as a classical test for the presence of olefins by the rapid disappearance of a drop of dark Br_2 when added to a solution of olefin. In our experiments, Br_2 rapidly reacted with PDCPD when it was exposed either as a vapor or as a 1 M solution in THF. In both examples, PDCPD was exposed to Br_2 for less than ten seconds and the olefins were brominated as seen by XPS and ATR-IR spectroscopy. Longer exposures of PDCPD to Br_2 leads to the polymer becoming dark and cracked but did not increase the ratio of carbon to Br in the XPS spectra. The procedure followed to generate PDCPD-Br for all of the samples was to dip the polymer in a 1M solution of Br_2 in THF for less than two seconds followed by extensive washing with organic solvents.

The reaction between PDCPD and Br_2 was so rapid that it was not possible to monitor its kinetics by XPS or ATR-IR spectroscopy, so the final polymer was studied. ATR-IR spectroscopy showed a near complete disappearance of the Csp^2-H peaks and a smoothing of the Csp^3-H peaks (Figure 29b). The peak assigned to the C=C bond at 1620 cm^{-1} in PDCPD was nearly absent in PDCPD-Br. This indicates that most of the olefin reacted, but that some of the olefins remained. That result is not surprising because the polymer was highly cross-linked and some olefins would not be accessible for reaction with Br_2. A new, broad peak appeared at 1705 cm^{-1} that was tentatively assigned to a weak carbonyl stretch due to oxidation of olefins to yield either ketones or aldehydes. Not surprisingly, ATR-IR spectra also showed a weak, broad signal for O-H at approximately 3375 cm^{-1}. It is well known that Br_2 in the presence of water – such as the water found in THF used to dissolve Br_2 – will react to add both Br and OH across an olefin (this is called the halohydrin reaction). Some O-H was expected, and it was found in the ATR-IR spectrum.

The XPS spectra of PDCPD-Br showed mostly C and Br with some oxygen (Table 4). Interestingly, the ratio of C to Br was approximately 6:1 although the ratio would be 5 to 2 if all of the olefins reacted with Br_2. Clearly, the surface was not completely brominated, but longer exposures to Br_2 did not result in a higher C to Br ratio. From the difference between the measured and expected C to Br ratio, it was determined that approximately half of the olefins reacted to yield the expected product. The likely reasons for the low C to Br ratio is that steric crowding around some olefins limited access to them, partial or full oxidation of the olefins with oxygen resulted in fewer olefins to react with Br_2, and advantageous water reacting with Br_2 and an olefin to form a halohydrin product with one C-Br and one C-OH bond. The ATR-IR spectrum of PDCPD-Br certainly shows the presence of an O-H bond, which is consistent with oxidation of the surface or formation of a halohydrin on the surface. Because of these limitations, the "yield" of bromination was approximately 50% as determined by XPS.

Synthesis and Characterization of PDCPD-Amine.

Amines readily react with alkyl bromides, and others have shown that they will react with alkyl bromides attached to monolayers. In contrast to the reaction between olefins and Br_2 which is complete in seconds, the reaction between alkyl bromides and amines is slower but can be completed in hours depending on the conditions used and the ability of an amine to approach the backside of an alkyl bromide. This reaction proceeds via a S_N2 mechanism, so it is sensitive to steric bulk around the amine and, to a greater extent, around the alkyl bromide. For instance, Fryxell et al. assembled monolayers of $Si(CH_2)_{17}Br$ on glass slides and studied the displacement of the bromide with azides.[402] The reaction was initially rapid with approximately 50% of the bromides displaced with azide in four hours, but complete reaction was not observed until 48 to 60 h.

Murray et al. studied the reaction between *n*-propyl, isopropyl, and *tert*-butyl amine with mixed monolayers assembled on monolayer-protected Au clusters composed

of approximately 145 Au atoms.[403] When mixed monolayers with ratios of 19.9 to 1 or 4.5 to 1 of $HS(CH_2)_{11}CH_3/HS(CH_2)_{11}CH_2Br$ were exposed to amines, the reaction with *n*-propyl amine was 95% complete in 3 h at room temperature and the other amines were more sluggish. The authors demonstrated that the reaction between these monolayers and *n*-propyl amine was as rapid as between 12-bromododecane and *n*-propyl amine freely dissolved in solution, so the steric environment of the monolayer did not hinder the desired reaction. When mixed monolayers were used with an alkyl thiol longer than the thiol with the alkyl bromide (a ratio of 4.2 to 1 of monolayers assembled from $HS(CH_2)_{11}CH_3/HS(CH_2)_7CH_2Br$ or a ratio of 10 to 1 of monolayers assembled from $HS(CH_2)_{11}CH_3/HS(CH_2)_2CH_2Br$), the alkyl bromides were buried within the monolayer. In the first example, the reaction went to only 59% conversion in 3 h, and in the second example, the conversion was only 5% in 3 h. Clearly, the reaction between *n*-propyl amine and the monolayers were slowed due to inability of the amine to do a backside attack on the C-Br bond.

These results indicate that the displacement of a Br with an amine will be rapid for alkyl bromides only at the surface and those that are buried within the polymer will be much less reactive. To study this reaction, an amine with a CF_3 group (molecule **A** in Figure 31) was used. This molecule was chosen because it contains fluorines that can be readily detected by XPS; yet, it will have similar reactivities to other alkyl amines.

Initial studies of the reaction between PDCPD-Br and **A** were carried out to determine how quickly surface alkyl bromides reacted with **A**. In Table 4, the atomic compositions measured by XPS are shown for various times for the exposure of the surface to molecule **A** dissolved in DMF. The surface was washed with copious amounts of organic solvents to remove any residual **A** that was not bonded to the surface. Only the survey scans and a high resolution scan of the carbon region were measured for each surface due to surface decomposition as the high resolution scans were acquired.

This decomposition was reported by others and was noticed in this work because the atomic compositions of the same surface were different depending on the order of acquisition of high resolution scans when carbon, fluorine, bromide, and silicon were obtained.[402] No noticeable decomposition was observed for the survey scans. The percent of fluorine measured from the survey scan versus the amount of time PDCPD-Br was exposed to the amine was plotted as shown in Figure 30. Clearly, the reaction was mostly complete within 4 h, although the amount of F continued to rise even at 88 h. These results were consistent with the results found by Murray for the reaction of bromide-terminated monolayers on Au clusters and freely dissolved amines.[403]

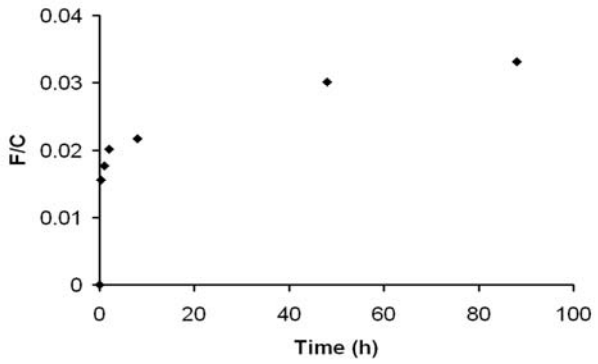

Figure 30 The F to C ratio for PDCPD-amine surfaces as a function of time PDCPD-Br was exposed to PDCPD-Br.

Only the surface alkyl bromides reacted and the fluorine was found as a monolayer on the surface rather than in the bulk near the surface. There are three pieces of evidence to support this assertion. First, the ATR-IR spectra of PDCPD-amine appeared unchanged from PDCPD-Br. If all of the alkyl bromides had reacted, the Csp^2-H peak would have grown in intensity along with an appearance of an aromatic C=C peak.

Table 4 XPS results from a variety of surfaces.

		[a]Atomic % Composition				[b]Carbon % Region		
	[c]Time	C	O	Br	F	C-C	C-Br	CF_3
PDCPD		98.6	0.9	0.0	0.0	100.0	0.0	0.00
PDCPD-Br		82.1	3.9	13.9	0.0	70.1	29.9	0.00
PDCPD-Amine	(20 min)	77.3	4.1	17.4	1.2	67.6	31.7	0.70
PDCPD-Amine	(1 h)	79.4	3.9	15.3	1.4	71.9	27.6	0.40
PDCPD-Amine	(2 h)	74.4	5.5	18.0	1.5	68.3	31.2	0.45
PDCPD-Amine	(8 h)	78.3	5.4	14.6	1.7	68.4	30.9	0.73
PDCPD-Amine	(48 h)	76.4	4.9	16.4	2.3	69.4	29.8	0.83
PDCPD-Amine	(88 h)	75.5	7.9	14.1	2.5	68.9	30.3	0.80

a Atomic compositions survey scans. b Atomic compositions from high resolution scans of the carbon region. c The time PDCPD-Br was exposed to the amine shown in Figure 27.

ATR-IR spectroscopy images the top 100 to 200 nm of a polymeric surface so a large increase in molecule **A** bonded to the surface and subsurface alkyl bromides would have been noticeable, but if molecule **A** only reacted with surface alkyl bromides the ATR-IR micrograph would be unchanged. A second piece of evidence was that the amount of Br in the XPS spectra for PDCPD-amine was similar to that found for PDCPD-Br. XPS is very sensitive to the top several nanometers of a surface; thus, it is an excellent technique for finding surface compositions. This analysis indicated that much of the alkyl bromides in the top ten nanometers did not react.

The most compelling piece of evidence for the location of molecule **A** on the surface is found by measuring the ratio of the peak area, Ap, to the background height, B, measured 30 eV below the peak energy in an XPS spectrum (Figure 31). This method was developed by Tougaard to investigate whether an atom is present only on the surface (Ap/B >30 eV), is uniformly distributed (Ap/B = 25 eV), or is localized beneath the surface (Ap/B <20 eV).[404-406] To test the validity of this method the Br peak in PDCPD-Br was examined (Figure 31a). The value for Ap/B was found to be 23.7 eV, which agrees with the prediction that Br is uniformly distributed as expected from the ATR-IR and XPS micrographs. To learn whether the fluorine was found only on the surface, PDCPD-Br was exposed to molecule **A** for 24 h and then studied by XPS. The value for Ap/B was found to be 109.8 eV, which was a high number in this analysis and provided critical evidence that the CF_3 group is found only on the surface and is not buried within the polymer.

Because molecule **A** is found only on the surface, an estimate for its surface coverage can be found by XPS. Approximately 1.37 molecules of A were found per nm^2; the calculations can be found in the supporting information. This result can be compared to the density of monolayers found on Au to provide a framework for understand the density of **A** on PDCPD. For instance, when a monolayer of $HSCH_2Ph$ on Au was

studied, the average density of the molecule was found to be 4.9 molecules nm^{-2}.[407] This value represents an upper limit for monolayers of this structure and clearly demonstrates

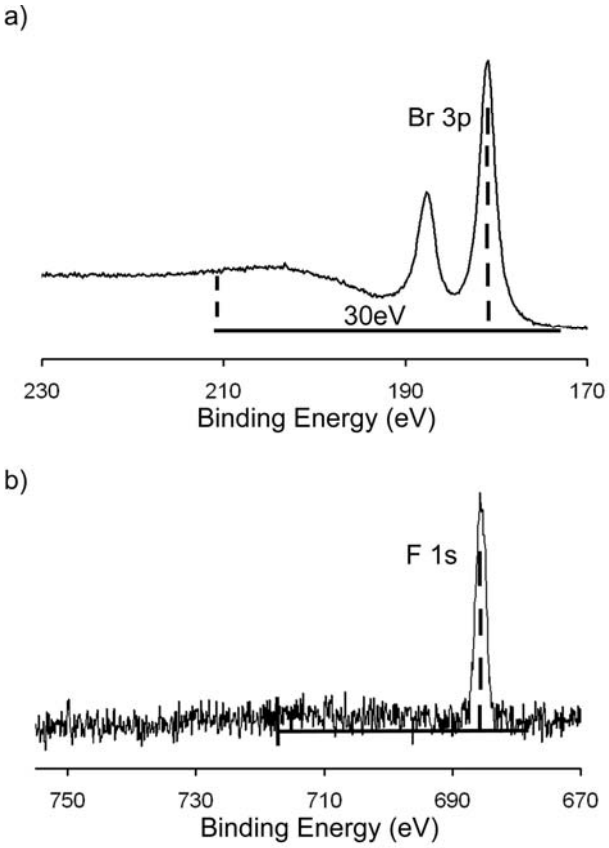

Figure 31 XPS spectra a) The high resolution scan of Br (3p) to demonstrate the increase in the background at higher binding energies. b) The high resolution scan of F (1s) does not show an appreciable increase the background for higher binding energies.

that our monolayers were less than a full monolayer and are better described as submonolayers.

These results make it possible to offer an interpretation of the curve in Figure 30. At short times of less than 4 h, the most sterically accessible alkyl bromides reacted with amines. The gradual increase of the F to C ratio at longer times indicates that some of the less sterically accessible surface alkyl bromides or, possibly, some that were buried near

the surface, reacted with the amines. The latter alkyl bromides were slower to react due to steric crowding that hindered the S_N2 reaction.

Patterning of Amines on PDCPD.

The formation of monolayers is important, but they must be patterned for many applications. To address this issue, PDCPD-Br was patterned with amines using polydimethylsiloxane (PDMS) slabs common in soft lithography.[296,299-301,408-411] A PDMS slab patterned in bas-relief was placed onto a flat surface of PDCPD and a solution of tris(2-aminoethyl)amine was flown through it for 16 h. After removal of the PDMS slab and copious washing with organic solvents, the sample was imaged by SEM. Initially, the pattern was challenging to observe because an organic monolayer on an organic polymer can have poor contrast.

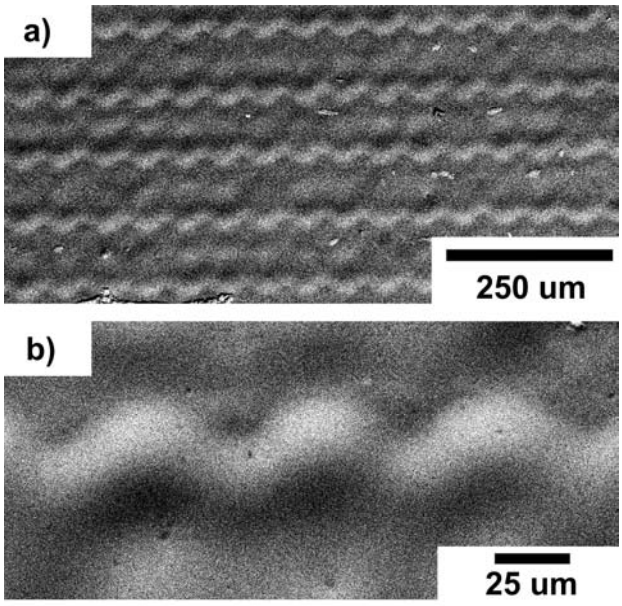

Figure 32 SEM micrographs of wavy lines patterned by soft lithography onto PDCPD.

To improve the contrast, the patterned sample was completely immersed into a solution of $CuBr_2$ in methanol prior to imaging by SEM. Cu(II) bonds well to the ligand that was patterned on the surface, and it would provide better contrast in the SEM micrographs. Because the entire polymer sample was exposed to $CuBr_2$ but only the monolayer was patterned, any contrast can be attributed to the formation of a monolayer of the amine. In Figure 32, SEM micrographs clearly show that the sample was patterned.

Conclusions

Due to its increasing importance, we developed the first method to assemble and pattern organic monolayers on PDCPD. This polymer has many attractive physical properties – such as high toughness, high corrosion resistance, optical transparency, and high impact resistance – and a low cost such that a variety of applications is possible. We assembled the first well characterized monolayers on this polymer using inexpensive reagents under reasonable periods of time. The reaction with Br_2 is complete in seconds, and the subsequent reaction with amines takes longer times but provides a monolayer in under 4 h. It is important to note that although we did not demonstrate it, our method is compatible with a wide variety of amines that expose different functional groups. Because many molecules that others attach to a variety of surfaces use amines as the linker, the flexibility of our method is important because it can be applied in many fields.

The monolayers assembled with this method were not densely packed; rather, they were at a density approximately 28% times less than a well-packed monolayer on a coinage metal. The low density of monolayers was attributed to incomplete reaction of surface carbon-bromide bonds that are not orientated correctly for a S_N2 reaction with an amine in solution, partial oxidation of the olefins resulting in a lower value for the density of carbon-bromide bonds, and the lack of a crystalline, dense arrangement of C-Br bonds on the surface. These limitations did not seem to have simple solutions, but are rather

limitations in working with this material. Regardless, these monolayers are dense enough for many applications where a full monolayer is not needed or even desired.

Experimental

Materials and Instruments.

Grubbs' 2nd Generation catalyst (Sigma Aldrich), dichloromethane (Fisher), bromine (Fisher), 4-(trifluoromethyl)benzylamine (Sigma Aldrich), tris(2-aminoethyl)amine (Fisher), and dicyclopentadiene >95% (Fluka) were used as received with no further purification.

SEM images where taken on an Hitachi S3400 SEM in variable pressure mode with a back scattered detector at pressures between 30 and 60 Pa and accelerating voltage of 15 KV. XPS spectra were recorded on an Axis Ultra using Al kα X-ray source at a 90° take off angle. Samples where placed in the sample exchange chamber until out gassing of any residual solvent or gas had diminished. Survey spectra were recorded at 1 eV intervals with a dwell time of 200 ms. High resolution spectra taken at 0.1 eV intervals with a dwell time of 1000 ms. ATR-IR spectra were recorded on a Brucker Tensor 27 with a liquid nitrogen cooled MCT detector. The samples where mounted on a Harrick GATR accessory. The ATR-IR spectra where taken at a resolution of 4 cm^{-1} for 1024 scans.

Synthesis of PDCPD.

10 mL of DCPD heated to 55 °C was mixed with 3.2 mg of Grubbs' 2nd generation catalyst dissolved in 100 μL of dichloromethane. This sample was transferred to a glass petri dish and filled to depth of 1-2 mm before being placed in a glass desiccator. The desiccator was placed under vacuum and backfilled with nitrogen three times to remove oxygen. It was then placed in oven at 80 ^{o}C for 30 minuets. Polydicyclopentadiene (PDCPD) was cut into pieces for use in experiments. Thin films,

for use in patterning, was cast as a solution prepared as above between two microscope slides and heated on a hot plate until cured. The slides were separated leaving the film behind on one of the slides.

Bromination of PDCPD.

PDCPD was immersed in 1 M bromine solution in THF for several seconds. Upon removal, the surface was rinsed with copious amounts of acetone. Exposure of PDCPD for greater than 30 sec caused the polymer to become dark and crack.

Reactions of PDCPD-Br with Amine.

A solution of 100 μL of 4-(trifluoromethyl)benzylamine in 10 ml DMF was prepared prior to reaction. PDCPD-Br was immersed into this solution for different times. The sample was washed with copious amounts of methanol and dried under a stream of nitrogen after removal from the solution.

Patterning of PDCPD.

Thin films of PDCPD-Br were prepared as described above. A slab of polydimethylsiloxane (PDMS) patterned in bas-relief to form microfluidic channels was placed on the surface. A solution of 0.5 ml tris(2-aminoethyl)amine in 10 mL of DMF was flown through the microfluidic channels for 16 hours at a flow rate of 500 μL h^{-1} with a syringe pump. The channels were flushed with DMF for 1 h before removal of the PDMS. These samples were of an organic monolayer on an organic polymer so the contrast under SEM was poor. To enhance the contrast, the patterned samples were completely immersed in a 0.1 M solution of $CuBr_2$ for 1 h, followed by washing with copious amounts of water.

Supporting Information Available.

Estimation of the surface coverage of the amine and the depth penetration of ATR-IR spectroscopy can be found in the supporting information in Appendix B.

CONCLUSION

Monolayers on silicon are important targets for the integration of semiconductor technology and chemistry. Some of the issues that we addressed that are necessary for monolayers on silicon to be useful to many scientists are their long term stability, what functional groups can be displayed on their surface, and whether they can be patterned.

The long term stability of monolayers on silicon has yet to be achieved. To be used in many applications, monolayers will have to be stable for months when exposed to atmospheric conditions. Monolayers that we assembled started to degrade by oxidation over several days when exposed to organic solvents. These monolayers showed an eventual degradation by oxidation, particularly in the presence of water.

The underlying concept that limits the stability of these monolayers is that their formation is a kinetic process. Once a reaction has occurred between a surface hydride and organic molecule, the molecule will not equilibrate between surface Si atoms. The radical mechanism for formation of a monolayer by a random walk on the surface is likely to create pinhole defects. These pinhole defects have been observed by electrical measurements through changes in impedance. The step-flow mechanism to assemble organic monolayers on silicon(111) is a contrast to monolayer formation of thiols on gold, which is a thermodynamic process under equilibrium conditions. SAMs on gold are well ordered and mostly free of defects that hinder their application. With a kinetic process any defects that form will persist.

The formation of silicon oxide is thermodynamically favored so any monolayers formed on silicon are inherently unstable. To prevent monolayers on silicon from degrading, the monolayer must be impenetrable to any molecules that cause silicon to oxidize. By contrast, monolayers on gold and diamond do not suffer this drawback as they do not oxidize.

The crystalline packing of the alkyl chains on silicon is critically important. The spacing of silicon atoms on the surface (3.84 Å) relative to the size of alkyl chains (4.2 Å) means that not all silicon atoms can be capped with an alkyl group and reactive hydrides will always be present. These silicon hydrides can react with small molecules that diffuse through the monolayer. Water can react with silicon hydrides to form hydroxyls that introduce disorder and lead to a layer of silicon oxide. Once formed, these defects can grow and degrade the monolayer. Oxidation of the silicon substrate alters its electrical properties, and this degradation has hindered the use of these monolayers in electronic devices.

To slow surface oxidation on silicon, denser monolayers should be assembled. However, because of the size of the alkyl chains (4.2Å) relative to the inter-silicon distance (3.84Å), it will never be possible to cap all the silicon hydrides on the surface.

One possible route to increase monolayer coverage that we briefly studied is the use of dendrimers to add steric bulk to the surface. Ester terminated monolayers generated by UV light[412] were previously reported, and we showed that it was possible to react these surface esters with amines to yield amides. A diamine reacted with the surface esters, and exposed a free amine on the surface. These amines can then be further reacted with methyl methacrylate through a Michael addition to yield a new ester terminated surface; each amine may undergo two Michael additions. This process can be repeated to increase the density of the monolayer. By using long alkyl chain diamines, the density of hydrophobic alkyl chains can be increased. We believe that this approach may cover defects to protect these sites from oxidation. Our preliminary work indicates this could be an interesting approach to address this problem.

The functionalization of surfaces will be important for potential applications of silicon monolayers, and carboxylic acids are a useful terminal group because of their various reactions. We demonstrated the ability to form carboxylic-acid terminated monolayers directly on a silicon surface. These monolayers were shown to be attached

through the olefin and not the acid group. These surfaces were modified by forming amides via an activated anhydride as observed by contact angle goniometry and IR spectroscopy. Reactions with amines are significant because they can be used to anchor important molecules, such as proteins or DNA, for the use in biosensors.

Mixed monolayers containing two different functional groups are one approach to protect the surface and incorporate useful functional groups. A thick alkane layer can protect the surface from oxidation and a second molecule with a different functional group can be assembled at the same time. Alkanes with diverse functional groups tend to occupy a different spatial conformation than alkyl chains, leading to disordered packing and a loss of surface protection from oxidation. This problem is alleviated with mixed monolayers. Mixed monolayers also have the added advantage that they reduce the steric crowding around the functional group, making them more accessible to reagents in further steps. We made mixed monolayers of methyl and olefin terminated surfaces. The olefin was accessible to react with Grubbs 1st generation catalyst, and it was possible to do both cross metathesis and ROMP to add new molecules to the surface. The Grubbs catalyst was tolerant towards many functional groups and opened up a range of molecules that could be exposed on a surface. This versatility was exploited in our work to pattern surfaces by performing two different reactions with the same catalyst on different regions of the surface.

Simple patterning was possible with PDMS microfluidic devices laminated to a surface. The limitations of the patterns were due to the fabrication method of the masters by rapid prototyping which resulted in rough edges along the inside of the channels. The edges of patterned surface exhibited the same roughness as the PDMS microchannels which demonstrated that the pattern conformed well to the stamp. We combined our different functionalization methods with this patterning technique to selectively functionalize the surface with micron-sized patterns.

Most importantly, we demonstrated a new soft lithographic technique, PENs, to pattern a silicon monolayer. By exploiting the reactivity of the Si-O bonds in PDMS, it was possible to controllably etch PDMS using fluoride containing species. We patterned polymer lines with widths from tens of nanometer to several microns. The lower limit of this technique was not found due to the difficulty in visualizing the resulting patterns with the chemistry that we used. Further work on this technique could involve the adaptation of this technique to another surface or to use an alternative set of reactions.

We demonstrated methods to functionalize the surface of polydicylcopentadiene. PDCPD has generated interest because it can be synthesized to a highly cross-linked network with the Grubbs catalyst, and it has a high concentration of double bonds throughout the polymer. Double bonds were exploited to functionalize the surface by using an intermediate alkyl bromide. The addition of bromine to double bonds was a rapid reaction that led to extensive bromination of the polymer. The bromide could be displaced in a substitution reaction on the surface by amines. Examination by XPS gave an estimated coverage of 0.9595 amines per nm^2 representing a 28% coverage compared to a reported phenyl monolayer on gold. PDMS was patterned with tris(2-aminoethyl)amine using a PDMS microfluidic device with dimensions in the tens of microns. Because of the similarity of PDCPD to the monolayer, the patterned region was decorated with copper to aid visualization by SEM.

Further work may be to explore the potential uses of surface functionalized PDCPD. It is anticipated that this hybrid material will have interesting properties in the gating of molecules through a PDCPD matrix. PDCPD thimbles have been used to perform site isolation reactions,[413] by adding certain functional groups it may be possible to alter which molecules diffuse through PDCPD. Surface functionalization can be used to add a layer of PEI that can be protonated and deprotonated. It is expected that this protonation will alter the diffusion properties through the layer. A dense amine

containing layer will also trap metals such as copper, preventing their diffusion. This increased control would be useful in development of site isolation reactions.

APPENDIX A CROSS METATHESIS ON OLEFIN-TERMINATED MONOLAYERS ON SI(111) USING THE GRUBBS' CATALYST

Abstract:

This appendix reports the functionalization and patterning of olefin-terminated monolayers on Si(111) through cross metathesis. A simple, one-step synthesis of a diolefin – CH_2=$CH(CH_2)_9O(CH_2)_9CH$=CH_2 – was developed from commercially available starting materials. Mixed partially olefin-terminated monolayers of this novel diolefin and 1-octadecene on hydrogen-terminated Si(111) were obtained. The olefins are raised above the rest of the monolayer and thus sterically accessible for further functionalization. Olefin-terminated monolayers were reacted with the Grubbs' first generation catalyst and olefins in solution that were terminated with fluorines, carboxylic acids, alcohols, aldehydes, and alkyl bromides. Characterization of these monolayers using X-ray photoelectron spectroscopy and horizontal attenuated total reflection infrared spectroscopy demonstrated that olefins on the surface had reacted via cross metathesis to expose fluorines, carboxylic acids, aldehydes, alcohols, and bromides. Through calibration experiments, we demonstrated a simple 1:1 correspondence between the ratio of olefins in solution used in the assembly and the final composition of the mixed monolayers. Finally, these monolayers on silicon were patterned on the micrometer-size scale by soft lithography using microfluidic channels patterned into PDMS stamps. Micrometer-wide lines of polymer brushes were synthesized on these monolayers and characterized by scanning electron microscopy. In addition, olefin-terminated monolayers were patterned into micrometer-sized lines exposing carboxylic acids by cross metathesis with olefins in solution. This method of patterning is broadly applicable and can find applications in a variety of fields including the development of biosensors and nanoelectronics.

Introduction

The field of monolayers on silicon is growing rapidly as new, mild methods for their assembly have been recently reported.[121,226-228,234-236,248,252-254,263,264,267,270,271,279,331-333,335,336,366,414-419] Self-assembled monolayers (SAMs) on silicon are an important area of research as they combine the selectivity of organic chemistry with the terrific electronic properties of silicon. For instance, new sensors that expose DNA, proteins, carbohydrates, porphyrins, or other biologically relevant functional groups on the surface of monolayers on silicon have been reported.[234,251-253,259,260,332,333] These sensors offer new possibilities to exploit the opportunities of combining biotechnology with silicon technology and will open up new avenues in science and technology.

Despite these advances, methods to assemble monolayers on silicon are intolerant of most functional groups or require multiple gram quantities of starting materials that make them impractical for the synthesis and assembly of complex, expensive molecules. Methods to assemble monolayers on silicon begin with hydrogen-terminated Si(111); this surface is unstable and readily oxidizes to form a thin layer of SiO_x on the surface.[281,282,420] Although crystalline monolayers on silicon protect it from oxidation, the assembly is slow such that side reactions between hydrogen-terminated Si(111) and most functional groups limits what can be displayed. The most successful approach around this problem is to first assemble an ordered monolayer and functionalize it in a second step.[121,226-228,234-236,248,252-254,263,264,267,270,271,279,331-333,335,336,366,414-419] In this paper we report a new, versatile approach that uses cross metathesis via the Grubbs' first generation catalyst to functionalize olefin-terminated monolayers on silicon with a wide variety of functional groups.

We and others recently reported mild methods to assemble well-ordered monolayers on Si(111) that can extend the range of functional groups displayed on its surface.[121,226-228,234-236,248,252-254,263,264,267,270,271,279,331-333,335,336,342,366,414-419,421] Monolayers on Si(111) that display esters, amides, alcohols, acids, alkyl halides, and acid chlorides

have been assembled and characterized. These monolayers are useful as they can be functionalized in subsequent steps, but important questions remain about their stabilities or whether these monolayers can be assembled over large areas. For instance, reports on acid-terminated monolayers demonstrated that they had limited stabilities in aqueous solvents or their stabilities were not reported.[248,249,257,259,260,279,421] Monolayers terminated with alkyl halides or acid chlorides were assembled by scribing silicon and yielded a monolayer covering a fraction of the area of a silicon wafer.[121,229,274,275,422] The field of monolayers on silicon would benefit greatly from more mild methods to assemble functional monolayers that protect the surface from oxidation.

We wished to assemble olefin-terminated monolayers as Si(111)-H is tolerant of this functional group and these olefins provide a useful functional group for further functionalization through cross metathesis (Scheme 1).[342,421] Cross metathesis is a simple reaction, the reaction between two terminal-olefins results in the formation of a double bond and the release of ethylene.[345,350-353,398,423-425] The release of ethylene can be used to drive this reaction to quantitative conversions. We choose to use the Grubbs' first generation catalyst as it is less sensitive to functional groups than those based on Ti, Mo, and W; it catalyzes cross metathesis reactions at low catalyst loadings; and it is over four times less expensive than the Grubbs' second generation catalyst.[345,350-353,398,423-425] This catalyst has been used to carry out cross metathesis reactions between proteins, carbohydrates, crown ethers, and numerous small molecules displaying acids, halides, alcohols, esters, amides, and amines.[345,350-353,398,423-425]

We and others have reported metathesis reactions on monolayers on gold, silicon dioxide, or silicon.[421,426-436] In most of these examples the Grubbs' catalyst was reacted with strained, cyclic olefins on a monolayer and used to grow polymer brushes from surfaces by ring opening metathesis polymerization (ROMP). In one example, crystalline monolayers of $HS(CH_2)_9CH=CH_2$ were assembled on gold and were reacted by cross metathesis with the Grubbs' second generation catalyst and olefins in solution.[437] These

monolayers were not patterned nor were the monolayers designed such that the olefins would be sterically accessible to react with the Grubbs' catalyst.

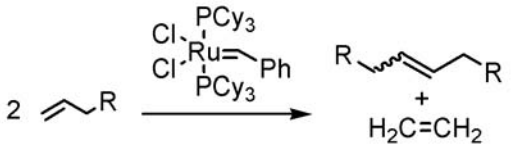

Figure A-1 An example of cross metathesis between two olefins and catalyzed by the Grubbs' first generation catalyst.

In previous work we showed that monolayers assembled from 1-octadecene and trace amounts of TEMPO-C_{10} (see Figure 1 for the structure of TEMPO-C_{10}) were stable and protected the silicon surface from oxidation upon exposure to ambient conditions for over two months, water at room temperature for over 20 days, chloroform at room temperature for over 14 days, and refluxing chloroform for over 4 days.[342] These results are critical as they show that these monolayers are stable enough to have practical applications in fields such as biochemistry, sensors, and tribology. Although these monolayers are crystalline and stable under a variety of conditions, being terminated with methyl groups limits their use, especially with respect to further functionalization.

In this paper we report the assembly of mixed monolayers of 1-octadecene and CH_2=$CH(CH_2)_9O(CH_2)_9CH$=CH_2, **A** (Figure 1). We designed **A** as a suitable precursor to assemble monolayers as it is easy to synthesize in one step from commercially available starting materials and it assembles into monolayers that are thicker than those assembled from 1-octadecene. The latter point is important: mixed monolayer of **A** and

1-octadecene will expose olefins on the monolayers above the methyl groups. Thus, the olefins will be easily accessible to react with the Grubbs' catalyst.

In this paper we will describe the straightforward, one-step synthesis of **A** and the assembly and characterization of mixed monolayers of **A** with 1-octadecene. These monolayers were characterized by X-ray photoelectron spectroscopy (XPS) and horizontal attenuated total reflection infrared spectroscopy (HATR-IR spectroscopy). In addition, we will describe our results for the functionalization of olefin-terminated monolayers with the Grubbs' first generation catalyst to yield monolayers terminated with acids, aldehydes, bromides, and alcohols. Finally, we will report mild methods to grow polymers from these monolayers and their patterning on the micrometer size scale.

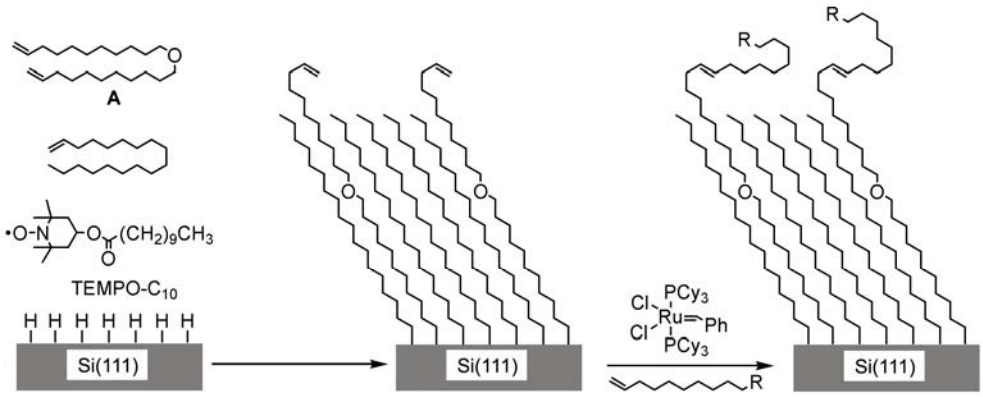

Figure A-2 Our method to assemble and functionalize olefin-terminated monolayers by cross metathesis. A silicon wafer with a native layer of SiO_x was cleaned and then placed in Ar purged 40% H_4NF for 30 min to form a hydrogen-terminated Si(111) surface. The wafer was immediately immersed in a solution of **A**, 1-octadecene, and trace amounts of TEMPO-C_{10} for 24 h. Cross metathesis between olefin-terminated monolayers and olefins with different "R" groups including carboxylic acids, alcohols, bromides, and aldehydes was catalyzed by the ruthenium-based Grubbs' first generation catalyst.

Experimental Section

Materials and Methods.

1-Octadecene (90%), 10-undecenoic acid (98%), 10-undecen-1-ol (99%), 10-undecenal (97%), 11-bromo-1-undecene (95%), 1,6-dichlorohexane (95%), 1-undecanol (98%), potassium *tert*-butoxide, 5-norbornene-2-carboxylic acid (98%), and 48% hydrofluoric acid were purchased from Acros or Aldrich and used as received. 40% NH_4F was purchased from J.T. Baker and used as received. All solvents were purchased from Acros and used as received. Single-side polished Si(111) wafers (n-type) were purchased from Silicon Inc, Boise, Idaho.

TEMPO-C_{10} was synthesized as described in a previous paper.[342,421] It was stored in a -30 ºC freezer in a glove box under N_2. 1-Octadecene and 10-undecenoic acid were distilled with a Vigreux column under reduced pressure. Typically, 500 mL were distilled and the middle third of the fractional distillation was used. The collected fraction was transferred to a Kontes flask. The Kontes flask was evacuated under reduced pressure for 48 h and back filled with N_2, this process was repeated three times. The Kontes flask was stored in the glove box.

Instrumentation

^1H and ^{13}C were recorded on a Bruker DPX 300 using $CDCl_3$. The solvent signal was used as internal standard.

X-ray Photoelectron Spectroscopy (XPS). X-ray photoelectron spectra were obtained on a Kartos Axis Ultra Imaging spectrometer. Spectra of C(1s) (275-295 eV binding energy), O(1s) (525-545 eV binding energy), F(1s) (675-695 eV binding energy), Si(2p) (90-110 eV binding energy), Cl(2p) (190-210 eV binding energy), and Br(3d) (60-70 eV binding energy) as well as survey scans (0-1100 eV) were recorded with a tilt angle of 45°. The atomic compositions were corrected for atomic sensitivities and

measured from high-resolution scans. The atomic sensitivities were 1.000 for F(1s), 0.780 for O(1s), 0.278 for C(1s), 0.328 for Si(2p), 0.891 for Cl(2p), and 1.055 for Br(3d).

Horizontal Attenuated Total Reflectance Infrared Spectroscopy

These spectra were recorded using a Bruker Tensor 27 equipped with an MCT detector cooled with liquid nitrogen. Monolayers were assembled on Si(111) HATR crystals with dimensions of 80X10X5 mm. The crystals were mounted in a dry air purged sample chamber. Background spectra were performed using freshly oxidized surfaces of HATR crystals. Scans were measured at a resolution of 4.0 cm^{-1} or 2.0 cm^{-1}.

Scanning Electron Microscopy

Si(111) shards that were patterned as shown in Figure 12 were examined with a Hitachi S-4000 Scanning Electron Microscope. Typically, an accelerating voltage of 5 kV was used to image the patterns on the surface.

Synthesis of 11,11/-Oxybis-1-undecene (A)

10-Undecen-1-ol (60 g, 0.352 mol), triethyl amine (28.4 g, 0.281 mol), and *p*-tolulenesulfonyl chloride (26.8 g, 0.140 mol) were stirred under nitrogen at room temperature for 24 h in 360 mL of THF. Potassium *tert*-butoxide (39.4 g, 0.352 mol) was added to the reaction mixture and stirred for 7 h. The solvent was evaporated and the product was extracted with methylene chloride. After evaporation the product was distilled as a colorless oil under vacuum at 200 °C and stored in a -30 °C freezer in a glove box. Yield: 61%. ^{1}H NMR (300 MHz, $CDCl_3$, ppm): δ 5.82 (2H, m), 4.96 (4H, m), 3.38 (4H, t, J = 6.9 Hz), 2.02 (4H, q, J = 6 Hz), 1.54 (4H, m), 1.28 (24H, m). ^{13}C NMR (300 MHz, $CDCl_3$, ppm): 138.9, 114.0, 70.8, 33.7, 29.7, 29.4 (3 peaks), 29.0, 28.8, 26.1.

Synthesis of $CH_2=CH(CH_2)_9O(CH_2)_{10}CH_3$

In a round bottom flask, 1-undecanol (58.3 g, 0.154 mol) and potassium *tert*-butoxide (38.0 g, 0.339 mol) were added under nitrogen to 250 mL of THF. The solution turned yellow and cloudy. 11-Bromo-1-undecene (35.9 g, 0.154 mol) was added and the mixture was refluxed under nitrogen. The product was isolated as a clear liquid by distillation under vacuum at 200 °C and stored in a -30 °C freezer in a glove box. Yield: 44%. ^{1}H NMR (300 MHz, $CDCl_3$, ppm): δ 5.76 (1H, m), 4.92 (2H, m), 3.36 (4H, t, J = 6 Hz), 1.99 (2H, m), 1.52-1.25 (32H, m), 0.85 (3H, t, J = 6 Hz). ^{13}C NMR (300 MHz, $CDCl_3$, ppm): δ 139.2, 114.0, 70.9, 33.8, 31.9, 29.8, 29.6, 29.5, 29.4 (4 peaks), 29.3, 29.1, 28.9, 26.2, 22.7, 14.1.

Synthesis of $CH_2=CH(CH_2)_9O(CH_2)_6Cl$

In a round bottom flask, 10-undecen-1-ol (26.5 g, 0.156 mol) and potassium *tert*-butoxide (20.9 g, 0.339 mol) were added under nitrogen to 450 mL of THF. 1,6-Dichlorohexane (72.4 g, 0.467 mol) was added and the mixture was refluxed under nitrogen. The solvent was removed by evaporation and the product was extracted with methylene chloride from water. The product was purified by column chromatography with 3% ethyl acetate/97% hexane. Yield: 22%. ^{1}H NMR (300 MHz, $CDCl_3$, ppm): δ 5.79 (1H, m), 4.94 (2H, m), 3.46 (2H, t, J = 6 Hz), 3.34 (4H, m), 1.97 (2H, m), 1.71 (2H, m), 1.52-1.33 (20H, m). ^{13}C NMR (300 MHz, $CDCl_3$, ppm): δ 138.8, 113.9, 70.7, 70.4, 44.7, 33.6, 32.4, 29.6, 29.3 (4 peaks), 28.9, 28.7, 26.5, 26.0, 25.3.

Assembly of Mixed Monolayers of 11,11/-Oxybis-1-undecene and 1-Octadecene

Silicon(111) shards cleaned with a nitrogen gun and rinsed with hexane, acetone, and methanol. The wafers were etched in 1:5 (v/v) of 48% HF/40% NH_4F solution for 30 sec.

The wafers were oxidized with 1:3 v/v of H_2O_2:H_2SO_4 for 1 h at 90 °C. *Caution*: *Pirhana solution is highly dangerous and should be handled with care.* The oxidized wafers were washed with water. The wafers were then etched with 40% NH_4F for 30 min under an atmosphere of argon. This process yielded hydrogen-terminated silicon(111). The wafer was dried with a nitrogen gun and immediately transferred to a glove box.

The shards were immersed in solution of 11,11′-oxybis-1-undecene and 1-octadecene with 0.1 mole% of TEMPO-C_{10} in the glove box. Typically, a mixed monolayer with a 1:1 mole ratio of 11,11′-oxybis-1-undecene / 1-octadecene was assembled on the hydrogen-terminated Si(111) shards by mixing 11,11′-oxybis-1-undecene (3 mL, 2.3 g, 7.0 mmol) and 1-octadecene (2.34 mL, 1.84 g, 7.0 mmol) with 0.1 mole% of TEMPO-C_{10} (0.005 g, 0.007 mmol). The wafer was sealed in a Schlenk flask under nitrogen for 24 h. After 24 h, the shards were washed with various solvents and sonicated with CH_2Cl_2.

Representative Procedure for Cross-Metathesis on Mixed Monolayers

A Si(111) shard with an olefin-terminated monolayer, Grubbs' first generation catalyst (0.054 g, 0.06 mmol), CH_2Cl_2 (3 mL), and 10-undecenoic acid (1 mL, 5.4 mmol) were added to a round bottom flask in a glove box. The flask was fitted with a reflux condenser and removed from the glovebox and attached to a nitrogen line. The reaction was refluxed under nitrogen for 48 h. The wafer was taken out and washed with hexanes, acetone and methanol. The yield of the cross-metathesis reaction was determined by ^{1}H NMR. These conditions always gave a yield of 100%. ^{1}H NMR (300 MHz, $CDCl_3$, ppm): δ 5.36 (2H, br), 2.34 (4H, t, J = 6 Hz), 1.98 (4H, m), 1.60 (4H, m), 1.29 (20H, br).

Patterning Brush Polymers using Soft Lithography

Typically, an olefin-terminated monolayer on a Si(111) shard was treated with a solution of Grubbs' first generation catalyst in methylene chloride for 30 min under ambient conditions. Next, the wafer was washed with methylene chloride and dried with nitrogen. A polydimethylsiloxane (PDMS) stamp patterned in bas-relief was then pressed onto the surface and a solution of 5-norbornene-2-carboxylic acid (0.01 g mL^{-1}) in DMF was passed through the microchannels with a syringe pump for 1 h at the rate of 200 μL h^{-1}. The channels were then flushed with DMF for 1 h. The PDMS stamp was then removed, rotated at an angle and the process was repeated. The wafer was washed with copious amounts of organic solvents and dried with nitrogen.

Results and Discussion

Assembly of Mixed Monolayers of 1-Octadecene and a Diolefin

We developed a simple, one pot synthesis of **A** from commercially available starting materials (Figure 2). This method was used to synthesize up to 56 grams of **A** that was readily cleaned by distillation. The full synthesis of **A** is described in the experimental section.

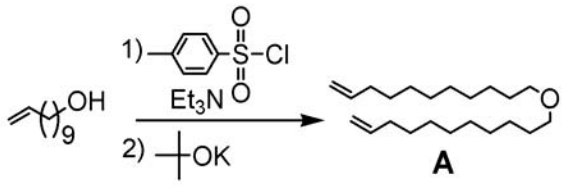

Figure A-3 One-step synthesis of **A** from commercially available starting materials.

Characterization of Monolayers of 1-Octadecene and **A**

Our method to assemble monolayers on Si(111) is shown in Figure 1. Higashi et al. reported a simple method to form hydrogen-terminated Si(111) with minimal defects (<1%).[281,282,420] Hydrogen-terminated Si(111) is air and water sensitive as it will readily oxidize to form a thin layer of silicon dioxide on the surface; however, well-ordered monolayers on Si(111) protect the surface from oxidation in air and solvents for days to months.[226,227,265,414] We used Higashi's method to form hydrogen-terminated Si(111) and then placed the wafer in mixtures of 1-octadecene, **A**, and TEMPO-C_{10}.

We characterized hydrogen-terminated Si(111) by horizontal attenuated total reflection infrared (HATR-IR) spectroscopy (Figure 3). The Si(111)-H bonds are perpendicular to the surface and only IR-active with *p*-polarized light and are not seen with *s*-polarized light. Higashi et al. reported that the Si(111)-H peak appears at 2083.7 cm^{-1} with a narrow FWHM of 0.95 cm^{-1}.[281] Our hydrogen-terminated Si(111) surfaces are well-ordered as we observed one peak with *p*-polarized light at 2084 cm^{-1} with a FWHM of 3.8 cm^{-1} and no peaks with *s*-polarized light. Our results demonstrated that we formed a well-ordered hydrogen-terminated Si(111) surface.

To fully characterize monolayers multiple methods must be used. We characterized our monolayers by XPS and HATR-IR spectroscopy. From our previous work on the assembly of monolayers of 1-octadecene with TEMPO , we learned several important characteristics of these monolayers that are important for the interpretation of the characterization of the monolayers reported in this paper.[342,421] First, we know that this method results in the assembly of a monolayer with a thickness given by ellipsometry of approximately 1.8 nm. Second, the monolayer is almost entirely composed of 1-octadecene with less than 1 mole % of TEMPO on the surface. Third, although TEMPO is necessary for the assembly of a well-ordered monolayer, we do not know the mechanism of assembly or the role of TEMPO.

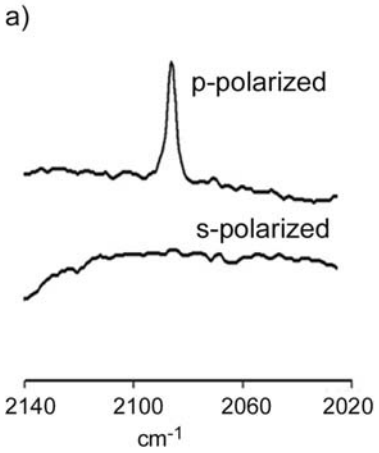

Figure A-4 The HATR-IR spectra of a hydrogen-terminated Si(111) surface under *p*- and *s*-polarized light. Di- and tri-hydrogen defects would appear at 2111, 2120, and 2139 cm^{-1} under both *p*- and *s*-polarized light.

In Table 1 and Figure 4 we show the XPS spectra of monolayers assembled from **A**. This surface was first characterized by a survey scan that showed the presence of Si, C, and O and high resolution scans of Si, C, O, and F. The region for F was examined as hydrogen-terminated Si(111) was formed in 40% H_4NF and we wished to look for the presence of Si-F or C-F bonds. The silicon region was interesting for what it did not show; we did not observe evidence for SiO_x. The bulk Si peak appears approximately 4 eV lower than the peak for SiO_x, and these peaks are thus easily separated and analyzed. We looked for SiO_x since unlike disordered monolayers well-ordered monolayers protect silicon from oxidation. The XPS samples were allowed to sit exposed to atmospheric conditions for 2 to 4 weeks prior to their characterization by XPS. If the monolayers were disordered the silicon surfaces would have oxidized during this time period. The lack of SiO_x in the XPS spectra indicates that well-ordered monolayers were assembled. The presence of a broad peak for O was consistent with our previous results for monolayers assembled from TEMPO-C_{10} and 1-octadecene. As there are many sources

for oxygen including the ether oxygen in **A**, the three oxygens in TEMPO-C_{10}, and SiO_x we can not make further assignments to this peak.

The C(1s) peak in the XPS spectra of monolayers assembled from 1-octadecene or **A** showed the presence of a Si-C bond and described the thickness of these monolayers. In a recent publication detailing the XPS characterization of organic monolayers on Si(111), Allongue et al. described the presence of a Si-C peak at binding energies approximately 0.9 eV lower than the main C-C peak.[438] They outlined how to use the integration of that peak relative to the integration of all carbon in the XPS to find a thickness for the monolayer. We fit the carbon peaks from monolayers assembled from 1-octadecene (Figure 5 b) or **A** (Figure 5a) using the values from Allongue et al. and found the presence of Si-C bonds. The Si-C peak from monolayers assembled only from 1-octadecene integrated to 4.1% of the total amount of carbon. This value gave a thickness for the monolayer of 20 Å which matches the predicted value for the monolayer and agreed well with the previously measured ellipsometric thickness of 18 Å.[342]

The C(1s) region in the XPS of monolayers assembled from **A** fit to three different peaks. The largest peak was assigned to the majority of the carbons on the monolayer. A smaller peak at a binding energy of 1.2 eV higher than the largest peak was assigned to the carbons next to the oxygen in **A**. This peak was not present in monolayers assembled from 1-octadecene as that molecule lacks an ether bond. Finally, a small peak at a binding energy 0.7 eV lower than the main carbon peak was assigned to carbon bonded to silicon. This peak integrated to 2.7 % of the total amount of carbon. Using the method of Allongue et al., this integration yielded a monolayer thickness of 25 Å.[438] This value agrees with predicted thicknesses for these monolayers and provides further evidence that an ordered monolayer was assembled.

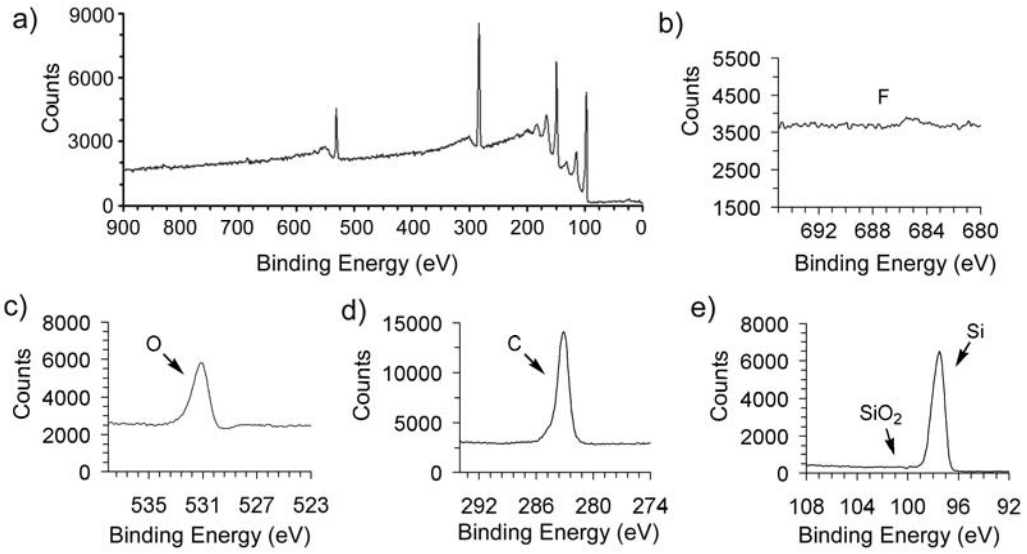

Figure A-5 The XPS of monolayers assembled from **A**. (a) A survey scan of this monolayer described the presence of C, O, and Si. High resolution scans of (b) F(1s); (c) O(1s); (d) C(1s); and (e) Si(2p) were obtained to find the compositions of these monolayers as described in Table 1.

The HATR-IR spectrum of a monolayer of 1-octadecene shows two important peaks (Figure 6). The peaks corresponding to the antisymmetric – $\nu_a(CH_2)$ – and symmetric – $\nu_s(CH_2)$ – stretches for methylene appear at 2920 and 2851 cm^{-1}. These results are significant as the $\nu_a(CH_2)$ peak for crystalline monolayers ranges from 2918 to 2920 cm^{-1} but for disordered monolayers it ranges from 2925 to 2928 cm^{-1}.[226,285,439] Similarly, the $\nu_s(CH_2)$ peak for crystalline monolayers appears at 2850 cm^{-1} but for disordered monolayers it appears at 2858 cm^{-1}.[226,285,439] The location of $\nu_a(CH_2)$ and $\nu_s(CH_2)$ peaks within these ranges describes the crystallinity of monolayers. Our results indicate that we assembled crystalline monolayers.

Table A-1 XPS and HATR-IR Spectroscopy of Monolayers on Si(111).

		[a]XPS Composition (%)				HATR-IR	
Entry	[b]Composition	C	Si	SiO_x	O	$\nu_a(CH_2)$ (cm^{-1})	$\nu_s(CH_2)$ (cm^{-1})
1	$CH_2=CH(CH_2)_{15}CH_3$	60	33	0	7.0	2920	2851
2	$CH_2=CH(CH_2)_9O(CH_2)_9CH=CH_2$	67	24	0	8.9	2925	2854
3	50% $CH_2=CH(CH_2)_{15}CH_3$/ 50% $CH_2=CH(CH_2)_9O(CH_2)_9CH=CH_2$	60	26	0	13	2924	2852
4	75% $CH_2=CH(CH_2)_{15}CH_3$/ 25% $CH_2=CH(CH_2)_9O(CH_2)_9CH=CH_2$	68	23	0	9	2924	2854
5	83% $CH_2=CH(CH_2)_{15}CH_3$/ 17% $CH_2=CH(CH_2)_9O(CH_2)_9CH=CH_2$	67	26	0	7	2923	2854
6	$CH_2=CH(CH_2)_9O(CH_2)_{10}CH_3$	c	c	c	C	2925	2854

[a]These compositions are from high resolution scans. We studied the C(1s), Si(2p), and O(1s) peaks. The peak for SiO_x appeared at 102 eV in the Si(2p) high resolution scan.

[b]This column refers to the composition of reagents used to assemble the monolayers. All monolayers were assembled in the presence of 0.1 mole % TEMPO-C_{10}. For monolayers assembled from two components, we list the mole % of each olefin that was used. [c]The XPS compositions of this monolayer was not determined.

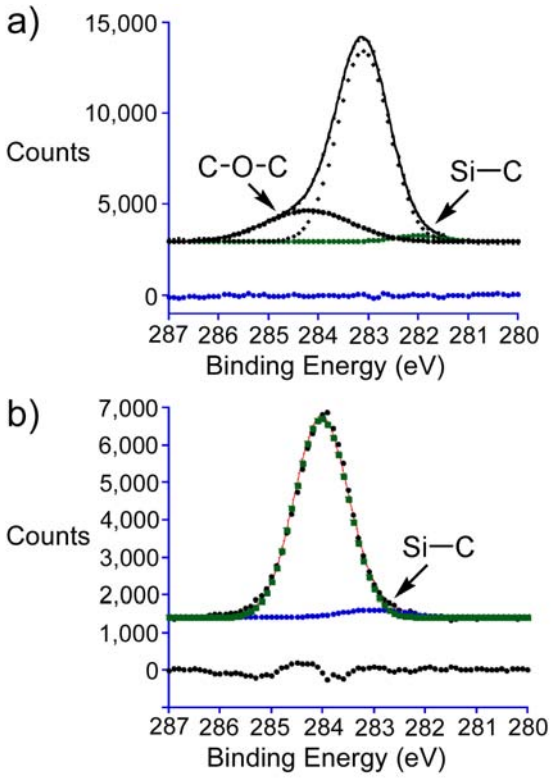

Figure A-6 XPS of the C(1s) region of a monolayer assembled from (a) **A** and (b) 1-octadecene. Each of these monolayers was assembled with 0.1 mole % TEMPO-C_{10}. We fit the peak in (a) to three peaks and the peak in (b) to two peaks. The residuals to the fits are shown beneath each peak.

To further investigate this discrepancy we assembled mixed monolayers of **A** and 1-octadecene. As we increased the ratio of 1-octadecene to **A** in solutions used for the assembly, the values for $\nu_a(CH_2)$ and $\nu_s(CH_2)$ decreased and indicated that mixed monolayers were more ordered than those assembled only from **A** (Table 1, entries 2 through 5). We also did not observe a peak for the olefin at approximately 1641 cm^{-1}. This peak is typically weak and difficult to observe, it also may have packed on the surface such that it was not IR active.[440,441]

Although we did not see this peak by HATR-IR spectroscopy it was present; in the following sections we will describe how these monolayers reacted by cross metathesis and ring opening metathesis polymerizations from the olefins on the surface.

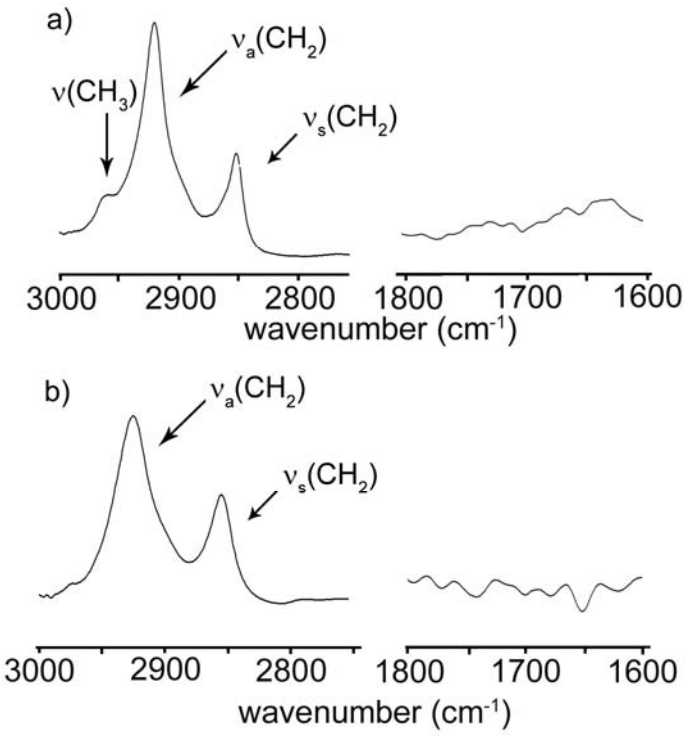

Figure A-7 HATR-IR spectrographs of monolayers assembled from 0.1 mole % TEMPO-C_{10} and (a) 1-octadecene and (b) **A**. We did not observe an olefin peak at in the spectrum of monolayers composed of **A.**

The two major differences between **A** and 1-octadecene are the presence of an ether and second olefin in **A**. From the literature of monolayers on gold we know several important characteristics about how molecules with these functional groups assemble into monolayers.[442-444] Ether bonds promote disorder in monolayers as they favor gauche over trans conformations by approximately 0.1 to 0.2 kcal mol^{-1}.[445] Whitesides et al. studied monolayers on gold assembled from thiols containing ether bonds by IR

spectroscopy and observed several unresolved components near the $\nu_a(CH_2)$ and $\nu_s(CH_2)$ peaks.[443,445] This work indicated, but did not prove, that the monolayer was not a homogeneous distribution of methylenes. Ether bonds are well known to affect the vibrational frequencies of methylenes and that this effect will increase as the tilt angle of the monolayer increases. These effects place shoulders at slightly higher vibrational frequencies for the $\nu_a(CH_2)$ and $\nu_s(CH_2)$ peaks of a crystalline hydrocarbon and, if the shoulders were not resolved from the $\nu_a(CH_2)$ and $\nu_s(CH_2)$ peaks, would cause the $\nu_a(CH_2)$ and $\nu_s(CH_2)$ peaks to appear to shift to higher frequencies. This is important as we did not observe shoulders on the $\nu_a(CH_2)$ and $\nu_s(CH_2)$ peaks in our spectra as expected. Thus, our reported values for $\nu_a(CH_2)$ and $\nu_s(CH_2)$ may not be the true values for these peaks.

In contrast, the presence of a terminal olefin on monolayers of $HS(CH_2)_9CH=CH_2$ on gold do not cause these monolayers to appear disordered.[437,441] From this we know that monolayers terminated with olefins can pack into an all trans, crystalline conformation. Of course it is important to note that monolayers on gold assemble through thiols whereas monolayers on silicon assemble through olefins. Thus, the interpretation of the HATR-IR of a diolefin such as **A** is more complicated as it may bond twice to silicon through both olefins and assemble into a disordered monolayer.

We synthesized $CH_2=CH(CH_2)_9O(CH_2)_{10}CH_3$ (**B**) to study whether how the presence of an ether affects the $\nu_a(CH_2)$ and $\nu_s(CH_2)$ peaks for monolayers on silicon. Monolayers assembled from **B** in 0.1 mole % TEMPO-C_{10} appeared disordered by HATR-IR spectroscopy (Table 1, entry 6). This result was surprising and indicated that one internal ether bond or a second olefin may affect the order of a monolayer on silicon. We are not surprised that a second olefin may introduce some disorder as it may bond to the surface twice and increase the disorder, but we expected that monolayers assembled from **B** would appear ordered. It is surprising that one ether bond would have such an impact on monolayers on Si(111) and this work suggests that the structure of monolayers

containing ether bonds or olefins deserves a full study that is beyond the scope of this paper.

Because of the limitations of HATR-IR spectroscopy, we were unable to determine if monolayers assembled from **A** were ordered or disordered. Our peaks were broad and we were unable to distinguish the presence of shoulders on the $\nu_a(CH_2)$ and $\nu_s(CH_2)$ peaks although Whitesides et al. described their presence on monolayers on Au. XPS data are consistent with an ordered monolayer, but HATR-IR data are consistent with a disordered monolayer.

Cross Metathesis on Olefin-Terminated SAMs

We first explored a simple cross metathesis reaction between two molecules of undecylenic acid to learn which conditions are needed to push the reaction to completion (Figure 7). These reactions were stopped after a period of time, the solvent was removed, and the yield was studied by ^{1}H NMR spectroscopy. Hydrogens on the starting olefin appeared at 5.0 and 5.8 ppm and those on the product appeared at 5.4 ppm; the yield was simple to determine based on this information. We choose to use undecylenic acid for our test reaction as it has a high boiling point that limited its loss under vacuum (boiling point of 137 ºC at 2 mm of Hg) and a carboxylic acid. Monolayers functionalized with carboxylic acids are important as they can be readily reacted to expose more complex molecules.

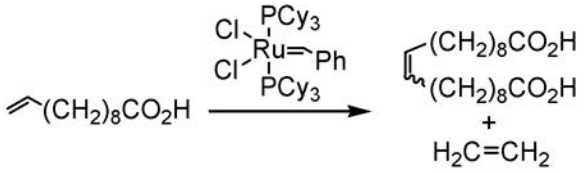

Figure A-8 The reaction conditions of this cross metathesis reaction were optimized to yield a quantitative yield of product.

The reaction conditions that we tried are shown in Table 2. Initial attempts in xylene, silicon oil, tetraethylene glycol, and polyethylene glycol were not successful due to poor catalyst solubility. Heating these reactions to speed the reaction or placing them under vacuum to remove ethylene increased the yield but were ultimately unsuccessful. Refluxing methylene chloride was attempted as the catalyst was soluble in this solvent and refluxing helped remove ethylene from the reaction mixture to drive the reaction forward. The yield of this reaction was >97% by ^{1}H NMR and worked for all olefins that we attempted.

Cross Metathesis Between Olefin-Terminated Monolayers and Fluorinated Olefins

Although we found reaction conditions that allow for low catalyst loadings and quantitative cross metathesis reactions, it is important to note that these conditions were for olefins in solution rather than those on monolayers. Olefins exposed on a monolayer may undergo three different reactions when reacted with the Grubbs' catalyst in the presence of an olefin in solution (Figure 9).

First, olefin-terminated monolayers may react with olefins in solution and yield functionalized surfaces (option #1 in Figure 9). Second, olefins on the monolayer may undergo cross metathesis with each other (option #2 in Figure 9). Third, olefins on the monolayer may be too sterically hindered from reacting with the Grubbs' catalyst (option # 3 in Figure 9). These three possible outcomes complicate our interpretation of olefin-terminated monolayers that reacted with the Grubbs' catalyst and an olefin in solution.

To study the yield of cross metathesis on olefins exposed on a monolayer, we synthesized CH_2=$CH(CH_2)_9OCH_2(CF_2)_6CF_3$ (Figure 9). The fluorines on this molecule gave us a unique handle in the XPS that we could use to study cross metathesis on monolayers. We first assembled monolayers on silicon from different ratios of **A** and 1-octadecene. Next, we reacted these monolayers with the Grubbs' catalyst and

$CH_2=CH(CH_2)_9OCH_2(CF_2)_6CF_3$ in refluxing methylene chloride. Finally, these surfaces were studied by XPS for C, F, Si, and O. The results are shown in Figure 9b.

These experiments showed that the highest concentration of fluorine on the surface was observed for monolayers assembled from 50% **A** and 50% 1-octadecene. Interestingly, monolayers assembled only from **A** had a lower amount of fluorine on the surface. This result suggests that either cross metathesis between olefins on the monolayer was significant or that the monolayers were too ordered to fully react with the Grubbs' catalyst. For surfaces with decreasing mole fractions of **A** used in their assembly, the amount of fluorine observed by XPS slowly decreased. These experiments also clearly demonstrated that monolayers assembled from CH2=CH(CH2)9O(CH2)9CH=CH2 exposed olefins on the surface that were reactive with the Grubbs' catalyst. Monolayers assembled from 1-octadecene that did not display olefins were not reactive with the Grubbs' catalyst. These monolayers did not and did not show any fluorine in the XPS after reaction with $CH_2=CH(CH_2)_9OCH_2(CF_2)_6CF_3$

We studied these surfaces by HATR-IR spectroscopy but could not distinguish between the three different outcomes shown in Figure 8. Due to strong absorptions below 1500 cm^{-1}, HATR-IR spectroscopy on Si(111) shards can not image peaks below this cutoff and the peaks in the C-H region were too broad to distinguish the different olefins that may be present on the surface. Nevertheless, these results are important as we learned how to optimize the ratio of **A** to 1-octadecene in solution to functionalize surfaces.

Composition of Mixed Monolayers

We do not know how the ratio of **A** to 1-octadecene used in the assembly of monolayers relates to their final composition. For instance, we do not know if a 1/1 molar ratio of **A** to 1-octadecene in solution results in a 1/1 ratio of these molecules in the monolayer. The studies that we discussed previously can not describe the composition on

the surface due to potential cross metathesis between olefins on the monolayers and incomplete cross metathesis between olefins in solution with those on the surface. We needed a cleaner system to study the composition of monolayers assembled from two different molecules.

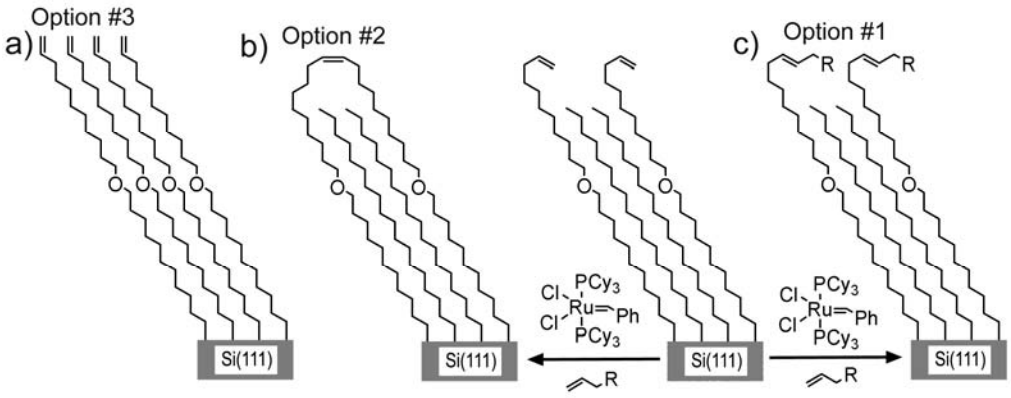

Figure A-9 Three possible outcomes for the reaction of monolayers of **A** and 1-octadecene with the Grubbs' catalyst and an olefin in solution. (a) Areas with well-ordered monolayers of **A** may be too sterically hindered to allow the Grubbs' catalyst to react. (b) Olefins on the monolayer may react with each other or (c) with an olefin in solution.

To learn how the composition of solutions used in the assembly relates to the final composition of monolayers, we synthesized $CH_2=CH(CH_2)_9O(CH_2)_6Cl$. Monolayers assembled from this molecule will have the same thickness as a monolayer assembled from 1-octadecene and expose a chlorine on the top of the monolayer. By measuring the ratio of chlorine to carbon by XPS for monolayers assembled from mixtures of $CH_2=CH(CH_2)_9O(CH_2)_6Cl$ and 1-octadecene we can learn the composition of these monolayers. Our results in Figure 10 demonstrate that the ratio of $CH_2=CH(CH_2)_9O(CH_2)_6Cl$ to 1-octadecene in solution closely follows the ratio of these molecules in the monolayer.

Table A-2 Different Reaction Conditions to Optimize the Cross Metathesis of 11-Undecylenic Acid as Shown in Figure 7.

[a]Amount of olefin (mL)	Solvent	Vol of solvent (mL)	[b]Grubbs' catalyst (mole %)	Temp (°C)	Vac	Time (h)	[c]Yield (%)
1.36	Xylenes	4.5	0.32	25	No	22	16
1.28	Xylenes	4.5	0.32	40	No	21	23
1.0	Xylenes	3.0	1.0	40	No	41	47
1.0	Xylenes	3.0	1.0	55	No	30	58
1.0	Xylenes	3.0	1.0	70	No	50	91
1.0	Xylenes	3.0	1.0	85	No	72	91
4.3	None	0.0	0.32	40	No	20	59
1.0	Tetraethylene glycol	3.0	1.0	25	Yes	46	54
1.0	Tetraethylene glycol	3.0	1.0	40	Yes	19	69
1.0	Poly(ethylene glycol) 600 M_w	3.0	1.0	60	Yes	113	72
1.0	Silicon oil	3.0	1.0	40	Yes	48	73
1.0	Methylene chloride	3.0	1.0	Reflux	No	48	100

[a]Each of these reactions were carried out under an atmosphere of N_2 or under vacuum (approximately 100 millitorr).
[b]The mole % of catalyst relative to undecylenic acid. [c]The yield refers to undecylenic acid that was cross metathesized to $=(CH(CH_2)_8CO_2H)_2$.

Cross Metathesis With Olefins Exposing Useful Functional Groups

As the Grubbs' catalyst is stable in the presence of many functional groups, monolayers displaying a variety of different functional groups can be synthesized. To demonstrate this potential, we reacted monolayers assembled from 50% **A** and 50% 1-octadecene with olefins terminated with alcohols, bromides, aldehydes, and carboxylic acids. We studied these surfaces by XPS and HATR-IR spectroscopy (Table 3 and Figure 11). These results indicated that each monolayer was functionalized with an olefin and exposed different functional groups on the surface.

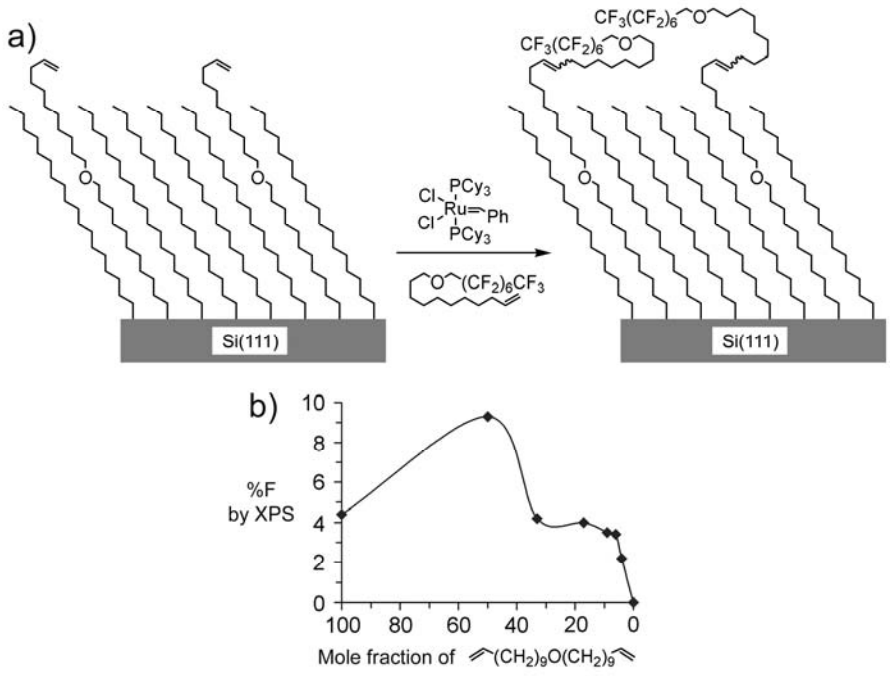

Figure A-10 Molefraction effects **(**a) Olefin-terminated monolayers were reacted with an olefin in solution with 15 fluorines to yield fluorinated surfaces. These surfaces were studied by XPS to describe the relative amounts of fluorine on the monolayers. (b) The amount of fluorine on these surfaces as a function of the mole fraction of **A** used in the assembly of the monolayer. The line is drawn as a guide to the reader and is not fitted from an equation.

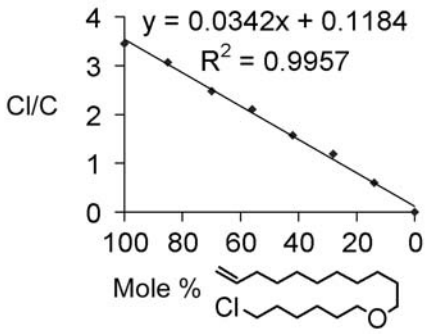

Figure A-11 The ratio of the areas of the Cl(2p) and C(1s) peaks from the XPS of monolayers assembled from $CH_2=CH(CH_2)_9O(CH_2)_6Cl$ and 1-octadecene. The x-axis shows the mole % of $CH_2=CH(CH_2)_9O(CH_2)_6Cl$ used in the assembly of the monolayers.

Table A-3 Cross Metathesis Between Olefin-Terminated Monolayers and Functional Olefins in Solution.

		XPS Composition (%)					HATR-IR Spectroscopy		
Entry	Olefin	C	Si	SiO_x	F	O	$\nu_a(CH_2)$ (cm^{-1})	$\nu_s(CH_2)$ (cm^{-1})	ν(C=O) (cm^{-1})
1	$CH_2=CH(CH_2)_8CO_2H$	58	22	0	0	20	2924	2854	1739, 1700
2	$CH_2=CH(CH_2)_9OH$	67	23	0	0	10	2925	2855	[a]1739
3	$CH_2=CH(CH_2)_8CHO$	68	19	0	0	12	2925	2854	1730

[a]After cross metathesis with the monolayer, the alcohol was reacted with acetyl chloride. We report the carbonyl peaks of the ester.

Patterning Monolayers on the Micrometer Size-Scale Using Soft Lithography

In this section we will report methods to pattern these monolayers on the micrometer-size scale by soft lithography. Specifically, we patterned PDMS on the

micrometer-size scale such that a series of microchannels were formed when a PDMS stamp was placed against a silicon wafer. These microchannels were easily accessible by an external syringe pump to add reagents only to the microchannels. Monolayers in contact with PDMS were protected from reaction. We choose soft lithography as these techniques have become well accepted in the scientific community, they are used to pattern monolayers on gold, and their applications to form microfluidic channels are becoming increasingly important.[296,298-301,408,410,446,447] Generating patterns by soft lithography is rapid as PDMS stamps are readily manufactured in under 24 h.[448]

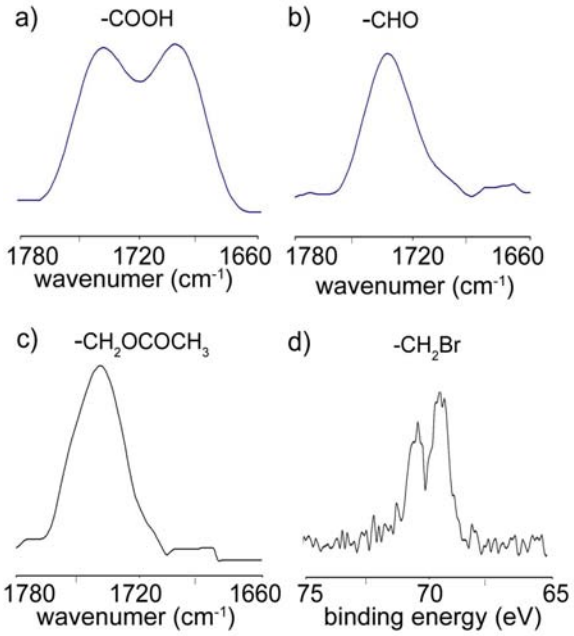

Figure A-12 HATR-IR spectrographs of the carbonyl regions for monolayers reacted with (a) CH_2=CH$(CH_2)_8CO_2H$, (b) CH_2=CH$(CH_2)_8$CHO, and (c) CH_2=CH$(CH_2)_9$OH. The alcohols on monolayers that were reacted with CH_2=CH$(CH_2)_9$OH were further functionalized with $ClCOCH_3$ to yield ester-terminated monolayers which were characterized by HATR-IR spectroscopy. These spectrographs show the presence of carbonyl peaks. (d) A high resolution XPS of the Br(3d) region for an olefin-terminated monolayer after reaction with CH_2=CH$(CH_2)_9$Br. This XPS shows the presence of Br on the surface.

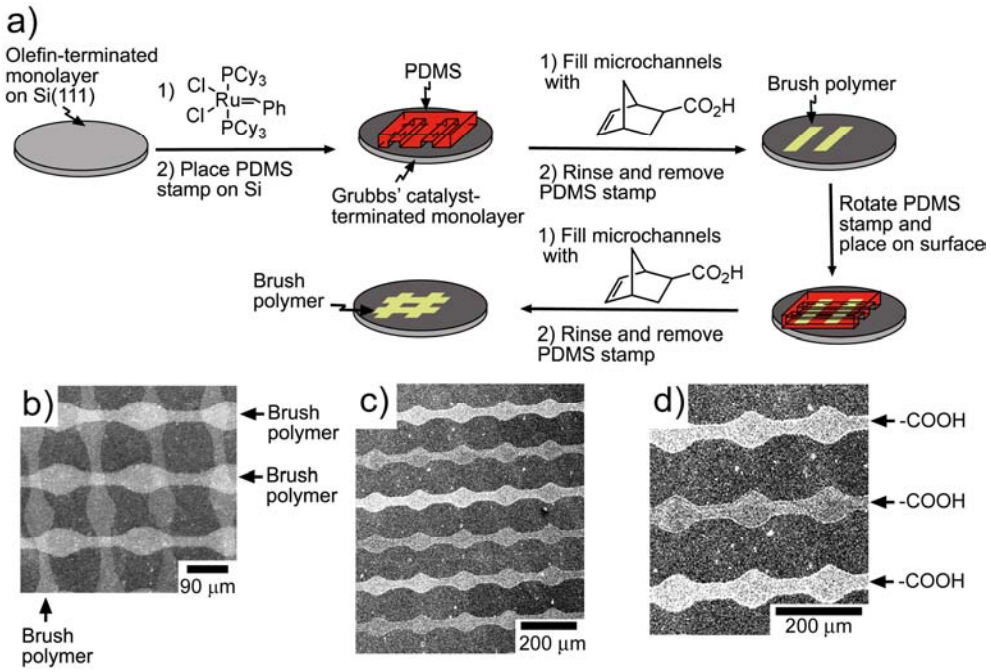

Figure A-13 Patterning on olefin terminated surfaces (a) The method for patterning olefin-terminated monolayers on Si(111) with the Grubbs' catalyst. First, we assembled a mixed monolayer of **A** and 1-octadecene. Next, we immersed the silicon wafer in a solution of the Grubbs' first generation catalyst for 15 min. The Grubbs' catalyst attached to the monolayer by cross metathesis with an olefin on the surface. A PDMS stamp was then placed on the monolayer to form microfluidic channels on the surface. Next, a solution of an olefin filled the channels by an external syringe (not shown). Monolayers in contact with PDMS were not exposed to the olefins and did not react. After 15 to 30 min the channels were rinsed, the PDMS stamp was removed and turned 90º before being placed on the monolayer again. A new solution of an olefin added to the channels. Finally, the channels were rinsed, the PDMS stamp was removed, and the silicon wafer was rinsed. (b) A SEM micrograph of crossed brush polymers synthesized as in part a). (c) and (d) SEM micrographs of monolayers reacted by cross metathesis with $CH_2=CH(CH_2)_8CO_2H$ to expose acids along the surface. In these experiments $CH_2=CH(CH_2)_8CO_2H$ was added to the microchannels rather than 5-norbornene-2-carboxylic acid. The image in d) is a close-up of the image in c).

Our general method is outlined in Figure 12. To demonstrate this method we patterned monolayers through cross metathesis and ring opening polymerizations (ROMP). In a one example we choose to grow polymer brushes from the surfaces using ROMP as the Grubbs' catalyst polymerizes strained monomers under living conditions.

We choose to synthesize polymer brushes of 5-norbornene-2-carboxylic acid as it polymerizes rapidly and exposes carboxylic acids on the surface (Figure 12b). These polymer brushes were covalently attached to the surface and could not be washed from the surface. In a second example we patterned monolayers by cross metathesis using solutions of $CH_2=CH(CH_2)_8CO_2H$ (Figures 12 c and d). These methods demonstrate that we can pattern monolayers using either cross metathesis or ROMP.

Conclusions

The main accomplishments of this work are the assembly and characterization of monolayers of **A**, the cross metathesis of olefin-terminated monolayers on Si(111), and the patterning of these monolayers using ROMP and cross metathesis. We patterned surfaces that exposed alkyl bromides, aldehydes, carboxylic acids, and alcohols and demonstrated how these surfaces may be patterned. These functional groups are important as we and others reported methods to further functionalize them to expose DNA, proteins, and other important molecules. Thus, the method we report in this paper is applicable to the complex functionalization of monolayers on silicon.

This work may have applications in a variety of areas that employ monolayers on silicon. Efforts to selectively functionalize its surface by organic chemistry are critical for applications in biotechnology and nanotechnology, such as biosensors and nanoelectronic chips that exploit the unique electronic properties of silicon. Our simple synthetic route to **A** facilitates use of the patterning methodology reported here also by researchers that are not skilled in organic synthesis. In addition, the ability to patternthese monolayers on silicon with a wide variety of end groups using soft lithography, i.e. microfluidic patterning, microcontact printing, further expands their applicability to cases where localized tailoring of physical and chemical surfaces properties is desired.

APPENDIX B SUPPORTING INFORMATION FOR THE ASSEMBLY OF ORGANIC MONOLAYERS ON POLYDICYCLOPENTADIENE

Estimation of Surface Coverage of Amine on PDCPD-Amine.

The surface coverage was estimated with the results from the XPS of the PDCPD-amine surface. Specifically, we reacted PDCPD-Br with 4-(trifluoromethyl)benzylamine for 24 h and obtained the XPS results reported in the paper. In the text of the paper, we discussed how the amine only reacted with surface alkyl bromides, so in this section we assumed that the amine does not significantly diffuse into the material and all the reactions occur at the surface.

It was first necessary to determine the attenuation length (Al) of electrons for C and F. Although this can be accomplished using a number of formulas, the Griess formula was used because its parameters could be readily determined. The Griess formula for inelastic mean free path (IMPF: Λ) is given below. It was assumed for our further calculations that the IMFP can be used to approximate the attenuation length, although the AL would be slightly longer than the IMPF. Determining a value for the attenuation length involves more approximations that may underestimate the surface coverage.

$$\Lambda = \frac{k_1\left(\frac{V_a}{z^*}\right)E}{LogE - k_2}$$

Equation B-2 Greiss Formula for the inelastic mean free path

All values were calculated using NIST standard reference database 71. Here, V_a was the atomic volume which was defined as the molar mass divided by density and z^*

was defined as $z^{1/2}$ where z was the atomic number of the element of interest. Both k_1 and k_2 were fitting parameters found in the NIST database, and the values used were 0.0018 and 1.0 respectively. E was the kinetic energy of the photoelectron for C 1s (1202 eV). A density of 1.30 $g.cm^{-3}$ was used based on an estimated from a survey of literature brominated compounds. The IMFP for C 1s was calculated to be 4.675 nm.

To find the density of the CF_3 groups on the surface, we used the IMPF to learn the depth of the carbon signals. The issue is that the intensity of the C peak will decrease as the distance from the surface increases. Because the intensity of the peak follows an exponential (shown below), we integrated it over the entire thickness. This argument leads to the conclusion that we can model the system as each C within the top 4.675 nm of the surface as having no attenuation due to being subsurface, but that all carbons buried farther than 4.675 nm from the surface will not contribute to the intensity of the peak. We found this model straightforward to use.

$$\int_0^\infty e^{-\frac{x}{AL}} dx = \left[-Al.e^{-\frac{x}{Al}} \right]_0^\infty = 4.675nm$$

Equation B-3 Density funtion

The ratio of carbon (75.5 %) to fluorine (2.5 %) was found from the XPS of the PDCPD-amine surface at 88 h. The ratio was 0.0331 or 1 CF_3 per 90.6 carbons.

$$V = x^2 h$$

Equation B-4 Area of Circle

We modelled our polymer surface as a box with one CF_3 group at the top and none buried within the interior based on arguments described in the paper. The height (h) of the box was equal to 4.675 nm. The volume (V) was the total volume for 90.6 carbon atoms in our polymer. The length of each segment of the square cross-section was labelled as x in the equation shown above. The volume was calculated using the atomic mass of polymer unit $C_{10}H_{12}Br_2$ (294.04 g mol^{-1}) and the estimated density for the brominated polymer (1.30 g cm^{-3}). We found a total volume of 3.403 nm^3 for 90.6 carbon atoms in our polymer. This value resulted in a value of 1.37 molecules of CF_3 per nm^2.

Depth Pentration of GATR-IR Spectroscopy.

GATR-IR spectroscopy can be used to find the functional groups in the surface layer of a material. The thickness that is measured by GATR-IR spectroscopy is a function of the wavelength, λ, and several other parameters as shown below.

$$\frac{d_{e\perp}}{\lambda_1} = \frac{n_{21}\cos\theta}{\pi(1-n_{21}^2)(\sin^2\theta - n_{21}^2)^{1/2}}$$

$$\frac{d_{e\Pi}}{\lambda_1} = \frac{n_{21}\cos\theta(2\sin^2\theta - n_{21}^2)}{\pi(1-n_{21}^2)[(1+n_{21}^2)\sin^2\theta - n_{21}^2](\sin^2\theta - n_{21}^2)^{1/2}}$$

Equation B-5

Here, λ_1 is the wavelength of light, θ is the incident angle of 65 degrees, and n_{21} is the refractive index of the sample relative to the Ge ATR crystal. The refractive index for Ge is 4.02 and we used the refractive index of polycarbonate (1.55) as approximation of PDCPD. It is important to note that the range of refractive index for typical polymers are

from 1.42-1.55 so our approximation is a close estimate. From these values, the depth of penetration is found to be 243 nm at 2000 cm^{-1} and 162 nm.

REFERENCES

(1) Pierstorff, E.; Ho, D. *Int. J. Nanomed.* **2008**, *3*, 425.

(2) Ghosh, P.; Han, G.; De, M.; Kim, C. K.; Rotello, V. M. *Adv. Drug Deliv. Rev.* **2008**, *60*, 1307.

(3) Liu, F. K. *J. Chromatogr. A* **2009**, *1216*, 9034.

(4) Zhou, J. F.; Ralston, J.; Sedev, R.; Beattie, D. A. *Journal of Colloid and Interface Science* **2009**, *331*, 251.

(5) Dutta, S.; Perring, M.; Barrett, S.; Mitchell, M.; Kenis, P. J. A.; Bowden, N. B. *Langmuir* **2006**, *22*, 2146.

(6) Shervedani, R. K.; Siadat-Barzoki, S. M.; Bagherzadeh, M. *Electroanalysis* **2010**, *22*, 969.

(7) Dharuman, V.; Chang, B. Y.; Park, S. M.; Hahn, J. H. *Biosensors & Bioelectronics* **2010**, *25*, 2129.

(8) Wang, Y. T.; Zhang, Z. Q.; Jain, V.; Yi, J. J.; Mueller, S.; Sokolov, J.; Liu, Z. X.; Levon, K.; Rigas, B.; Rafailovich, M. H. *Sens. Actuator B-Chem.* **2010**, *146*, 381.

(9) Boujday, S.; Briandet, R.; Salmain, M.; Herry, J. M.; Marnet, P. G.; Gautier, M.; Pradier, C. M. *Microchim. Acta* **2008**, *163*, 203.

(10) Yuan, S. J.; Pehkonen, S. O.; Liang, B.; Ting, Y. P.; Neoh, K. G.; Kang, E. T. *Corrosion Sci.* **2010**, *52*, 1958.

(11) Leska, B.; Pankiewicz, R.; Gierczyk, B.; Schroeder, G.; Brzezinski, B. *J. Mater. Sci.* **2008**, *43*, 3459.

(12) Li, Y.; Wong, C. P. *Applied Physics Letters* **2006**, *89*.

(13) Belser, T.; Stohr, M.; Pfaltz, A. *J. Am. Chem. Soc.* **2005**, *127*, 8720.

(14) Simon, A.; Cohen-Bouhacina, T.; Porte, M. C.; Aime, J. P.; Baquey, C. *Journal of Colloid and Interface Science* **2002**, *251*, 278.

(15) Nagel U.; E., K. *J. Chem. Soc., Chem. Commun.* **1986**, 1098.

(16) Huc V.; Saveyroux M.; Bourgoin J.-P.; Valin F.; Zalczer G.; Albouy P.-A.; Palacin S. *Langmuir* **2000**, 1770.

(17) Qiu, L.; Liu, D. J.; Zhang, Y.; He, W. J. *Chin. J. Inorg. Chem.* **2006**, *22*, 1745.

(18) Lu, F. T.; Gao, L. N.; Li, H. H.; Ding, L. P.; Fang, Y. *Applied Surface Science* **2007**, *253*, 4123.

(19) Reddy, V. R.; Currao, A.; Calzaferri, G. *Journal of Materials Chemistry* **2007**, *17*, 3603.

(20) Ozturk, S.; Akata, B. *Microporous and Mesoporous Materials* **2009**, *126*, 228.

(21) Guleryuz, H.; Kaus, I.; Filiatre, C.; Grande, T.; Einarsrud, M. A. *Journal of Sol-Gel Science and Technology* **2010**, *54*, 249.

(22) Gawish, S. M.; Ramadan, A. M.; Mosleh, S.; Morcellet, M.; Martel, B. *J. Appl. Polym. Sci.* **2006**, *99*, 2586.

(23) Gupta, A.; Matsui, K.; Lo, J.-F.; Silver, S. *Nat. Med. (N. Y.)* **1999**, *5*, 183.

(24) Jiang, H.; Manolache, S.; Wong, A. C. L.; Denes, F. S. *J. Appl. Polym. Sci.* **2004**, *93*, 1411.

(25) Silver, S. *FEMS Microbiol. Rev.* **2003**, *27*, 341.

(26) Brito, R.; Tremont, R.; Feliciano, O.; Cabrera, C. R. *Journal of Electroanalytical Chemistry* **2003**, *540*, 53.

(27) Silien, C.; Dreesen, L.; Cecchet, F.; Thiry, P. A.; Peremans, A. *J. Phys. Chem. C* **2007**, *111*, 6357.

(28) Vercelli, B.; Zotti, G. *Chemistry of Materials* **2006**, *18*, 3754.

(29) Laibinis, P. E.; Whitesides, G. M. *Journal of the American Chemical Society* **1992**, *114*, 9022.

(30) Zhang, D. Q.; He, X. M.; Cai, Q. R.; Gao, L. X.; Kim, G. S. *Thin Solid Films* **2010**, *518*, 2745.

(31) Gassull, D.; Ulman, A.; Grunze, M.; Tanaka, M. *Journal of Physical Chemistry B* **2008**, *112*, 5736.

(32) Wampler, H. P.; Zemlyanov, D. Y.; Lee, K.; Janes, D. B.; Ivanisevic, A. *Langmuir* **2008**, *24*, 3164.

(33) Adlkofer, K.; Eck, W.; Grunze, M.; Tanaka, M. *Journal of Physical Chemistry B* **2003**, *107*, 587.

(34) Shaporenko, A.; Adlkofer, K.; Johansson, L. S. O.; Tanaka, M.; Zharnikov, M. *Langmuir* **2003**, *19*, 4992.

(35) Goncalves, A. M.; Mezailles, N.; Mathieu, C.; Le Floch, P.; Etcheberry, A. *Chemistry of Materials* **2010**, *22*, 3114.

(36) Clare, T. L.; Clare, B. H.; Nichols, B. M.; Abbott, N. L.; Hamers, R. J. *Langmuir* **2005**, *21*, 6344.

(37) Sun, B.; Baker, S. E.; Butler, J. E.; Kim, H.; Russell, J. N.; Shang, L.; Tse, K. Y.; Yang, W. S.; Hamers, R. J. *Diamond and Related Materials* **2007**, *16*, 1608.

(38) Sun, B.; Colavita, P. E.; Kim, H.; Lockett, M.; Marcus, M. S.; Smith, L. M.; Hamers, R. J. *Langmuir* **2006**, *22*, 9598.

(39) Tse, K. Y.; Nichols, B. M.; Yang, W. S.; Butler, J. E.; Russell, J. N.; Hamers, R. J. *Journal of Physical Chemistry B* **2005**, *109*, 8523.

(40) Sirikittikul, D.; Fuongfuchat, A.; Booncharoen, W. *Polym. Adv. Technol.* **2009**, *20*, 802.

(41) Lee, W.; Prinz, F. B. *J. Electrochem. Soc.* **2009**, *156*, G125.

(42) Finklea, H. O.; Hanshew, D. D. *Journal of Electroanalytical Chemistry* **1993**, *347*, 327.

(43) Camillone, N.; Chidsey, C. E. D.; Liu, G. Y.; Scoles, G. *Journal of Chemical Physics* **1993**, *98*, 3503.

(44) Bertilsson, L.; Liedberg, B. *Langmuir* **1993**, *9*, 141.

(45) Walczak, M. M.; Popenoe, D. D.; Deinhammer, R. S.; Lamp, B. D.; Chung, C. K.; Porter, M. D. *Langmuir* **1991**, *7*, 2687.

(46) Czanderna, A. W.; King, D. E.; Spaulding, D. *Journal of Vacuum Science & Technology a-Vacuum Surfaces and Films* **1991**, *9*, 2607.

(47) Widrig, C. A.; Chung, C.; Porter, M. D. *Journal of Electroanalytical Chemistry* **1991**, *310*, 335.

(48) Uosaki, K.; Sato, Y.; Kita, H. *Langmuir* **1991**, *7*, 1510.

(49) Collard, D. M.; Fox, M. A. *Langmuir* **1991**, *7*, 1192.

(50) Mar, W.; Klein, M. L. *Langmuir* **1994**, *10*, 188.

(51) Sun, F.; Grainger, D. W.; Castner, D. G.; Leachscampavia, D. K. *Macromolecules* **1994**, *27*, 3053.

(52) Forster, R. J.; Faulkner, L. R. *Journal of the American Chemical Society* **1994**, *116*, 5444.

(53) A. Shaporenko; P. Cyganik; M. Buck; A. Terfort; Zharnikov, M. *J. Phys. Chem. B* **2005**, *109*, 13630.

(54) T. Weidner; A. Shaporenko; J. Muller; M. Holtig; A. Terfort; Zharnikov, M. *J. Phys. Chem. C* **2007**, *111*, 11627.

(55) Sondaghuethorst, J. A. M.; Schonenberger, C.; Fokkink, L. G. J. *Journal of Physical Chemistry* **1994**, *98*, 6826.

(56) Schonenberger, C.; Sondaghuethorst, J. A. M.; Jorritsma, J.; Fokkink, L. G. J. *Langmuir* **1994**, *10*, 611.

(57) Folkers, J. P.; Laibinis, P. E.; Whitesides, G. M. *Journal of Adhesion Science and Technology* **1992**, *6*, 1397.

(58) Venkataramanan, M.; Pradeep, T. *Chem. Phys. Lett.* **2000**, *327*, 299.

(59) Tao, Y. T.; Pandian, K.; Lee, W. C. *Journal of the American Chemical Society* **2000**, *122*, 7072.

(60) Nishimura, N.; Ooi, M.; Shimazu, K.; Fujii, H.; Uosaki, K. *Journal of Electroanalytical Chemistry* **1999**, *473*, 75.

(61) Brockman, J. M.; Frutos, A. G.; Corn, R. M. *Journal of the American Chemical Society* **1999**, *121*, 8044.

(62) Hostetler, M. J.; Templeton, A. C.; Murray, R. W. *Langmuir* **1999**, *15*, 3782.

(63) Spinke, J.; Liley, M.; Schmitt, F.-J.; Guder, H.-J.; Angermaier, L.; Knoll, W. *J. Chem. Phys.* **1993**, *99*, 7012.

(64) Spinke, J.; Liley, M.; Guder, H.-J.; Angermaier, L.; Knoll, W. *Langmuir* **1993**, *9*, 1821.

(65) Allen, C. T.; Hostetler, M. J.; Kraft, C. T.; Murray, R. W. *J. Am. Chem. Soc.* **1998**, *120*, 1906.

(66) Voicu, R.; Boukherroub, R.; Bartzoka, V.; Ward, T.; Wojtyk, J. T. C.; Wayner, D. D. M. *Langmuir* **2004**, *20*, 11713.

(67) Yan, L.; Marzolin, C.; Terfort, A.; Whitesides, G. M. *Langmuir* **1997**, *13*, 6704.

(68) Peckys, D. B.; de Jonge, N.; Simpson, M. L.; McKnight, T. E. *Nanotechnology* **2008**, *19*.

(69) Kavanagh, P.; Leech, D. *Analytical Chemistry* **2006**, *78*, 2710.

(70) Han, G.; Martin, C. T.; Rotello, V. M. *Chemical Biology & Drug Design* **2006**, *67*, 78.

(71) Xiao, Z. W.; Xu, M. X.; Ohgi, T.; Ishikawa, N.; Fujita, D. *Physica E-Low-Dimensional Systems & Nanostructures* **2004**, *21*, 1098.

(72) Lu, X. Q.; Zhang, M.; Kang, J. W.; Wang, X. Q.; Zhuo, L.; Liu, H. D. *Journal of Inorganic Biochemistry* **2004**, *98*, 582.

(73) Sakao, Y.; Ueno, N.; Nakamura, F.; Ito, E.; Hayasi, J.; Hara, M. *Molecular Crystals and Liquid Crystals* **2003**, *407*, 537.

(74) Bernard, A.; Delamarche, E.; Schmid, H.; Michel, B.; Bosshard, H. R.; Biebuyck, H. *Langmuir* **1998**, *14*, 2225.

(75) Mirsky, V. M.; Riepl, M.; Wolfbeis, O. S. *Biosensors & Bioelectronics* **1997**, *12*, 977.

(76) Yang, Z. P.; Engquist, I.; Wirde, M.; Kauffmann, J. M.; Gelius, U.; Liedberg, B. *Langmuir* **1997**, *13*, 3210.

(77) Jiang, L.; Glidle, A.; Griffith, A.; McNeil, C. J.; Cooper, J. M. *Bioelectrochemistry and Bioenergetics* **1997**, *42*, 15.

(78) Sadhu, V. B.; Perl, A.; Duan, X. X.; Reinhoudt, D. N.; Huskens, J. *Soft Matter* **2009**, *5*, 1198.

(79) Brondijk, J. J.; Li, X.; Akkerman, H. B.; Blom, P. W. M.; de Boer, B. *Applied Physics a-Materials Science & Processing* **2009**, *95*, 1.

(80) Li, X. M.; Huskens, J.; Reinhoudt, D. N. *Journal of Materials Chemistry* **2004**, *14*, 2954.

(81) He, H. X.; Li, Q. G.; Zhou, Z. Y.; Zhang, H.; Li, S. F. Y.; Liu, Z. F. *Langmuir* **2000**, *16*, 9683.

(82) Jeon, N. L.; Choi, I. S.; Whitesides, G. M.; Kim, N. Y.; Laibinis, P. E.; Harada, Y.; Finnie, K. R.; Girolami, G. S.; Nuzzo, R. G. *Applied Physics Letters* **1999**, *75*, 4201.

(83) Libioulle, L.; Bietsch, A.; Schmid, H.; Michel, B.; Delamarche, E. *Langmuir* **1999**, *15*, 300.

(84) Biebuyck, H. A.; Larsen, N. B.; Delamarche, E.; Michel, B. *Ibm Journal of Research and Development* **1997**, *41*, 159.

(85) Lagutchev, A. S.; Song, K. J.; Huang, J. Y.; Yang, P. K.; Chuang, T. J. *Chemical Physics* **1998**, *226*, 337.

(86) Feng, X.; Fryxell, G. E.; Wang, L. Q.; Kim, A. Y.; Liu, J.; Kemner, K. M. *Science* **1997**, *276*, 923.

(87) Guidotti, B. R.; Caseri, W. R.; Suter, U. W. *Langmuir* **1996**, *12*, 4391.

(88) Fagerholm, H. M.; Rosenholm, J. B.; Horr, T. J.; Smart, R. S. *Colloids and Surfaces a-Physicochemical and Engineering Aspects* **1996**, *110*, 11.

(89) Banga, R.; Yarwood, J.; Morgan, A. M.; Evans, B.; Kells, J. *Langmuir* **1995**, *11*, 4393.

(90) Choi, K. M.; Eom, T.-J.; Lee, C. *Thin Solid Films* **2003**, *435*, 223.

(91) Duke, C. B. *Chem. Rev.* **1996**, *96*, 1237.

(92) H. N. Waltenburg; Jr., J. T. Y. *Chem. Rev.* **1995**, *95*, 1589.

(93) Yang, L.; Lua, Y.; Tan, M.; Scherman, O. A.; Grubbs, R. H.; Harb, J. N.; Davis, R. C.; Linford, M. R. *Chemistry of Materials* **2007**, *19*, 1671.

(94) Lua, Y.; Niederhauser, T. L.; Matheson, R.; Bristol, C.; Mowat, I. A.; Asplund, M. C.; Linford, M. R. *Langmuir* **2002**, *18*, 4840.

(95) Ledung, G.; Bergkvist, M.; Quist, A. P.; Geluis, U.; Carlsson, J.; Oscarsson, S. *Langmuir* **2001**, *17*, 6056.

(96) Bansal A.; Li X.; Lauermann I.; Lewis, N. S. *J. Am. Chem. Soc.* **1996**, *118*, 7225.

(97) Bansal A.; Li X.; Yi S. I.; Weinberg W. H.; Lewis, N. S. *J. Phys. Chem. B* **2001**, *105*, 10266.

(98) Zhu, X.-Y.; Boiadjiev V.; Mulder J. A.; Hsung R. P.; C., M. R. *Langmuir* **2000**, *16*, 6766.

(99) Eves, B. J.; Lopinski G. P. *Surf. Sci.* **2005**, *579*, L89.

(100) Narducci D.; Pedemonte L.; G., B.; . *Appl. Surf. Sci.* **2003**, *212*, 649.

(101) Lauerhaas J. M.; Sailor M. J *Science (Washington, D. C.)* **1993**, *261*, 1567.

(102) Lauerhaas J. M.; Sailor M. J. *Mater. Res. Soc. Symp. Proc.* **1993**, *298*, 259.

(103) Joy V. T.; Mandler D. *ChemPhysChem* **2002**, *3*, 973.

(104) Higashi, G. S.; Chabal, Y. J.; Trucks, G. W.; Raghavachari, K. *Applied Physics Letters* **1990**, *56*, 656.

(105) Wade, C. P.; Chidsey, C. E. D. *Applied Physics Letters* **1997**, *71*, 1679.

(106) Allongue, P.; de Villeneuve, C. H.; Morin, S.; Boukherroub, R.; Wayner, D. D. M. *Electrochim. Acta* **2000**, *45*, 4591.

(107) Jakob, P.; Chabal, Y. J. *J. Chem. Phys.* **1991**, *95*, 2897.

(108) Hessel, H. E.; Feltz, A.; Reiter, M.; Memmert, U.; Behm, R. J. *Chem. Phys. Lett.* **1991**, *186*, 275.

(109) P. Allongue; J. Kasparian *Microsc. Microanal. Microstruct.* **1994**, *5*, 257.

(110) Allongue, P.; Kieling, V.; Gerischer, H. *Electrochim. Acta* **1995**, *40*, 1353.

(111) Y.-C. Huang; J. Flidr; Newton, T. A.; M. A. Hines *Phys. Rev. Lett.* **1998**, *80*, 4462.

(112) J. Flidr; Huang, Y.-C.; M. A. Hines, J. *Journal of Chemical Physics* **1999**, *111*, 6970.

(113) Y. C. Huang; J. Flidr; Newton, T. A.; Hines, M. A. *Journal of Chemical Physics* **1998**, *109*, 5025.

(114) M.R. Linford; C.E.D. Chidsey *J. Am. Chem. Soc.* **1993**, *115*, 12631.

(115) Sung, M. M.; Kluth, G. J.; Yauw, O. W.; Maboudian, R. *Langmuir* **1997**, *13*, 6164.

(116) J. Terry; M.R. Linford; C. Wigren; R. Cao; P. Pianetta; C.E.D. Chidsey *Appl. Phys. Lett.* **1997**, *71*, 1056.

(117) Cicero, R. L.; Linford, M. R.; Chidsey, C. E. D. *Langmuir* **2000**, *16*, 5688.

(118) C.H. de Villeneuve; J. Pinson; M.C. Bernard; P. Allongue *J. Phys. Chem. B* **1997**, *101*, 2415.

(119) de Smet, L.; Pukin, A. V.; Sun, Q. Y.; Eves, B. J.; Lopinski, G. P.; Visser, G. M.; Zuilhof, H.; Sudholter, E. J. R. *Applied Surface Science* **2005**, *252*, 24.

(120) Cicero, R. L.; Wagner, P.; Linford, M. R.; Hawker, C. J.; Waymouth, R. M.; Chidsey, C. E. D. *Polym. Prepr.(Am. Chem. Soc.,Div. Polym. Chem.)* **1997**, *38*, 904.

(121) Sieval A. B.; Demirel A. L.; Nissink J. W. M.; Linford M. R.; van der Maas J. H.; de Jeu W. H.; Zuilhof H.; Sudholter E. J. R. *Langmuir* **1998**, *14*, 1759.

(122) Boukherroub R.; Morin S.; Bensebaa F.; M., W. D. D. *Langmuir* **1999**, *15*, 3831.

(123) Fabre, B.; Lopinski, G. P.; Wayner, D. D. M. *Journal of Physical Chemistry B* **2003**, *107*, 14326.

(124) Boukherroub R.; Wayner, D. D. M. *J. Am. Chem. Soc.* **1999**, *121*, 11513.

(125) Mitchell S. A.; Ward T. R.; Wayner D. D. M.; P., L. G. *J. Phys. Chem. B* **2002**, *106*, 9873.

(126) Perring, M.; Dutta, S.; Arafat, S.; Mitchell, M.; Kenis, P. J. A.; Bowden, N. B. *Langmuir* **2005**, *21*, 10537.

(127) Rosso, M.; Giesbers, M.; Schroen, K.; Zuilhof, H. *Langmuir* **2010**, *26*, 866.

(128) Heise A; Stamm M; Rauscher M; Duschner H; H., M. *Thin Solid Films* **1998**, 327.

(129) Sieval A. B.; Vleeming V.; Zuilhof H.; R., S. E. J. *Langmuir* **1999**, *15*, 8288.

(130) Huang A.; Scherman, O. R.; Grubbs R. H.; S., L. N. *Langmuir* **2001**, *17*, 1321.

(131) Zhang, X. C.; Teplyakov, A. V. *Langmuir* **2008**, *24*, 810.

(132) Sieval A. B.; Linke R.; Heij G.; Meijer G.; Zuilhof, H.; R., S. l. J. *Langmuir* **2001**, *17*, 7554.

(133) Hart B. R.; Le´tant S. E.; Kane S. R.; Hadi M. Z.; Shields S.J.; G., R. J. *Chem. Commun.* **2003**, 322.

(134) Aswal, D. K.; Lenfant, S.; Guerin, D.; Yakhmi, J. V.; Vuillaume, D. *Analytica Chimica Acta Molecular Electronics and Analytical Chemistry* **2006**, *568*, 84.

(135) Voicu, R.; Boukherroub, R.; Bartzoka, V.; Ward, T.; Wojtyk, J. T. C.; Wayner, D. D. M. *Langmuir* **2004**, *20*, 11713.

(136) Strother, T.; Hamers, R. J.; Smith, L. M. *Nucleic Acids Res.* **2000**, *28*, 3535.

(137) Ren, S. L.; Yang, S. R.; Zhao, Y. P. *Appl. Surf. Sci.* **2004**, *227*, 293.

(138) Pike A. R.; Lie L. H.; Eagling R. A.; Ryder L. C.; Patole S. N.; Connolly B. A.; Horrocks B. R.; Houlton A. *Angew. Chem., Int. Ed.* **2002**, *41*, 615.

(139) Fryxell G. E.; Rieke P. C.; Wood L. L.; Engelhard M. H.; Williford R. E.; Graff G. L.; Campbell A. A.; Wiacek R. J.; Lee L.; Halverson A. *Langmuir* **1996**, *12*, 5064.

(140) Arafat, S. N.; Dutta, S.; Perring, M.; Mitchell, M.; Kenis, P. J. A.; Bowden, N. B. *Chemical Communications* **2005**, 3198.

(141) Sieval, A. B.; Linke, R.; Zuilhof, H.; Sudhlter, E. J. R. *Adv. Mater.* **2000**, *12*, 1457.

(142) Linford, M. R.; Chidsey, C. E. D. *Langmuir* **2002**, *18*, 6217.

(143) Linford, M. R.; Fenter, P.; Eisenberger, P. M.; Chidsey, C. E. D. *J. Am. Chem. Soc.* **1995**, *117*, 3145.

(144) Holmes-Farley, S. R.; Reamey, R. H.; McCarthy, T. J.; Deutch, J.; Whitesides, G. M. *Langmuir* **1985**, *1*, 725.

(145) Eriksson, J. C.; Golander, C. G.; Baszkin, A.; Terminassiansaraga, L. *Journal of Colloid and Interface Science* **1984**, *100*, 381.

(146) Kong, J. S.; Lee, D. J.; Kim, H. D. *Journal of Applied Polymer Science* **2001**, *82*, 1677.

(147) Rasmussen, J. R.; Bergbreiter, D. E.; Whitesides, G. M. *Journal of the American Chemical Society* **1977**, *99*, 4746.

(148) Holmberg, K.; Hyden, H. *Prep Biochem* **1985**, *15*, 309.

(149) Tanahashi, M.; Yao, T.; Kokubo, T.; Minoda, M.; Miyamoto, T.; Nakamura, T. *J. Appl. Biomater.* **1994**, 339.

(150) Cheng, J. Y.; Wei, C. W.; Hsu, K. H.; Young, T. H. *Sens. Actuators B* **2004**, *99*, 186.

(151) Desai. S; Singh, R. P. *Surface modification of polyethylene.*; Springer: New York, 2004.

(152) Kim, Y. J.; Kang, I. K.; Huh, M. W.; Yoon, S. C. *Biomaterials* **2000**, *21*, 121.

(153) Aouinti, M.; Bertrand, P.; Poncin-Epaillard, F. *Plasmas Polymers* **2003**, *8*, 225.

(154) Wang, M.-J.; Chang, Y.-I.; Poncin-Epaillard, F. *Surf. Interface Anal.* **2005**, *37*, 348.

(155) Hu, Y.; Winn, S. R.; Krajbich, I.; Hollinger, J. O. *J. Biomed. Mater. Res., Part A* **2003**, *64A*, 583.

(156) Crombez, M.; Chevallier, P.; Gaudreault, R. C.; Petitclerc, E.; Mantovani, D.; Laroche, G. *Biomaterials* **2005**, *26*, 7402.

(157) Cheng, Z.; Teoh, S.-H. *Biomaterials* **2004**, *25*, 1991.

(158) Wang, P.; Tan, K. L.; Kang, E. T.; Neoh, K. G. *J. Mater. Chem.* **2001**, *11*, 2951.

(159) Kang, E. T.; Tan, K. L.; Kato, K.; Uyama, Y.; Ikada, Y. *Macromolecules* **1996**, *29*, 6872.

(160) Situma, C.; Wang, Y.; Hupert, M.; Barany, F.; McCarley, R. L.; Soper, S. A. *Anal. Biochem.* **2005**, *340*, 123.

(161) Welle, A.; Horn, S.; Schimmelpfeng, J.; Kalka, D. *J. Neurosci. Methods* **2005**, *142*, 243.

(162) Xing, C.-M.; Deng, J.-P.; Yang, W.-T. *J. Appl. Polym. Sci.* **2005**, *97*, 2026.

(163) Long, T. M.; Prakash, S.; Shannon, M. A.; Moore, J. S. *Langmuir* **2006**, *22*, 4104.

(164) Prissanaroon, W.; Brack, N.; Pigram, P. J.; Hale, P.; Kappen, P.; Liesegang, J. *Synth. Met.* **2005**, *154*, 105.

(165) Kawase, T.; Sawada, H. *J. Adhes. Sci. Technol.* **2002**, *16*, 1121.

(166) Goddard, J. M.; Hotchkiss, J. H. *Progress in Polymer Science* **2007**, *32*, 698.

(167) Della Martina, A.; Garamszegi, L.; Hilborn, J. G. *Reactive & Functional Polymers* **2003**, *57*, 49.

(168) Gries, W. H. *Surf. Inter. Anal.* **1996**, *24*, 38.

(169) Tanuma, S.; Powell, C. J.; Penn, D. R. *Surf. Inter. Anal.* **1994**, *21*, 165.

(170) Tougaard, S. *Surf. Inter. Anal.* **1988**, *11*, 453.

(171) Tougaard, S.; Hansen, H. S. *Surf. Inter. Anal.* **1989**, *14*, 730.

(172) Tougaard, S. *J. Electron Spec. Related Phenomena* **1990**, *52*, 243.

(173) Walton, J.; Fairley, N. *J. Electron Spectrosc. Relat. Phenom.* **2005**, *148*, 29.

(174) Johansson, L. S.; Campbell, J.; Koljonen, K.; Kleen, M.; Buchert, J. *Surface and Interface Analysis* **2004**, *36*, 706.

(175) Idla, K.; Johansson, L. S.; Campbell, J. M.; Inganas, O. *Surface and Interface Analysis* **2000**, *30*, 557.

(176) Hansen, H. S.; Tougaard, S.; Biebuyck, H. *J. Electron Spec. Related Phenomena* **1992**, *58*, 141.

(177) Hajati, S.; Tougaard, S. *Anal. Bioanal. Chem.* **2010**, *396*, 2741.

(178) Wayner, D. D. M.; Wolkow, R. A. *J. Chem. Soc.-Perkin Trans. 2* **2002**, 23.

(179) Lummerstorfer, T.; Hoffmann, H. *Langmuir* **2004**, *20*, 6542.

(180) Harrick-Scientific, http://www.harrricksci.com/files/Thin%20Films%20on%20Polycarbonates.pdf.

(181) Bain, C. D.; Whitesides, G. M. *J. Am. Chem. Soc.* **1988**, *110*, 3665.

(182) Holmes-Farley, S. R.; Reamey, R. H.; McCarthy, T. J.; Deutch, J.; Whitesides, G. M. *Langmuir* **1985**, *1*, 725.

(183) Lopez G. P.; Biebuyck H. A.; Whitesides G. M. *Langmuir* **1993**, *9*, 1513.

(184) Wollman E. W.; Frisbie C. D.; Wrighton M. S. *Langmuir* **1993**, *9*, 1517.

(185) Lopez G. P.; Biebuyck H. A.; Harter R.; Kumar A.; Whitesides G. M. *J. Am. Chem. Soc.* **1993**, *115*, 10774.

(186) Mack N. H.; Dong R.; Nuzzo R. G. *J. Am. Chem. Soc.* **2006**, *128*, 7871.

(187) Xia, Y.; Whitesides, G. M. *Angew. Chem., Int. Ed.* **1998**, *37*, 550.

(188) Xia, Y.; Rogers, J. A.; Paul, K. E. *Chem. Rev.* **1999**, *99*, 1823.

(189) Xia, Y.; Tien, J.; Qin, D.; Whitesides, G. M. *Langmuir* **1996**, *12*, 4033.

(190) Xia, Y.; Whitesides, G. M. *Adv. Mater.* **1996**, *8*, 765.

(191) Schmid, H.; Michel, B. *Macromolecules* **2000**, *33*, 3042.

(192) Odom, T. W.; Love, J. C.; Wolfe, D. B.; Paul, K. E.; Whitesides, G. M. *Langmuir* **2002**, *18*, 5314.

(193) Choi, K. M.; Rogers, J. A. *J. Am. Chem. Soc.* **2003**, *125*, 4060.

(194) Clarson, S. J.; Semlyen, J. A. *Siloxan Polymers*; Prentice Hall: Engelwoods Cliff, NJ.

(195) Chadudhury, M. K.; Whitesides, G. M. *Langmuir* **1991**, *7*, 1013.

(196) Gates, B. D.; Xu, Q.; Love, J. C.; Wolfe, D. B.; Whitesides, G. M. *Annual Review of Materials Research* **2004**, *34*, 339.

(197) Geissler, M.; Schmid, H.; Bietsch, A.; Michel, B.; Delamarche, E. *Langmuir* **2002**, *18*, 2374.

(198) Balmer, T. E.; Schmid, H.; Stutz, R.; Delamarche, E.; Michel, B.; Spencer, N. D.; Wolf, H. *Langmuir* **2005**, *21*, 622.

(199) Kraus, T.; Stutz, R.; Balmer, T. E.; Schmid, H.; Malaquin, L.; Spencer, N. D.; Wolf, H. *Langmuir* **2005**, *21*, 7796.

(200) Brock A.; Chang E.; Ho C-C.; LeDuc P.; X., J. *Langmuir* **2003**, *19*, 1611.

(201) Delamarche E.; Donzel C.; Kamounah F. S.; Wolf H.; M., G. *Langmuir* **2003**, *19*, 8749.

(202) Delamarche E.; Geissler M.; Wolf H.; B., M. *J. Am. Chem. Soc.* **2002**, *124*, 3834.

(203) Kim E.; Xia Y.; Zhao X. M.; M., W. G. *Adv. Mater.* **1997**, *9*, 651.

(204) Pavlovic E.; Quist AP.; Nyholm L.; Pallin A.; Gelius U. *Langmuir* **2003**, *19*, 10267.

(205) Geissler M; Schmid H.; Michel B.; E., D. *Microelectron. Eng.* **2003**, *67-68*, 326.

(206) Wilbur J. L.; Kumar A.; Kim E.; M., W. G. *Adv. Mater.* **1994**, *6*, 600.

(207) Renault J. P.; Bernard A.; Bietsch A.; Michel B.; R., B. H. *J. Phys. Chem. B* **2003**, *107*, 703.

(208) Losic D.; Shapter J. G.; Gooding J. J. *Langmuir* **2001**, *17*, 3307.

(209) Geissler M.; Wolf H.; Stutz R.; Delamarche E.; U-W., G. *Langmuir* **2003**, *19*, 6301.

(210) Tormen M.; Borzenko T.; Steffen B.; Schmidt G.; W., M. L. *Appl. Phys. Lett.* **2002**, *81*, 2094.

(211) Martin B. D.; Brandow S. L.; Dressick W. J.; L., S. T. *Langmuir* **2000**, *16*, 9944.

(212) Trimbach D.; Feldman K.; Spencer N. D.; Broer D. J.; M., B. C. W. *Langmuir* **2003**, *19*, 10957.

(213) Wolfe D. B.; Love J. C.; Paul K. E.; Chabinyc M. L.; M., W. G. *Appl. Phys. Lett.* **2002**, *80*, 2222.

(214) Xia Y.; Tien J.; Qin D.; M., W. G. *Langmuir* **1996**, *12*, 4033.

(215) Koide Y.; Such M. W.; Basu R.; Evmenenko G.; J., C. *Langmuir* **2003**, *19*, 86.

(216) Xia Y.; Kim E.; M., W. G. *J. Electrochem. Soc.* **1996**, *143*, 1070.

(217) Duffy, D. C.; McDonald, J. C.; Schueller, O. J. A.; Whitesides, G. M. *Analytical Chemistry* **1998**, *70*, 4974.

(218) Kim, J. S.; Knapp, D. R. *Journal of the American Society for Mass Spectrometry* **2001**, *12*, 463.

(219) Linder, V.; Verpoorte, E.; Thormann, W.; de Rooij, N. F.; Sigrist, M. *Analytical Chemistry* **2001**, *73*, 4181.

(220) McDonald, J. C.; Duffy, D. C.; Anderson, J. R.; Chiu, D. T.; Wu, H. K.; Schueller, O. J. A.; Whitesides, G. M. *Electrophoresis* **2000**, *21*, 27.

(221) Bunyakul, N.; Edwards, K. A.; Promptmas, C.; Baeumner, A. J. *Anal. Bioanal. Chem.* **2009**, *393*, 177.

(222) Seguin, C.; McLachlan, J. M.; Norton, P. R.; Lagugne-Labarthet, F. *Applied Surface Science* **2010**, *256*, 2524.

(223) Yu, L.; Li, C. M.; Liu, Y. S.; Gao, J.; Wang, W.; Gan, Y. *Lab on a Chip* **2009**, *9*, 1243.

(224) Klammer, I.; Hofmann, M. C.; Buchenauer, A.; Mokwa, W.; Schnakenberg, U. *Journal of Micromechanics and Microengineering* **2006**, *16*, 2425.

(225) Lee J. N.; Park C.; M., W. G. *Anal. Chem.* **2003**, *75*, 6544.

(226) Sieval, A. B.; Linke, R.; Zuilhof, H.; Sudhölter, E. J. R. *Adv. Mater.* **2000**, *12*, 1457.

(227) Linford, M. R.; Fenter, P.; Eisenberger, P. M.; Chidsey, C. E. D. *J. Am. Chem. Soc.* **1995**, *117*, 3145.

(228) Wayner, D. D. M.; Wolkow, R. A. *J. Chem. Soc., Perkin Trans.* **2002**, *2*, 23.

(229) Wagner, P.; Nock, S.; Spudich, J. A.; Volkmuth, W. D.; Chu, S.; Cicero, R. L.; Wade, C. P.; Linford, M. R.; Chidsey, C. E. D. *J. Struct. Biol.* **1997**, *119*, 189.

(230) Arafat, S. N.; Dutta, S.; Perring, M.; Mitchell, M.; Kenis, P. J. A.; Bowden, N. B. *Chem. Commun.* **2005**, In press.

(231) Yeo, W.-S.; Mrksich, M. *Angew. Chem. Int. Ed.* **2003**, *42*, 3121.

(232) Guisinger, N. P.; Greene, M. E.; Basu, R.; Baluch, A. S.; Hersam, M. C. *Nano Lett.* **2004**, *4*, 55.

(233) Zhao, J.; Uosaki, K. *J. Phys. Chem. B* **2004**, *108*, 17129.

(234) de Smet, L. C. P. M.; Pukin, A. V.; Stork, G. A.; Ric de Vos, C. H.; Visser, G. M.; Zuilhof, H.; Sudhoelter, E. J. R. *Carbohydr. Res.* **2004**, *339*, 2599.

(235) Sun, Q.-Y.; De Smet, L. C. P. M.; Van Lagen, B.; Giesbers, M.; Thuene, P. C.; Van Engelenburg, J.; De Wolf, F. A.; Zuilhof, H.; Sudhoelter, E. J. R. *J. Am. Chem. Soc.* **2005**, *127*, 2514.

(236) Sun, Q.-Y.; de Smet, L. C. P. M.; van Lagen, B.; Wright, A.; Zuilhof, H.; Sudhoelter, E. J. R. *Angew. Chem. Int. Ed.* **2004**, *43*, 1352.

(237) Xu, D.; Kang, E. T.; Neoh, K. G.; Tay, A. A. O. *Langmuir* **2004**, *20*, 3324.

(238) Altavilla, C.; Ciliberto, E.; Gatteschi, D.; Sangregorio, C. *Adv. Mater.* **2005**, *17*, 1084.

(239) Pei, Y.; Ma, J. *J. Am. Chem. Soc.* **2005**, *127*, 6802.

(240) Zanoni, R.; Cattaruzza, F.; Coluzza, C.; Dalchiele, E. A.; Decker, F.; Di Santo, G.; Flamini, A.; Funari, L.; Marrani, A. G. *Surf. Sci.* **2005**, *575*, 260.

(241) Yasseri, A. A.; Syomin, D.; Loewe, R. S.; Lindsey, J. S.; Zaera, F.; Bocian, D. F. *J. Am. Chem. Soc.* **2004**, *126*, 15603.

(242) Liao, W.; Wei, F.; Qian, M. X.; Zhao, X. S. *Sens. Actuators, B* **2004**, *B101*, 361.

(243) Kim, K.; Shin, K.; Kim, H.; Kim, C.; Byun, Y. *Langmuir* **2004**, *20*, 5396.

(244) Kolbel, M.; Tjerkstra, R. W.; Kim, G.; Brugger, J.; van Rijn, C. J. M.; Nijdam, W.; Huskens, J.; Reinhoudt, D. N. *Adv. Func. Mater.* **2003**, *13*, 219.

(245) Roth, K. M.; Yasseri, A. A.; Liu, Z.; Dabke, R. B.; Malinovskii, V.; Schweikart, K.-H.; Yu, L.; Tiznado, H.; Zaera, F.; Lindsey, J. S.; Kuhr, W. G.; Bocian, D. F. *J. Am. Chem. Soc.* **2003**, *125*, 505.

(246) Yamada, T.; Takano, N.; Yamada, K.; Yoshitomi, S.; Inoue, T.; Osaka, T. *Mat. Phys. Mech.* **2001**, *4*, 67.

(247) Yamada, T.; Takano, N.; Yamada, K.; Yoshitomi, S.; Inoue, T.; Osaka, T. *J. Electroanal. Chem.* **2002**, *532*, 247.

(248) Boukherroub, R.; Morin, S.; Bensebaa, F.; Wayner, D. D. M. *Langmuir* **1999**, *15*, 3831.

(249) Cattaruzza, F.; Cricenti, A.; Flamini, A.; Girasole, M.; Longo, G.; Mezzi, A.; Prosperi, T. *J. Mater. Chem.* **2004**, *14*, 1461.

(250) Yamada, T.; Takano, N.; Yamada, K.; Yoshitomi, S.; Inoue, T.; Osaka, T. *Electrochem. Commun.* **2001**, *3*, 67.

(251) Pike, A. R.; Lie, L. H.; Eagling, R. A.; Ryder, L. C.; Patole, S. N.; Connolly, B. A.; Horrocks, B. R.; Houlton, A. *Angew. Chem. Int. Ed.* **2002**, *41*, 615.

(252) de Smet, L. C. P. M.; Stork, G. A.; Hurenkamp, G. H. F.; Sun, Q.-Y.; Topal, H.; Vronen, P. J. E.; Sieval, A. B.; Wright, A.; Visser, G. M.; Zuilhof, H.; Sudhoelter, E. J. R. *J. Am. Chem. Soc.* **2003**, *125*, 13916.

(253) Lasseter, T. L.; Clare, B. H.; Abbott, N. L.; Hamers, R. S. *J. Am. Chem. Soc.* **2004**, *126*, 10220.

(254) Zhu, X.-Y.; Jun, Y.; Staarup, D. R.; Major, R. C.; Danielson, S.; Boiadjiev, V.; Gladfelter, W. L.; Bunker, B. C.; Guo, A. *Langmuir* **2001**, *17*, 7798.

(255) Cha, T.-W.; Boiadjiev, V.; Lozano, J.; Yang, H.; Zhu, X.-Y. *Anal. Biochem.* **2002**, *311*, 27.

(256) Jun, Y.; Cha, T.-W.; Guo, A.; Zhu, X.-Y. *Biomaterials* **2004**, *25*, 3503.

(257) Cai, W.; Peck, J. R.; van der Weide, D. W.; Hamers, R. J. *Biosens. Bioelectron.* **2004**, *19*, 1013.

(258) Lin, Z.; Strother, T.; Cai, W.; Cao, X.; Smith, L. M.; Hamers, R. J. *Langmuir* **2002**, *18*, 788.

(259) Strother, T.; Cai, W.; Zhao, X.; Hamers, R. J.; Smith, L. M. *J. Am. Chem. Soc.* **2000**, *122*, 1205.

(260) Voicu, R.; Boukherroub, R.; Bartzoka, V.; Ward, T.; Wojtyk, J. T. C.; Wayner, D. D. M. *Langmuir* **2004**, *20*, 11713.

(261) Cai, W.; Lin, Z.; Strother, T.; Smith, L. M.; Hamers, R. J. *J. Phys. Chem. B* **2002**, *106*, 2656.

(262) Sigal, G. B.; Mrksich, M.; Whitesides, G. M. *J. Am. Chem. Soc.* **1998**, *120*, 3464.

(263) Kim, N. Y.; Laibinis, P. E. *J. Am. Chem. Soc.* **1997**, *199*, 2297.

(264) Kim, N. Y.; Laibinis, P. E. *J. Am. Chem. Soc.* **1998**, *120*, 4516.

(265) Cicero, R. L.; Linford, M. R.; Chidsey, C. E. D. *Langmuir* **2000**, *16*, 5688.

(266) Effenberger, F.; Gotz, G.; Bidlingmaier, B.; Wezstein, M. *Angew. Chem. Int. Ed.* **1998**, *37*, 2462.

(267) Zhang, L.; Wesley, K.; Jiang, S. *Langmuir* **2001**, *17*, 6275.
(268) Linford, M. R.; Chidsey, C. E. D. *Langmuir* **2002**, *18*, 6217.

(269) Wojtyk, J. T. C.; Tomietto, M.; Boukherroub, R.; Wayner, D. D. M. *J. Am. Chem. Soc.* **2001**, *123*, 1535.

(270) Buriak, J. M.; Allen, M. J. *J. Am. Chem. Soc.* **1998**, *120*, 1339.

(271) Buriak, J. M. *Chem. Commun.* **1999**, *12*, 1051.

(272) Bateman, J. E.; Eagling, R. D.; Worrall, D. R.; Horrocks, B. R.; Houlton, A. *Angew. Chem. Int. Ed.* **1998**, *37*, 2683.

(273) Miramond, C.; Vuillaume, D. *J. Appl. Phys.* **2004**, *96*, 1529.

(274) Lua, Y.-Y.; Fillmore, W. J. J.; Linford, M. R. *Appl. Surf. Sci.* **2004**, *231-232*, 323.

(275) Jiang, G.; Niederhauser, T. L.; Davis, S. D.; Lua, Y.-Y.; Cannon, B. R.; Dorff, M. J.; Howell, L. L.; Magleby, S. P.; Linford, M. R. *Colloids Surf., A* **2003**, *226*, 9.

(276) Liu, Y.-J.; Navasero, N. M.; Yu, H.-Z. *Langmuir* **2004**, *20*, 4039.

(277) Bent, S. F. *J. Phys. Chem. B* **2002**, *106*, 2830.

(278) Sieval, A. B.; Demirel, A. L.; Nissink, J. W. M.; Linford, M. R.; Maas, J. H. v. d.; Jeu, W. H. d.; Zuilhof, H.; Sudholter, E. J. R. *Langmuir* **1998**, *14*, 1759.

(279) Li, Y. J.; Tero, R.; Nagasawa, T.; Ngata, T.; Urisu, T. *Appl. Surface Sci.* **2004**, *238*, 238.

(280) Lee, T. R.; Carey, R. I.; Biebuyck, H. A.; Whitesides, G. M. *Langmuir* **1994**, *10*, 741.

(281) Higashi, G. S.; Chabal, Y. J.; Trucks, G. W.; Raghavachari, K. *Appl. Phys. Lett.* **1990**, *56*, 656.

(282) Burrows, V. A.; Chabal, Y. J.; Higashi, G. S.; Raghavachari, K.; Christman, S. B. *Appl. Phys. Lett.* **1988**, *53*, 998.

(283) Jakob, P.; Chabal, Y. J. *J. Chem. Phys.* **1991**, *95*, 2897.

(284) Snyder, R. G.; Strauss, H. L.; Elliger, C. A. *J. Phys. Chem.* **1982**, *86*, 5145.

(285) Porter, M. D.; Bright, T. B.; Allara, D. L.; Chidsey, C. E. D. *J. Am. Chem. Soc.* **1987**, *109*, 3559.

(286) Chidsey, C. E. D.; Loiacono, D. N. *Langmuir* **1990**, *6*, 682.

(287) Yuan, S.; Zhang, Y.; Li, Y.; Guiying, X. *Colloids Surf., A* **2004**, *242*, 129.

(288) Yan, L.; Marzolin, C.; Terfort, A.; Whitesides, G. M. *Langmuir* **1997**, *13*, 6704.

(289) Holmes-Farley, S. R.; Bain, C. D.; Whitesides, G. M. *Langmuir* **1988**, *4*, 921.

(290) Bain, C. D.; Whitesides, G. M. *J. Am. Chem. Soc.* **1989**, *111*, 7164.

(291) E., D.; B., M.; A., B. H.; C., G. *Adv. Mater.* **1996**, *8*, 719.

(292) Laibinis, P. E.; Whitesides, G. M.; Allara, D. L.; Tao, Y.-T.; Parikh, A. N.; Nuzzo, R. G. *J. Am. Chem. Soc.* **1991**, *113*, 7152.

(293) Laibinis, P. E.; Bain, C. D.; Nuzzo, R. G.; Whitesides, G. M. *J. Phys. Chem.* **1995**, *99*, 7663.

(294) Kim, E.; Xia, Y.; Whitesides, G. M. *J. Am. Chem. Soc.* **1996**, *118*, 5722.

(295) McDonald, J. C.; Whitesides, G. M. *Accts. Chem. Res.* **2002**, *35*, 491.

(296) McDonald, J. C.; Duffy, D. C.; Anderson, J. R.; Chiu, D. T.; Wu, H.; Schueller, O. J.; Whitesides, G. M. *Electrophoresis* **2000**, *21*, 27.

(297) Odom, T. W.; Love, J. C.; Wolfe, D. B.; Paul, K. E.; Whitesides, G. M. *Langmuir* **2002**, *18*, 5314.

(298) Xia, Y.; Whitesides, G. M. *Angew. Chem. Int. Ed.* **1998**, *37*, 550.

(299) Kane, R. S.; Stroock, A. D.; Jeon, N. L.; Ingber, D. E.; Whitesides, G. M. *Opt. Biosens.* **2002**, 571.

(300) Kane, R. S.; Takayama, S.; Ostuni, E.; Ingber, D. E.; Whitesides, G. M. *Biomaterials* **1999**, *20*, 2363.

(301) Whitesides, G. M.; Ostuni, E.; Takayama, S.; Jiang, X.; Ingber, D. E. *Ann. Rev. Biomed. Eng.* **2001**, *3*, 335.

(302) Sampson, N. S.; Mrksich, M.; Bertozzi, C. R. *Proc. Natl. Acad. Sci. U.S.A.* **2001**, *98*, 12870.
(303) Headrick, J. E.; Armstrong, M.; Cratty, J.; Hammond, S.; Sheriff, B. A.; Berrie, C. L. *Langmuir* **2005**, *21*, 4117.

(304) Heath, J. R.; Ratner, M. A. *Phys. Today* **2003**, *56*, 43.

(305) Sun, S.; Chong, K. S. L.; Leggett, G. J. *Nanotechnology* **2005**, *16*, 1798.

(306) Fresco, Z. M.; Frechet, J. M. J. *J. Am. Chem. Soc.* **2005**, *127*, 8302.

(307) Luderer, F.; Walschus, U. *Top. Curr. Chem.* **2005**, *260*, 37.

(308) Weibel, D. B.; Garstecki, P.; Whitesides, G. M. *Curr. Opin. Neurobio.* **2005**, *15*, 560.

(309) Senaratne, W.; Andruzzi, L.; Ober, C. K. *Biomacromolecules* **2005**, *6*, 2427.

(310) Davis, J. J. *Chem. Commun.* **2005**, 3509.

(311) Salaita, K.; Lee, S. W.; Wang, X.; Huang, L.; Dellinger, T. M.; Liu, C.; Mirkin, C. A. *Small* **2005**, *1*, 940.

(312) Jung, H.; Dalal, C. K.; Kuntz, S.; Shah, R.; Collier, C. P. *Nano. Lett.* **2004**, *4*, 2171.

(313) Mossman, K. D.; Campi, G.; Groves, J. T.; Dustin, M. L. *Science* **2005**, *310*, 1191.

(314) Wallraff, G. M.; Hinsberg, W. D. *Chem. Rev.* **1999**, *99*, 1801.

(315) Vion, D.; Aassime, A.; Cottet, A.; Joyez, P.; Pothier, H.; Urbina, C.; Esteve, D.; Devoret, M. H. *Science* **2002**, *296*, 886.

(316) Tseng, A. A. *Small* **2005**, *1*, 594.

(317) Tseng, A. A. *Small* **2005**, *1*, 924.

(318) Okinaka, M.; Inoue, S.-I.; Tsukagoshi, K.; Aoyagi, Y. *J. Vac. Sci. Technol., B* **2006**, *24*, 271.

(319) Maury, P.; Escalante, M.; Reinhoudt, D. N.; Huskens, J. *Adv. Mater.* **2005**, *17*, 2718.

(320) Liang, X.; Zhang, W.; Li, M.; Xia, Q.; Wu, W.; Ge, H.; Huang, X.; Chou, S. Y. *Nano. Lett.* **2005**, *5*, 527.

(321) Gates, B. D.; Xu, Q.-B.; Stewart, M.; Ryan, D.; Willson, C. G.; Whitesides, G. M. *Chem. Rev.* **2005**, *105*, 1171.

(322) Charvet, R.; Novak, B. M. *Macromolecules* **2004**, *37*, 8808.

(323) Mahanthappa, M. K.; Bates, F. S.; Hillmyer, M. A. *Macromolecules* **2005**, *38*, 7890.

(324) Nomura, K.; Takahashi, S.; Imanishi, Y. *Macromolecules* **2001**, *34*, 4712.

(325) Notestein, J. M.; Lee, L.-B. W.; Register, R. A. *Macromolecules* **2002**, *35*, 1985.

(326) Pollino, J. M.; Stubbs, L. P.; Weck, M. *Macromolecules* **2003**, *36*, 2230.

(327) Schmeltzer, J. M.; Buriak, J. M. *Chem. Nanomater.* **2004**, *2*, 518.

(328) Buriak, J. M. *Chem. Rev.* **2002**, *102*, 1271.

(329) Buriak, J. M. *Chem. Commun.* **1999**, 1051.

(330) Ahn, S. J.; Kaholek, M.; Lee, W.-K.; LaMattina, B.; LaBean, T. H.; Zauscher, S. *Adv. Mater.* **2004**, *16*, 2141.

(331) Bergerson, W. F.; Mulder, J. A.; Hsung, R. P.; Zhu, X.-Y. *J. Am. Chem. Soc.* **1999**, *121*, 454.

(332) Ara, M.; Tada, H. *Appl. Phys. Lett.* **2003**, *83*, 578.

(333) Liao, W.; Wei, F.; Qian, M. X.; Zhao, X. S. *Sens. Actuators, B* **2004**, *B101*, 361.

(334) Sieval, A. B.; Demirel, A. L.; Nissink, J. W. M.; Linford, M. R.; van der Maas, J. H.; de Jeu, W. H.; Zuilhof, H.; Sudholter, E. J. R. *Langmuir* **1998**, *14*, 1759.

(335) Sieval, A. B.; Vleeming, V.; Zuilhof, H.; Sudholter, E. J. R. *Langmuir* **1999**, *15*, 8288.

(336) Sung, M. M.; Kluth, G. J.; Yauw, O. W.; Maboudian, R. *Langmuir* **1997**, *13*, 6164.

(337) Basu, R.; Guisinger, N. P.; Greene, M. E.; Hersam, M. C. *Applied Physics Letters* **2004**, *85*, 2619.

(338) Peng, Y.-c.; Fu, G.-s.; Wang, Y.-l.; Shang, Y. *Semicon. Photonics Tech.* **2004**, *10*, 158.

(339) Yu, H.-Z.; Morin, S.; Wayner, D. D. M.; Allongue, P.; de Villeneuve, C. H. *J. Phys. Chem. B* **2000**, *104*, 11157.

(340) France, M. B.; Alty, L. T.; Earl, T. M. *J. Chem. Ed.* **1999**, *76*, 659.

(341) Dutta, S.; Perring, M.; Mitchell, M.; Kenis, P. J. A.; Bowden, N. B. *Langmuir* **2006**, *22*, 2146.

(342) Arafat, S. N.; Dutta, S.; Perring, M.; Mitchell, M.; Kenis, P. J. A.; Bowden, N. B. *Chem. Commun.* **2005**, *25*, 3198.

(343) Perring, M.; Dutta, S.; Arafat, S.; Mitchell, M.; Kenis, P. J. A.; Bowden, N. B. *Langmuir* **2005**, *21*, 10537.

(344) Chatterjee, A. K.; Choi, T.-L.; Sanders, D. P.; Grubbs, R. H. *J. Am. Chem. Soc.* **2003**, *125*, 11360.

(345) Trnka, T. M.; Grubbs, R. H. *Accts. Chem. Res.* **2001**, *34*, 18.

(346) Grubbs, R. H. *Handbook of Metathesis*; Wiley-VCH: Weinheim, Germany, 2003.

(347) Bielawski, C. W.; Grubbs, R. H. *Angew. Chem. Int. Ed.* **2000**, *39*, 2903.

(348) Lynn, D. M.; Kanaoka, S.; Grubbs, R. H. *J. Am. Chem. Soc.* **1996**, *118*, 784.

(349) Weck, M.; Schwab, P.; Grubbs, R. H. *Macromolecules* **1996**, *29*, 1789.

(350) Blackwell, H. E.; O'Leary, D. J.; Chatterjee, A. K.; Washenfelder, R. A.; Bussmann, D. A.; Grubbs, R. H. *J. Am. Chem. Soc.* **2000**, *122*, 58.

(351) Sanford, M. S.; Henling, L. M.; Day, M. W.; Grubbs, R. H. *Angew. Chem. Int. Ed.* **2000**, *39*, 3451.

(352) Connon, S. J.; Blechert, S. *Angew. Chem. Int. Ed.* **2003**, *42*, 1900.

(353) Schmidt, B. *Angew. Chem. Int. Ed.* **2003**, *42*, 4996.

(354) Lee, J. N.; Park, C.; Whitesides, G. M. *Anal. Chem.* **2003**, *75*, 6544.

(355) Chemoweth, K.; Cheung, S.; van Duin, A. C. T.; Goddard III, W. A.; Kober, E. M. *J. Am. Chem. Soc.* **2005**, *127*, 7192.

(356) Andruzzi, L.; Senaratne, W.; Hexemer, A.; Sheets, E. D.; Ilic, B.; Kramer, E. J.; Baird, B.; Ober, C. K. *Langmuir* **2005**, *21*, 2495.
(357) Arvizo, R. R.; Verma, A.; Rotello, V. M. *Supramolecular Chemistry* **2005**, *17*, 155.

(358) Yan, L.; Huck, W. T. S.; Whitesides, G. M. *J. Macromolecular Sci., Polymer Rev.* **2004**, *C44*, 175.

(359) Xu, F. J.; Zhong, S. P.; Yung, L. Y. L.; Kang, E. T.; Neoh, K. G. *Biomacromolecules* **2004**, *5*, 2392.

(360) Seminario, J. M. *Nature Mater.* **2005**, *4*, 111.

(361) Schoning, M. J. *Sensors* **2005**, *5*, 126.

(362) Paul, K. E.; Prentiss, M.; Whitesides, G. M. *Adv. Funct. Mater.* **2003**, *13*, 259.

(363) Mrksich, M.; Grunwell, J. R.; Whitesides, G. M. *J. Am. Chem. Soc.* **1995**, *117*, 12009.

(364) Caster, K. C. *Polymer Brushes* **2004**, 331.

(365) Flink, S.; van Veggel, F. C. J. M.; Reinhoudt, D. N. *Sens. Update* **2001**, *8*, 3.

(366) Li, X.-M.; Huskens, J.; Reinhoudt, D. N. *J. Mater. Chem.* **2004**, *14*, 2954.

(367) Medintz, I. L.; Goldman, E. R.; Lassman, M. E.; Hayhurst, A.; Kusterbeck, A. W.; Deschamps, J. R. *Anal. Chem.* **2005**, *77*, 365.

(368) E., O.; L., Y.; M., W. G. *Colloids Surf., B* **1999**, *15*, 3.

(369) Swanson, S. A.; McClain, R.; Lovejoy, K. S.; Alamdari, N. B.; Hamilton, J. S.; Scott, J. C. *Langmuir* **2005**, *21*, 5034.

(370) Sylvia, J. M.; Spencer, K. M.; Janni, J. A. *J. Proc. Anal. Chem.* **2001**, *6*, 146.

(371) MacBeath, G.; Schreiber, S. L. *Science*, *289*, 1760.

(372) Bulyk, M. L.; Gentalen, E.; Lockhart, D. J.; Church, G. M. *Nature Biotech.* **1999**, *17*, 573.

(373) Wang, A.-J.; Feng, J.-J.; Fan, J. *Journal of Chromatography, A* **2008**, *1192*, 173.

(374) Sugiura, S.; Edahiro, J.-i.; Sumaru, K.; Kanamori, T. *Colloids and Surfaces, B: Biointerfaces* **2008**, *63*, 301.

(375) Mora, M. F.; Giacomelli, C. E.; Garcia, C. D. *Analytical Chemistry (Washington, DC, United States)* **2007**, *79*, 6675.

(376) Henry, A.; Tutt, T.; Galloway, M.; Davidson, Y.; McWhorter, C.; Soper, S.; McCarley, R. *Anal. Chem.* **2000**, *72*, 5331.

(377) Zhu, Y.; Gao, C.; Liu, X.; Shen, J. *Biomacromolecules* **2002**, *3*, 1312.

(378) Zhu, Y.; Gao, C.; Shen, J. *Biomaterials* **2002**, *23*, 4889.

(379) Inagaki, N.; Narushima, K.; Tsutsui, Y.; Ohyama, Y. *Journal of Adhesion Science and Technology* **2002**, *16*, 1041.

(380) Cai, K.; Yao, K.; Cui, Y.; Yang, Z.; Li, X.; Xie, H.; Qing, T.; Gao, L. *Biomaterials* **2002**, *23*, 1603.

(381) Rouzes, C.; Gref, R.; Leonard, M.; De Sousa Delgado, A.; Dellacherie, E. *Journal of Biomedical Materials Research* **2000**, *50*, 557.

(382) Jung, S.; Angerer, B.; Loscher, F.; Niehren, S.; Winkle, J.; Seeger, S. *ChemBioChem* **2006**, *7*, 900.

(383) Ifuku, S.; Tsujii, Y.; Kamitakahara, H.; Takano, T.; Nakatsubo, F. *Journal of Polymer Science, Part A: Polymer Chemistry* **2005**, *43*, 5023.

(384) Holmes-Farley, S. R.; Reamey, R. H.; McCarthy, T. J.; Deutch, J.; Whitesides, G. M. *Langmuir* **1985**, *1*, 725.

(385) Holmes-Farley, S. R.; Whitesides, G. M. *Langmuir* **1987**, *3*, 62.

(386) Holmes-Farley, S. R.; Bain, C. D.; Whitesides, G. M. *Langmuir* **1988**, *4*, 921.

(387) Martina, A. D.; Garamszegi, L.; Hilborn, J. G. *J. Polym. Sci., Part A: Polym. Chem.* **2003**, *41*, 2036.

(388) Martina, A. D.; Graf, R.; Hilborn, J. G. *J. Appl. Polym. Sci.* **2005**, *96*, 407.

(389) Rule, J. D.; Moore, J. S. *Macromolecules* **2002**, *35*, 7878.

(390) Ren, F.; Feldman, A. K.; Carnes, M.; Steigerwald, M.; Nuckolls, C. *Macromolecules (Washington, DC, United States)* **2007**, *40*, 8151.

(391) Lee, J. K.; Gould, G. L. *Journal of Sol-Gel Science and Technology* **2007**, *44*, 29.

(392) Lee, J. K.; Liu, X.; Yoon, S. H.; Kessler, M. R. *Journal of Polymer Science, Part B: Polymer Physics* **2007**, *45*, 1771.

(393) Liu, X.; Lee, J. K.; Yoon, S. H.; Kessler, M. R. *Journal of Applied Polymer Science* **2006**, *101*, 1266.

(394) Bellan, L. M.; Coates, G. W.; Craighead, H. G. *Macromolecular Rapid Communications* **2006**, *27*, 511.

(395) Jones, A. S.; Rule, J. D.; Moore, J. S.; White, S. R.; Sottos, N. R. *Chemistry of Materials* **2006**, *18*, 1312.

(396) Lubbad, S.; Buchmeiser, M. R. *Macromol. Rapid Commun.* **2003**, *24*, 580.

(397) Love, J. A.; Sanford, M. S.; Day, M. W.; Grubbs, R. H. *J. Am. Chem. Soc.* **2003**, *125*, 10103.

(398) Schwab, P.; Grubbs, R. H.; Ziller, J. W. *J. Am. Chem. Soc.* **1996**, *118*, 100.

(399) Milosevic, M.; Milosevic, V.; Berets, S. L. *Applied Spectroscopy* **2007**, *61*, 530.

(400) Swanson, S. A.; McClain, R.; Lovejoy, K. S.; Alamdari, N. B.; Hamilton, J. S.; Scott, J. C. *Langmuir* **2005**, *21*, 5034.

(401) Ishino, Y.; Ishida, H. *Applied Spectroscopy* **1988**, *42*, 1296.

(402) Fryxell, G. E.; Rieke, P. C.; Wood, L. L.; Engelhard, M. H.; Williford, R. E.; Graff, G. L.; Campbell, A. A.; Wiacek, R. J.; Lee, L.; Halverson, A. *Langmuir* **1996**, *12*, 5064.

(403) Templeton, A. C.; Hostetler, M. J.; Kraft, C. T.; Murray, R. W. *J. Am. Chem. Soc.* **1998**, *120*, 1906.

(404) Hansen, H. S.; Jansson, C.; Tougaard, S. *J. Vac. Sci. Technol. A* **1992**, *10*, 2938.

(405) Tougaard, S. *Surf. Inter. Anal.* **1988**, *11*, 453.

(406) Tougaard, S. *J. Electron Spec. Related Phenomena* **1990**, *52*, 243.

(407) Tao, Y.-T.; C.-C., W.; Eu, J.-Y.; Lin, W.-L. *Langmuir* **1997**, *13*, 4018.

(408) Bruinink, C. M.; Peter, M.; de Boer, M.; Kuipers, L.; Huskens, J.; Reinhoudt, D. N. *Adv. Mater.* **2004**, *16*, 1086.

(409) Huang, Y.; Paloczi, G. T.; Yariv, A.; Zhang, C.; Dalton, L. R. *J. Phys. Chem. B* **2004**, *108*, 8606.

(410) Rolland, J.; Hagberg, E. C.; Dension, G. M.; Carter, K. R.; De Simone, J. M. *Angew. Chem. Int. Ed.* **2004**, *43*, 5796.

(411) Rolland, J. P.; Zhou, Z.; Kelly, J. Y.; Denison, G. M.; van Dam, R. M.; Hagberg, E. C.; Carter, K. R.; Quake, S. R.; DeSimone, J. M. *Polym. Mat.: Sci. Eng.* **2004**, *91*, 254.

(412) Bocking, T.; James, M.; Coster, H. G. L.; Chilcott, T. C.; Barrow, K. D. *Langmuir* **2004**, *20*, 9227.

(413) Rungee, M. B.; Mwangi, M. T.; Miller, A. L. I.; Perring, M.; Bowden, N. B. *Angew. Chem. Int. Ed. Engl.* **2008**, *120*, 949.

(414) Linford, M. R.; Chidsey, C. E. D. *Langmuir* **2002**, *18*, 6217.

(415) Boukherroub, R.; Wayner, D. D. M. *J. Am. Chem. Soc.* **1999**, *121*, 11513.

(416) Uosaki, K.; Quayum, M. E.; Nihonyanagi, S.; Kondo, T. *Langmuir* **2004**, *20*, 1207.

(417) Bansal, A.; Li, X.; Lauermann, I.; Lewis, N. S. *J. Am. Chem. Soc.* **1996**, *118*, 7225.

(418) Bansal, A.; Li, X.; Yi, S. I.; Weinberg, W. H.; Lewis, N. S. *J. Phys. Chem. B* **2001**, *105*, 10266.

(419) Liu, Y.-J.; Navasero, N. M.; Yu, H.-Z. *Langmuir* **2004**, *20*, 4039.

(420) Wade, C. P.; Chidsey, C. E. D. *Appl. Phys. Lett.* **1997**, *71*, 1679.

(421) Perring, M.; Dutta, S.; Arafat, S.; Mitchell, M.; Kenis, P. J. A.; Bowden, N. B. *Langmuir* **2005**, In Press.

(422) Niederhauser, T. L.; Lua, Y.-Y.; Jiang, G.; Davis, S. D.; Matheson, R.; Hess, D. A.; Mowat, I. A.; Linford, M. R. *Angew. Chem. Int. Ed.* **2002**, *41*, 2353.

(423) Liu, Z.; Rainier, J. D. *Org. Lett.* **2005**, *7*, 131.

(424) Bielawski, C. W.; Grubbs, R. H. *Macromolecules* **2001**, *34*, 8838.

(425) Sanford, M. S.; Love, J. A.; Grubbs, R. H. *J. Am. Chem. Soc.* **2001**, *123*, 6543.

(426) Liu, X.; Guo, S.; Mirkin, C. A. *Angew. Chem. Int. Ed.* **2003**, *42*, 4785.

(427) Li, X.-M.; Huskens, J.; Reinhoudt, D. N. *Nanotechnology* **2003**, *14*, 1064.

(428) Harada, Y.; Girolami, G. S.; Nuzzo, R. G. *Langmuir* **2003**, *19*, 5104.

(429) Rutenberg, I. M.; Scherman, O. A.; Grubbs, R. H.; Jiang, W.; Garfunkel, E.; Bao, Z. *J. Am. Chem. Soc.* **2004**, *126*, 4062.

(430) Watson, K. J.; Zhu, J.; Nguyen, S. T.; Mirkin, C. A. *J. Am. Chem. Soc.* **1999**, *121*, 462.

(431) Jeon, N. L.; Choi, I. S.; Whitesides, G. M.; Kim, N. Y.; Laibinis, P. E.; Harada, Y.; Finnie, K. R.; Girolami, G. S.; Nuzzo, R. G. *Appl. Phys. Lett.* **1999**, *75*, 4201.

(432) Weck, M.; Jackiw, J. J.; Rossi, R. R.; Weiss, P. S.; Grubbs, R. H. *J. Am. Chem. Soc.* **1999**, *121*, 4088.

(433) Jordi, M. S.; Seery, T. A. P. *J. Am. Chem. Soc.* **2005**, *127*, 4416.

(434) Gomez, F. J.; Chen, R. J.; Wang, D.; Waymouth, R. M.; Dai, H. *Chem. Commun.* **2003**, 190.

(435) Agnes, J.; Scherman, O. A.; Grubbs, R. H.; Lewis, N. S. *Langmuir* **2001**, *17*, 1321.

(436) Kim, N. Y.; Jeon, N. L.; Choi, I. S.; Takami, S.; Harada, Y.; Finnie, K. R.; Girolami, G. S.; Nuzzo, R. G.; Whitesides, G. M.; Laibinis, P. E. *Macromolecules* **2000**, *33*, 2793.

(437) Lee, J. K.; Lee, K.-B.; Kim, D. J.; Choi, I. S. *Langmuir* **2003**, *19*, 8141.

(438) Wallart, X.; de Villeneuve, C. H.; Allongue, P. *J. Am. Chem. Soc.* **2005**, *127*, 7871.

(439) Snyder, R. G.; Strauss, H. L.; Elliger, C. A. *J. Phys. Chem.* **1982**, *86*, 5145.

(440) Dubowski, Y.; Vieceli, J.; Tobias, D. J.; Gomez, A.; Lin, A.; Nizkoorodor, S. A.; Mcintire, T. M.; Finlayson-Pitts, B. J. *J. Phys. Chem. A* **2004**, *108*, 10473.

(441) Peanasky, J. S.; McCarley, R. L. *Langmuir* **1998**, *14*, 113.

(442) Wenzel, I.; Yam, C. M.; Barriet, D.; Lee, T. R. *Langmuir* **2003**, *119*, 10217.

(443) Laibinis, P. E.; Bain, C. D.; Nuzzo, R. G.; Whitesides, G. M. *J. Phys. Chem.* **1995**, *99*, 7663.

(444) Sinniah, K.; Cheng, J.; Terrettaz, S.; Reutt-Robey, J. E.; Miller, C. J. *J. Phys. Chem.* **1995**, *99*, 14500.

(445) Miwa, Y.; Machida, K. *J. Am. Chem. Soc.* **1989**, *111*, 7733.

(446) Aizenberg, J. *Adv. Mater.* **2004**, *16*, 1295.

(447) Lee, C. J.; Blumenkranz, M. S.; Fishman, H. A.; Bent, S. F. *Langmuir* **2004**, *20*, 4155.

(448) Qin, D.; Xia, Y.; Whitesides, G. M. *Adv. Mater.* **1996**, *8*, 917.